Kinetic, electrochemical and spectroscopic investigation of the oxidation of CO and C_2H_4 on YSZ-supported metal model electrodes

Christoph Bachmann

zur Erlangung des akademischen Grades eines

Doktors der Naturwissenschaften

vom Fachbereich Biologie und Chemie

der Justus-Liebig-Universität Gießen

Gießen

2015

Referent: Prof. Dr. Jürgen Janek

Koreferent: Prof. Dr. Herbert Over

Erklärung zur eigenständigen Anfertigung

Hiermit erkläre ich, dass ich die vorliegende Arbeit selbständig verfasst und keine anderen als die angegebenen Hilfsmittel benutzt habe.
Die Stellen der Arbeit, die anderen Quellen im Wortlaut oder dem Sinn nach entnommen wurden, sind durch Angaben der Herkunft kenntlich gemacht. Dies gilt auch für Zeichnungen, Skizzen und bildliche Darstellungen.
Bei den von mir durchgeführten und in der Dissertation erwähnten Untersuchungen habe ich die Grundsätze guter wissenschaftlicher Praxis, wie sie in der Satzung der Justus-Liebig-Universität Gießen zur Sicherung guter wissenschaftlicher Praxis niedergelegt sind, eingehalten.

Murr, 2015

(Christoph Bachmann)

"Tue es oder tue es nicht. Es gibt kein Versuchen"

Für meinen Sohn Luke

Eine wissenschaftliche Arbeit ist nie das Werk einer einzelnen Person, deshalb ist es jetzt an der Zeit, mich bei allen Menschen zu bedanken, die mir die Erstellung meiner Dissertation ermöglicht haben.

- Prof. Dr. Jürgen Janek möchte ich für die Betreuung dieser Arbeit, die hilfreichen Diskussionen und die immer neuen Ideen danken.
- Prof. Dr. Herbert Over danke ich für die Übernahme des Korreferats und die Anregungen und die konstruktive Kritik, die mich stets weiter brachten.
- Dr. Bjoern Luerßen danke ich für die Betreuung meiner Arbeit.
- Allen Mitarbeiter/innen des PCI danke ich für die vielen schönen beruflichen aber auch privaten Momente.
- Meiner Frau und meinem Sohn danke ich, dass sie mir stets Mut zugesprochen und mich in meiner Arbeit bestärkt haben.
- Und nicht zuletzt danke ich meinen Eltern, die in jeglicher Hinsicht die Grundsteine für meinen Weg gelegt haben.

Abstract

Catalysis research is one of the most important topics in physical chemistry. Without catalytic processes many materials, chemicals and pharmaceutical products would not be available today. In many ways the catalyst plays a decisive role. Due to the possibility of stereochemical synthesis the selective and pure preparation of particular substances (for example avoiding Kontagan problematic) and/or the production of substances by avoiding undesirable and hazardous side-products is possible. Besides the material sector catalysis is of fundamental importance for one of the big upcoming topics, the energy supply in the future. Most of the processes of energy production and storage are based upon catalytic processes. Catalysis plays an important role in the chemical processes of batteries, but also in relation to hydrogen technology. For example, during the use of fuel cells a catalytic reforming process is connected ahead which ensures the availability of pure fuel (hydrogen).

Other important new research fields are the availability of resources, the recuperation of certain materials and waste avoidance. Today, the use of specific active catalysts is seen as the only possibility to recover plastic materials.

An important branch of catalysis represents the combination of catalysis with electrochemistry, the so-called electrocatalysis. What makes this new field special is that the electrode material represents also the catalytic active material. The efficiency of the catalyst is hereby mainly determined by the morphology and composition of the surface. Up till now improvements of the catalytic properties have been mainly obtained by enlargement of the active surface, e.g. the development of nano crystalline surfaces, nano particles or

high-porosity materials. Another approach is to modify the surface properties by an external switch, for example pressure, temperature, magnetic fields or electric fields in the case of electrocatalysis. This allows completely new technical applications like the realization of switchable systems and surfaces.

A very impressive example of a switchable catalyst has been recently shown by a French research team [Andr13]. They developed a new material which could be used as catalyst during electrolysis for hydrogen production. Up till now hydrogen has not been produced in industrial scale by electrolysis due to high energy costs and the costly platinum catalyst. New developed catalyst materials on the base of cobalt are capable of catalyzing both reactions of the electrolysis (oxidation on the anode and reduction on the cathode). Therefore the catalyst is used in two different states. The reduced state consists of cobalt nano particles surrounded by a cobalt(II)oxophosphate for the production of hydrogen while the material exists in an oxidized state as a complex cobalt trioxide which is used for the production of oxygen. The French research team points out that the electrolysis can be operated cost efficient and eco-friendly in the future by the utilization of these materials.

In our daily life switchable surfaces will also play an important role in the future. At the moment materials are developed, which allow a reversible change between an adhesive and non-adhesive state [Jung10, Hein12]. This could be utilized in the clothing industry for tailoring functionalized clothes which are water-repellent (waterproof) or water wettable (airy) depending on the external conditions.

This work arouses in the scope of a research focus (DFG project JA 648/17-1) which concentrates on the influence of an electrochemical potential on the surface properties of solid cells and thereby on the development of switchable solid cells and electrocatalysts. A key point of this work has been the investigation of the so-called NEMCA effect (**N**on-faradaic **E**lectrochemical **M**odification of **C**atalytic **A**ctivity) or EPOC effect (**E**lectrochemical **P**romotion **o**f **C**atalysis) which explains the modification of the reaction rate of a catalytic reaction like CO or ethylene oxidation by application of an electrochemical potential on a metal electrode placed on an ion conducting solid electrolyte. The effect is generally explained by the migration of charged ions (spillover species) originating from the electrolyte onto the surface of the catalyst thereby modifying the surface properties. The focus of this work has been drawn on the combination of spectroscopic and microscopic methods with electrochemical techniques to get a deeper understanding into the NEMCA effect and the nature of the electrochemical created spillover species. The utilization of model electrodes with geometric well defined and spectroscopic accessible electrode surfaces (triple phase boundary (TPB) length) were of importance. Besides the buildup of the setup to measure the catalytic activity of solid cells and the accompanied measurements of the influence of an applied potential on the reaction rate the spectroscopic and microscopic techniques have been refined to a point where a coupling with electrochemical methods is possible and changes on the surface and the TPB can be monitored in-situ. The following measurements have been conducted in detail:

- Characterization of different electrode types and different electrode materials on different orientated substrate materials in reference to sinter effects. X-Ray Diffraction (XRD, polfigure measurements), Scanning Electron Microscopy (SEM), Electron Backscatter Diffraction (EBSD) show oxidation and dewetting effects depending on the material combined with grain growth and reduction of different orientated grains.

- Electrochemical investigations of Pt/YSZ and Ag/YSZ cells under high vacuum conditions with and without reactive gases have been done. The results reveal a storage of oxygen at the metal/YSZ interface and a small (persistent) NEMCA effect.

- Kinetic measurements for different Pt electrodes in the presence of CO and O_2 reveal a strong influence of the TPB length for the kinetic behavior and the overall conversion. Additionally a strong influence of the underlying substrate could be found.

- Electrochemical investigations under different NEMCA typical conditions for different temperatures have been done. The results show that a NEMCA effect is only visible after prolonged heat treatment. Due to the thermodynamic stability of platinum and platinum oxide a change between both states upon temperature treatment is likely. An obtained metastable state upon decreasing temperature can be destabilized by electrochemical polarization therefore showing a NEMCA effect.

- Surface XRD (S-XRD) measurements have been conducted to identify the conditions necessary for a platinum oxide forma-

tion on the surface of the catalyst under different oxygen partial pressures as well as under reaction conditions. Here, a thin platinum oxide could be found under low oxygen partial pressures (down to 10 mbar), but not under reaction conditions in the presence of CO. Additionally, high pressure X-Ray Photoelectron Spectroscopy (XPS) measurements have been done to identify a possible platinum oxide. A platinum oxide formation under higher oxygen partial pressures and under polarization conditions (NEMCA conditions) could not be found.

Zusammenfassung

Die Katalyseforschung ist eines der wichtigen Themengebiete der physikalischen Chemie. Ohne katalytische Prozesse wären viele Materialien, Chemikalien und Pharmaprodukte heute gar nicht erhältlich. Hierbei spielen Katalysatoren in vielerlei Hinsicht eine entscheidende Rolle. Sei es, dass sie aufgrund der besonderen stereochemischen Synthese die gezielte und reine Herstellung bestimmter Stoffe (meist Pharmawirkstoffe, zum Beispiel Vermeidung des Kontaganproblems) oder die Herstellung bestimmter Produkte unter Vermeidung unerwünschter und gefährlicher Nebenprodukte ermöglichen. Neben dem stofflichen Sektor ist die Katalyse auch von grundlegender Bedeutung für eines der großen Themengebiete der nahen Zukunft, der künftigen Energieversorgung. Die meisten Prozesse der Energieerzeugung oder Speicherung basieren auf katalytischen Prozessen. So spielt die Katalyse eine wichtige Rolle bei den chemischen Prozessen in einer Metall-Luft Batterie aber auch eine bedeutende Rolle in Bezug auf die Wasserstofftechnologie. Zum Beispiel muss bei der Verwendung einer Brennstoffzelle ein katalytischer Reformierungsprozess vorgeschaltet sein, der die Verfügbarkeit des reinen Brennstoffes (Wasserstoff) ermöglicht. In der Automobilindustrie ist man sich einig, dass aus Sicherheitsgründen das Mitführen eines Wasserstoff-Druckbehälters vermieden werden muss, was dazu führt, dass unmittelbar vor dem Gebrauch alternative Kraftstoffe, wie zum Beispiel Methanol katalytisch effizient in ein hochwasserstoffhaltiges Gas reformiert werden müssen.
Ein weiteres wichtiges und recht neues Forschungsgebiet, in dem die Katalyse eine grundlegende Bedeutung spielen wird, ist die zukünftige Ressourcenverfügbarkeit und Rückgewinnung bestimmter

Materialien sowie die Müllvermeidung. So sieht man heutzutage in der Verwendung spezifisch wirksamer Katalysatoren die einzige Möglichkeit, Kunststoffe wieder zurückzubauen.
Ein bedeutendes Teilgebiet der Katalyse stellt die Kombination mit der Elektrochemie dar, die sogenannte Elektrokatalyse. Hierbei ist das Besondere, dass das Elektrodenmaterial gleichzeitig das katalytisch aktive Material darstellt. Für die Effizienz eines Katalysators ist hierbei vor allem die Morphologie der Oberfläche und die Oberflächenzusammensetzung von Bedeutung.
Eine Verbesserung der katalytischen Eigenschaften wurde bisher meist durch eine Vergrößerung der aktiven Oberfläche versucht zu erzeugen, zum Beispiel durch die Entwicklung von nanokristallinen Oberflächen, nano-Partikeln oder hoch porösen Materialien.
Ein anderer Ansatz besteht darin, die Oberflächeneigenschaften durch einen externen Schalter, zum Beispiel Druck, Temperatur, magnetische Felder oder im Falle der Elektrokatalyse ein elektrisches Feld zu verändern. Dies ermöglicht völlig neue technische Anwendungen wie die Realisierung schaltbarer Systeme und Oberflächen.
Ein sehr beeindruckendes Beispiel für einen Katalysator hat vor kurzem ein französisches Forscherteam vorgestellt [Andr13]. Sie entwickelten ein neues Material, das als Katalysator für die Wasserstofferzeugung durch Elektrolyse genutzt werden kann. Bisher wurde Wasserstoff im industriellen Maßstab aufgrund der hohen Kosten nicht auf elektrolytischem Wege erzeugt, was vor allem an den hohen Energiekosten und dem bisher verwendeten Katalysator Platin lag. Das neu entwickelte Katalysatormaterial ist auf Kobaltbasis aufgebaut und kann beide Teilreaktionen der Elektrolyse (Oxida-

tion an der Anode und Reduktion an der Kathode) katalysieren. Hierzu wird der Katalysator in zwei Zuständen genutzt, die reduzierte Form besteht aus Kobalt-Nanopartikeln umgeben von einem Kobalt(II)-Oxophosphat zur Herstellung des Wasserstoffes während das Material in oxidierter Form als komplexes Kobalttrioxid zur Erzeugung von Sauerstoff dient. Das Forscherteam geht davon aus, dass mit diesem Material die Elektrolyse in Zukunft kostengünstig und umweltfreundlich umgesetzt werden kann.

Auch in unserem Alltag werden schaltbare Oberflächen in Zukunft eine wichtige Rolle spielen. So werden derzeit Materialien entwickelt, die es ermöglichen, reversibel zwischen adhäsivem und nichtadhäsivem Zustand zu wechseln [Jung10, Hein12]. Dies findet Verwendung in der Textilindustrie und ermöglicht es, Kleidung zu entwickeln die je nach äußeren Bedingungen Wasser abweisend (wasserdicht) oder von Wasser benetzbar (luftig) ist.

Die vorliegende Arbeit ist im Rahmen eines Forschungsschwerpunktes (DFG Projekt JA 648/17-1) entstanden, der sich mit dem Einfluss eines elektrochemischen Potentials auf die Oberflächeneigenschaften von Festköperzellen beschäftigt und auf diesem Wege die Entwicklung von schaltbaren Festkörperzellen und Elektrokatalysatoren ermöglicht. Im Mittelpunkt der Arbeit steht die Untersuchung des NEMCA-Effektes (**N**on-faradaic **E**lectrochemical **M**odification of **C**atalytic **A**ctivity) oder EPOC-Effektes (**E**lectrochemical **P**romotion **o**f **C**atalysis), bei dem durch Anlegen eines elektrochemischen Potentials an einer Metallelektrode auf einem ionenleitenden Festelektrolyten die Umsatzrate einer katalytischen Reaktion, wie die Reaktion von CO zu CO_2 oder Ethylen zu CO_2 und H_2O gesteigert oder verringert werden kann. Die gängige Erklärung für diesen

Effekt geht davon aus, dass während der elektrochemischen Polarisation (anodische Polarisation) Spillover Sauerstoffspezies aus dem Elektrolyten auf die Elektrodenoberfläche gepumpt werden und dort katalytisch aktiv sind. Der Fokus der vorliegenden Arbeit bestand darin, spektroskopische und mikroskopische Methoden mit elektrochemischen Techniken zu kombinieren, um ein tieferes Verständnis des NEMCA-Effektes und der Natur der elektrochemisch erzeugten Spillover Spezies zu bekommen. Dabei stand die Verwendung von gut definierten Modellsystemen mit einer geometrisch klar definierten und spektroskopisch zugänglichen Elektrodenoberfläche und Dreiphasengrenzlänge im Mittelpunkt. Neben dem Aufbau einer Anlage zur Untersuchung des Einflusses eines angelegten elektrochemischen Potentials auf die Umsatzrate der jeweils betrachteten Reaktion wurden in dieser Arbeit vor allem spektroskopische und mikroskopische Techniken dahingehend weiterentwickelt, dass sie mit elektrochemischen Methoden gekoppelt wurden, um so in-situ während der elektrochemischen Polarisation Veränderungen an der Katalysatoroberfläche und der Dreiphasengrenze zu beobachten. Im Detail wurden die folgenden Untersuchungen durchgeführt:

- Verschiedene Metallelektroden (Pt, Ag und Pd) wurden auf unterschiedlichen Substraten (YSZ mit verschiedenen Orientierungen sowie Saphir (0001)) mittels PLD abgeschieden und der Einfluss der Orientierung des Substrates, der Ablationstemperatur und einer anschließende Nachbehandlung auf die Schichteigenschaften wurde mittels Röntgendiffraktometrie (XRD), Rasterelektronenmikroskopie (SEM) und Rückstreuelektronenbeugung (EBSD) untersucht.

- Elektrochemische Untersuchungen an den Elektrodensystemen Pt|YSZ und Ag|YSZ unter Hochvakuum (HV) Bedingungen wurden sowohl ohne als auch unter Reaktionsbedingungen durchgeführt. Dabei konnte eine Speicherung von Sauerstoff an der Metal|YSZ-Grenzfläche nachgewiesen werden sowie ein schwach ausgeprägter persistenter NEMCA-Effekt.

- An Platinelektroden mit verschiedenen geometrisch gut definierten Dreiphasengrenzlängen wurden kinetische Messungen durchgeführt, um den Einfluss der Dreiphasengrenzlänge auf das kinetische Verhalten während der CO Oxidation zu untersuchen. Zusätzlich wurde noch der Einfluss verschiedener Substrate auf die Oxidationsreaktion untersucht.

- Elektrochemische Messungen unter NEMCA typischen Bedingungen wurden an verschiedenen Platinelektroden (deckende, entnetzte, poröse und lithografische Elektrodem) durchgeführt. Hierbei konnte gezeigt werden, dass ein NEMCA-Effekt nur nach thermischer Vorbehandlung der Elektroden nachgewiesen werden kann. Als mögliche Erklärung wurde ein Modell basierend auf thermodynamischen Stabilitäten verschiedener Oberflächenzustände (Platinoxid und reines Platin) vorgeschlagen. Während der Temperaturbehandlung wird ein entsprechend metastabiler aktiver Oberflächenzustand (Platinoxid) destabilisiert, der während der entsprechenden elektrochemischen Polarisation aufgrund des erhöhten Sauerstoffpartialdruckes wieder erzeugt werden kann und somit eine Ratensteigerung während der elektrochemischen Polarisation erzeugt.

- Oberflächen-XRD Messungen wurden durchgeführt, um den Stabilitätsbereich und die Bildungsbedingungen des Platinoxids auf der Platinoberfläche zu untersuchen. Desweiteren wurden Hochdruck-XPS Messungen durchgeführt um eine mögliche Platinoxidbildung unter höheren Sauerstoffpartialdrücken und während der elektrochemischen Polarisation nachzuweisen.

Table of Contents

Chapter 1

Theoretical Part

1.1 The Theory of Electrochemical Promotion of Catalysis (EPOC) on metal electrodes

The phenomenon of electrochemical promotion of catalysis (EPOC) is often considered as one of the important discoveries in electrochemistry and was proven for more than 80 different systems till now. The current theory explains the effect with a work function change of the catalyst by a spillover process of oxygen out of the solid electrolyte onto the free electrode surface by either temperature treatment or electrochemical polarization. Although a lot of surface analytical techniques were used to confirm this theory, the interpretation of some results has to be questioned critically. New explanatory approaches were published recently, mainly because of the development of (in situ) surface analysis techniques which allow new mechanistic insights. The aim of this chapter is to give a critical overview of the current understanding of electrochemical promotion. First of all, the experimental procedure of a classical EPOC experiment and the different mechanisms of electrochemical promotion will be presented. In the next part, the use of ap-

propriate analytical techniques for investigation of the underlying mechanism and the influence of sample preparation conditions and different sample morphologies will be discussed. The last part deals with possible future directions of EPOC research and perspective industrial applications.

1.2 Introduction

In the early 80s the NEMCA effect (**N**on-faradaic **E**lectrochemical **M**odification of **C**atalytic **A**ctivity) or EPOC (**E**lectrochemical **P**romotion **o**f **C**atalysis) was firstly reported by Costas G. Vayenas and Mike Stoukidis [Stou81]. The goal of their studies was to control the oxygen activity of a silver electrode deposited on an oxygen ion conducting electrolyte during epoxidation by application of an external electrical field. They observed a non-faradaic behavior (the reaction rate increased by a factor of 300 in comparison to the expected one calculated with the faradaic law) which they attributed to the nature of the specific system and formation of subsurface silver oxide by mistake [Stou81]. In 1988 it was recognized that this effect is a general phenomenon which is not limited to a few reaction systems, but is assigned to a wide number of catalytic reactions [Vaye88]. This was the beginning of years of research resulting in more than 1000 publications and numerous explanatory approaches. The working group of C. G. Vayenas has contributed to develop the phenomenon of electrochemical promotion to an important area of catalysis. So far, researchers have succeeded to show on 80 different catalytic systems an increase of reaction rate and an impact on reaction se-

lectivity by applying an electrochemical potential on a (mixed) conducting electrode onto an ion-conducting solid electrolyte. A comprehensive overview of the topic is given in a 2001 published book [Vaye01] and in review articles [Kats10, Bely00, Imbi10]. Besides the work of Vayenas, the following working groups have gained reputation in the research field of electrochemical promotion: Sobyanin [Poli90, Mar92], Valverde [deLu07, Jime12, Mate13], Anastasijevic [Anas93, Anas09], Lambert [Lamb95, Lamb96], Imbihl [Imbi10, Togh10], Pachioni [Pacc96, Pacc97], Haller [Cava93, Cava98], Stoukidis [Stou81, Stou84, Stou88], Tsiakaras [Douv02, Tsia02], Yentakis [Vaye95, Yent98], Vernoux [Roch10, Kamb12, Tsam13], Smotkin [Sala06, Ploe97, Ploe00], Katsaounis [Kats10, Thel12, Nako10], Comninellis [Vark95], Metcalfe [Metc02, Emer98, Poul07], Bjerrum [Petr00], Janek [Popp99, Jane00, Muto10].

Although a lot research effort has been carried out to get a deeper understanding of electrochemical promotion there still exist a lot of open questions and critical responses mainly according to the spillover mechanism proposed by Vayenas et al. and the associated identification of a spillover oxygen species [Imbi10, Togh10]. In the present work, a critical overview over the different studies presented in the research field of electrochemical promotion is given. In addition to the pioneering work of Vayenas, studies which favored an alternative explanation will be discussed. The first section starts with a classical NEMCA experiment and the introduction of all important physical variables. The second part focuses on different mechanisms explaining the electrochemical promotion as well as a discussion of some critical facts concerning previous publications. The last section is devoted to possible industrial applications of elec-

trochemical promotion. First the problems hampering an industrial use till now will be identified followed by possible directions for future research projects leading to optimized solutions for industrial applications.

1.3 Theory of Electrochemical Promotion

In a typical NEMCA experiment an electrochemical cell composed of an oxygen ion conducting electrolyte, a metal catalyst and a counter and reference electrode is heated up in a gastight reactor in a reaction mixture which typically contains 0 % - 10 % of the reaction gas (e.g. hydrocarbons and oxygen) and helium as carrier gas. The reaction mixture is fed by mass flow controller and the reaction products are analyzed with an infrared (IR) analyzer.
The catalyst electrode commonly consists of a porous Pt paste which is painted onto the solid electrolyte (commonly YSZ) followed by an annealing step to reveal thermic stability and high porosity. Depending on the reactor design, the counter and reference electrode on the backside of the solid electrolyte are exposed to the reaction mixture (single chamber system) or supplied with fresh air as reference gas (two chamber system) (Fig. 1.1). By using a single chamber system, it is of prime importance that the counter and reference electrode consist of electrode materials which are inert with reference to the observed reaction. In most cases gold paste is used to inhibit a contribution to the reaction rate. In both cases the potential of the reference electrode is fixed and can be measured

against the potential of the catalyst (open circuit potential) which is given by the Nernst equation (assuming the following reaction balance on the three phase boundary (TPB) on both electrodes: $O_2 + 4e^- \rightleftharpoons 2O^{2-}$):

$$U_{(\mathrm{WR})} = \frac{RT}{zF} + \ln\left(\frac{p(\mathrm{O}_{2(\mathrm{W})})}{p(\mathrm{O}_{2(\mathrm{R})})}\right) \tag{1.1}$$

($U_{(\mathrm{WR})}$: potential between working and reference electrode, R: universal gas constant (8.314 $\frac{\mathrm{J}}{\mathrm{molK}}$), z: the number of electrons transferred in the cell reaction, F: Faraday constant (96 485.34 $\frac{C}{mol}$), $p(\mathrm{O}_{2(W)})$: oxygen partial pressure on the working electrode and $p(\mathrm{O}_{2(R)})$: oxygen partial pressure on the reference electrode; activities can be substituted by $\frac{p}{p^0}$ for sufficent partial pressures).

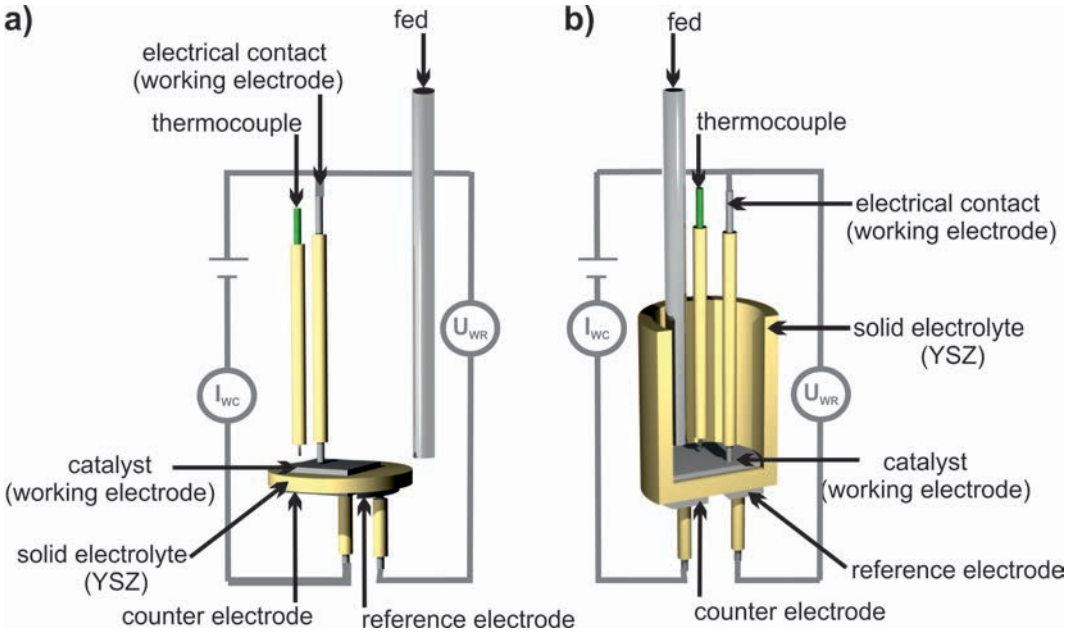

Figure 1.1: Scheme of the setup of a NEMCA experiment: a) single chamber system with working, reference and counter electrode in the reaction mixture; b) in a two chamber system only the working electrode is exposed to the reaction mixture.

The classical reaction in electrochemical promotion is the total oxidation of ethylene to carbon dioxide and water. By applying an anodic potential between working and counter electrode and the associated flux of oxygen ions from the counter electrode to the working electrode, the initial reaction rate increases more than expected by Faraday's law. After finishing the polarization step the reaction rate changes back to the initial value as demonstrated by a typical reaction process in a NEMCA experiment in Fig. 1.2.

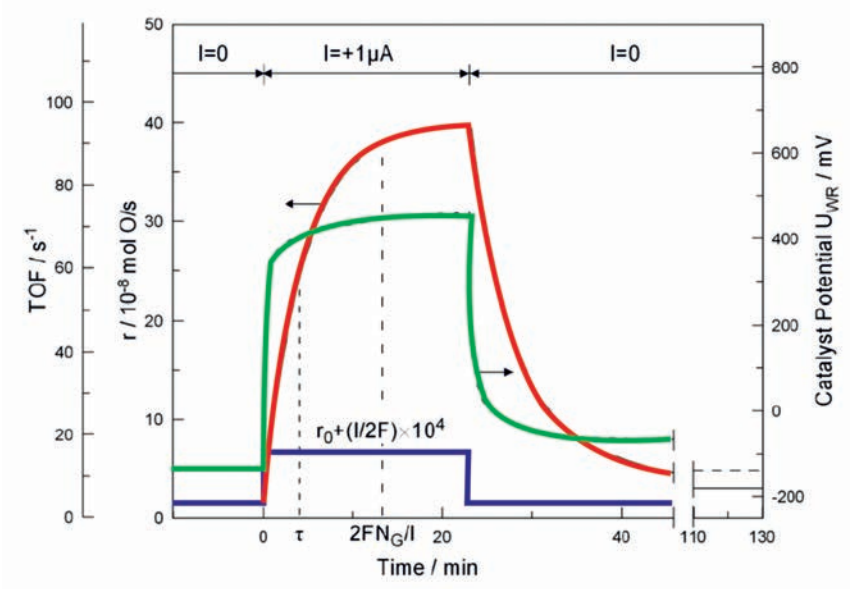

Figure 1.2: Example of a typical NEMCA reaction scheme for the total oxidation of ethylene to carbon dioxide and water on a Pt/YSZ electrode (T = 643 K, $p(O_2)$ = 46 mbar und $p(C_2H_4)$ = 3.6 mbar). The red line indicates the reaction rate, the green one the potential between working and reference electrode and the blue one shows the galvanostatic controlled current [modified from Bebe89].

For quantification of the increased reaction rate under electrochemical polarization and for comparison of different results, Vayenas et al. defined two important ratios:

The **lambda factor** (Λ) or **faradaic efficiency** is a measure of the efficiency of electrochemical promotion and results from the dif-

ference between the reaction rate with applied electrochemical potential (r) and without *(r_0)* divided by the number of moles of electrons transferred in the cell reaction and the number of coulombs per mole of electrons. In essence, the lambda factor describes the number of product molecules formed per pumped oxygen ion during electrochemical polarization. Typical values of Λ are between 1 and 10^5.

$$\Lambda = \frac{r - r_0}{\frac{I}{zF}} = \frac{\Delta r}{\frac{I}{zF}} \tag{1.2}$$

(Λ: lambda factor or faradaic efficiency, r: reaction rate during electrochemical polarization, r_0: reaction rate without polarization, I: current, z: the valency number of ions of the substance (electrons transferred per ion) and F: Faraday constant (96 485.34 $\frac{\mathrm{C}}{\mathrm{mol}}$))

The **enhancement factor** (ρ) describes the reaction rate increase during electrochemical promotion. Here should be noted that the definition of ρ contains neither an applied electrochemical potential nor the electrons transferred per ion, meaning that both the lambda and rho factor are necessary for a complete characterization of electrochemical promotion. Typical values of ρ are between 1 and 30.

$$\rho = \frac{r}{r_0} \tag{1.3}$$

(ρ: enhancement factor, r: reaction rate during electrochemical polarization and r_0: reaction rate without polarization)

The effect of electrochemical promotion is a change of reaction rate (r) by applying an electrochemical potential between working and counter electrode (U_{WC}). An empirical relation between both has been proposed by Vayenas and is given by equation 1.4.

$$\ln(\frac{r}{r_0}) = \frac{\alpha F \Delta U_{\mathrm{WR}}}{RT} \tag{1.4}$$

(r : reaction rate during electrochemical polarization, r_0: reaction rate without polarization, α : NEMCA coefficient, F: Faraday constant (96 485.34 $\frac{\mathrm{C}}{\mathrm{mol}}$), U_{WR}: potential between working and reference electrode, R: universal gas constant (8.314 $\frac{J}{\mathrm{molK}}$) and T : temperature)

α is an experimental variable and depends on the type of catalytic reaction. If α is positive, the reaction rate will increase by applying a positive potential to the working electrode relative to the reference electrode (anodic polarization, oxygen pumping to the WE) whereas the reaction rate will decrease by negative applied potentials (cathodic polarization, pumping oxygen away from WE) ($\alpha > 0 \Rightarrow$ electrophobic reaction), but this also means that the reaction rate will decrease with positive potentials and increase with negative potentials if the value of α is negative ($\alpha < 0 \Rightarrow$ electrophilic reaction). Furthermore, more complex reaction behaviors are already described in literature, for example, some working groups reported a maximum (vulcano behavior [Yent98]) or a minimum (inverted vulcano behavior [Alex97]) of the reaction rate during electrochemical polarization.

Equation (1.5) describes the relation between current densities and potential differences between working and reference electrode and is basically the high field approximation of the Butler-Volmer equation.

$$\ln\left(\frac{j}{j_0}\right) = \frac{\alpha_j F \Delta U_{(\mathrm{WR})}}{RT} \tag{1.5}$$

(j: electrode current density, j_0: exchange current density, α_j: charge transfer coefficient: ($|\alpha_j| \leq 1$, with $\alpha_j > 0 \Rightarrow$ anodic charge transfer coefficient and $\alpha_j < 0 \Rightarrow$ cathodic charge transfer coefficient), $U_{(\mathrm{WR})}$: potential between working and reference electrode, R: universal gas constant (8.314 $\frac{\mathrm{J}}{\mathrm{molK}}$) and T: temperature)

In the case of $\alpha \approx \alpha_j$ and $\Delta r >> r_0$ the following approximation is possible:

$$|\Lambda| = \left|\frac{\Delta r}{\frac{I}{zF}}\right| \approx \frac{r}{\frac{I}{zF}} \approx \frac{r_0}{\frac{I_0}{zF}} \tag{1.6}$$

(Λ: lambda factor or faradaic efficiency, r : reaction rate during electrochemical polarization, r_0: reaction rate without electrochemical polarization, I: electrode current, z: the valency number of ions of the substance (electrons transferred per ion) and F: Faraday constant (96485.34 $\frac{C}{mol}$))

The exchange current density can be calculated on the basis of equation (1.6) with the knowledge of the reaction rate under open circuit conditions and the faradaic efficiency. As a result, systems with low TPB length and in consequence, low oxygen exchange currents (strongly polarisable electrodes) show high lambda values

and vice versa [Vaye01]. In this context, it is important to mention that the exchange current density depends not only on the TPB length but also on the reaction gas composition [Wang79, Wang79.2, Wang81].

1.3.1 Spillover mechanism of Vayenas et al. [Vaye01, Flei05, Emer98, Jane00]

The widely accepted mechanism for electrochemical promotion was already presented in the early 1990s by Costas G. Vayenas. The main element of this mechanism is a spillover process of a special oxygen species (backspillover oxygen) from the ion conducting electrolyte onto the surface of the catalyst by applying an electrochemical potential. It is assumed that this affects the properties of the catalyst in relation to the rate and selectivity of the catalyzed reaction surface. The nature of the oxygen spillover species differs from gas phase oxygen in the sense that it has a partial negative valence state (examination has shown that the valence state is between -1 and -2 [Lada93, Neop98, Vaye01], more specifically the oxygen spillover is assumed to be a neutral species containing of a negatively charged oxygen ion and a positive counter-charge in the catalyst (double layer)).

$$O^{2-}_{(YSZ)} \rightarrow \left[O^{\delta-} - \delta+\right](Pt) + 2e^{-} \tag{1.7}$$

From the negative charge of the spillover oxygen species it is concluded that this species is stronger bound to the catalyst surface in comparison to normal chemisorbed oxygen, which causes a much lower uptake rate due to the lower sticking coefficient with the elec-

trode. The migration of spillover oxygen is assumed to be fast, mainly because of repulsive interactions between spillover species themselves. This and the fast bonding onto the catalyst forms a neutral charged double-layer ("effective double layer" to distinguish this gas/metal interface from the interface Pt/YSZ) consisting of the negative charged oxygen species and the positive charge in the catalyst material (Fig. 1.3). The double layer generates a strong dipole moment on the surface of the catalyst leading to a change of the bonding strength of the adsorbed species with the catalyst by repulsive (electronegative adsorbate) or attractive interactions (electropositive adsorbate) with the oxygen spillover species. These interactions are hypothesized to influence the activation barriers for the surface reaction and the surface coverage, which ultimately results in the observed change of the reaction rate and selectivity. One consequence of the effective double layer is a measurable change of the work function.

The catalyst work function during electrochemical polarization is considered as an important confirmation of the spillover theory of Vayenas et al.. The definition of the work function is closely related to the processes and corresponding energies of an electron brought from the Fermi level of the catalyst to vacuum. The electron has an electrical component (charge) and a chemical component (material). The electrical component results in the Galvani potential (φ) by subtracting the electron from the catalyst and bringing it to infinite distance in vacuum. The Galvani potential consists of the surface potential χ for the overcome of the electrochemical double layer at the metal/vacuum interface due to the adsorption of gas phase molecules on the surface of the catalyst resulting in a dipole

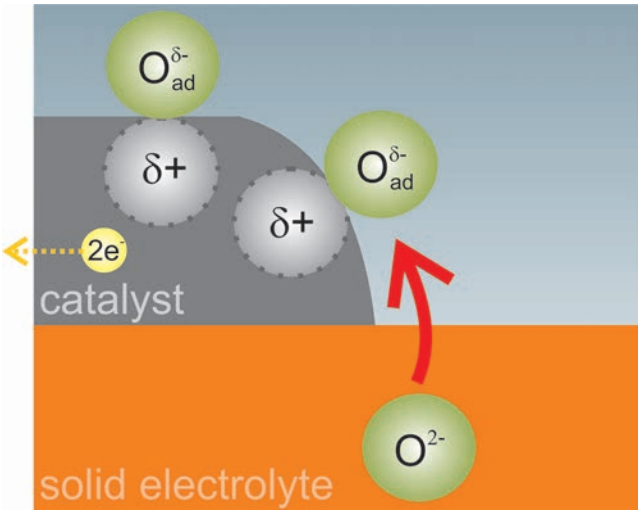

Figure 1.3: A special oxygen species (spillover oxygen) migrates from the solid electrolyte onto the catalyst surface by applying an electrochemical potential, forming an effective double layer which affects the properties of the catalyst in relation to its reaction rate and selectivity (Illustration of spillover model by C. G. Vayenas).

moment at the interface and the Volta potential ψ for the electrostatic attraction of the negatively charged electron and the (after leaving of the electron) positively charged catalyst (Fig. 1.4, left (electrical part)).

$$\varphi = \chi + \psi \tag{1.8}$$

(φ: Galvani potential, χ: surface potential, ψ: Volta potential)

The chemical component takes the mass transfer of the electron from one phase ($\mu_{e,\text{metal}}$, metal) to another phase ($\mu_{e,\text{vacuum}}$, vacuum) into account (Fig. 1.4, middle (chemical part)). By combining the electrical and chemical component one obtains the electrochemical potential $\widetilde{\mu_e}$. The electrochemical potential is defined

as the energy which is needed to bring an electron from infinite distance in the vacuum to the Fermi level (chemical potential + Galvani potential).

$$\tilde{\mu} = \mu - e_0\varphi \tag{1.9}$$

($\tilde{\mu}$: electrochemical potential, μ: chemical potential, e_0: charge of an electron, φ: Galvani potential)

The electrochemical potential is not measurable, but the work function Φ is measurable. The work function is defined as the energy which is needed to bring an electron from the Fermi level to the vacuum level (10^{-4} cm away from the sample, but approximately free of interactions between the electron and the sample). It also consists of the chemical potential μ_e and the surface potential energy χ for the crossing of the electrochemical double layer at the metal/vacuum interface (Fig. 1.4, right (electrochemical part)).

$$\Phi = \mu - e_0\chi \tag{1.10}$$

(Φ: work function, μ: chemical potential, e_0: charge of an electron, φ: Galvani potential)

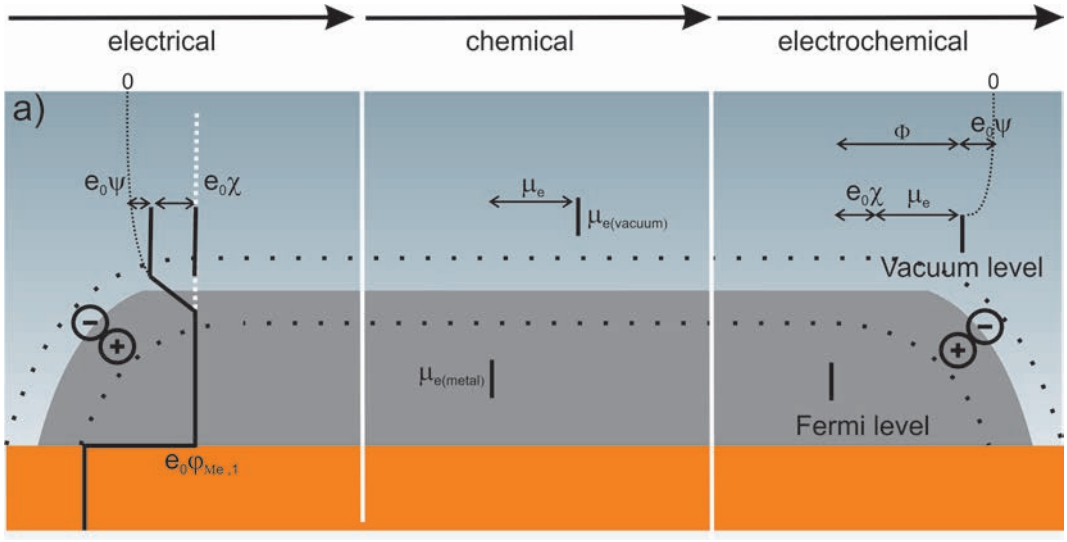

Figure 1.4: Potentials and energy levels of electrons on the metal/vacuum interface without an applied electrochemical potential.

Electrochemical polarization without spillover species

Due to anodic polarization between working and reference electrode (ΔU_{WR}) the Galvani potential (φ) shifts by the overpotential η (assumption: $\Delta U_{\mathrm{WR}} = \eta$, the applied potential represents exclusively the overpotential at the working electrode). Since there is no spillover at the metal/vacuum interface (at low temperatures where the ion conductivity of the electrolyte is low, for completely dense electrodes or at the very beginning of the polarization where the spillover ions have not been moved to the catalyst because of finite diffusion) the surface potential χ cannot change meaning that the contribution of the overpotential η is reflected in the Volta potential ψ. Ultimately the positively charged electrode causes the electron leaving the electrode to pass a stronger outer potential (Volta potential) in order to reach the vacuum at infinite distance (Fig. 1.5, left (electrical part)). The polarization is also reflected in the electrochemical potential resulting in a lower Fermi level. As

already shown the surface potential and the chemical potential of the electrons are not affected by polarization and the work function can therefore not change. Due to the lower Fermi level the vacuum level is shifted by the value of the overpotential η. Comparable to the electrical part the overpotential η is used for the Volta potential ψ (Fig. 1.5, right (electrochemical part)).

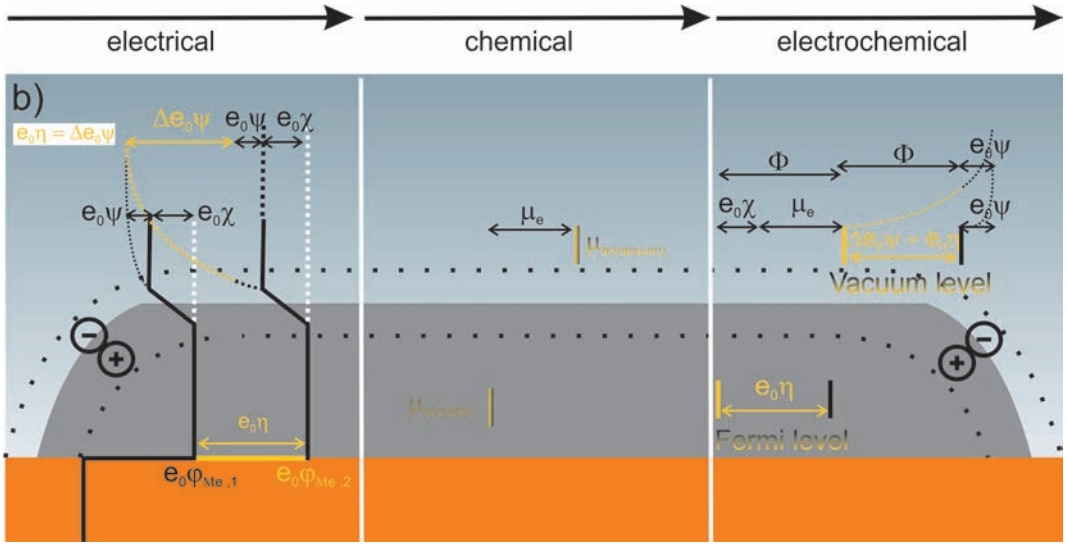

Figure 1.5: Potentials and energy levels of electrons on the metal/vacuum interface with an applied electrochemical potential but without spillover process.

Electrochemical polarization with spillover species

By anodic polarization spillover ions move towards the surface and the surface concentration of these species remains constant at the metal/vacuum interface at equilibrium. Accordingly to the above mentioned case the Galvani potential (φ) shifts by the factor of the overpotential η. Because of the presence of the spillover species the dipole moment at the metal/vacuum interface changes, therefore changing the surface potential χ. At the same time the contribution for the Volta potential has to be smaller in comparison to

the case without spillover (Fig. 1.6, left (electrical part)). The spillover species bind the positive charge of the electrode therefore shielding the escaping electron from the positive charge, explaining the smaller contribution of the Volta potential.

The Fermi level of the system is changed by the overpotential $e\eta$, but because of the higher contribution of the surface potential χ the work function also changes (Fig. 1.6, right (electrochemical part)).

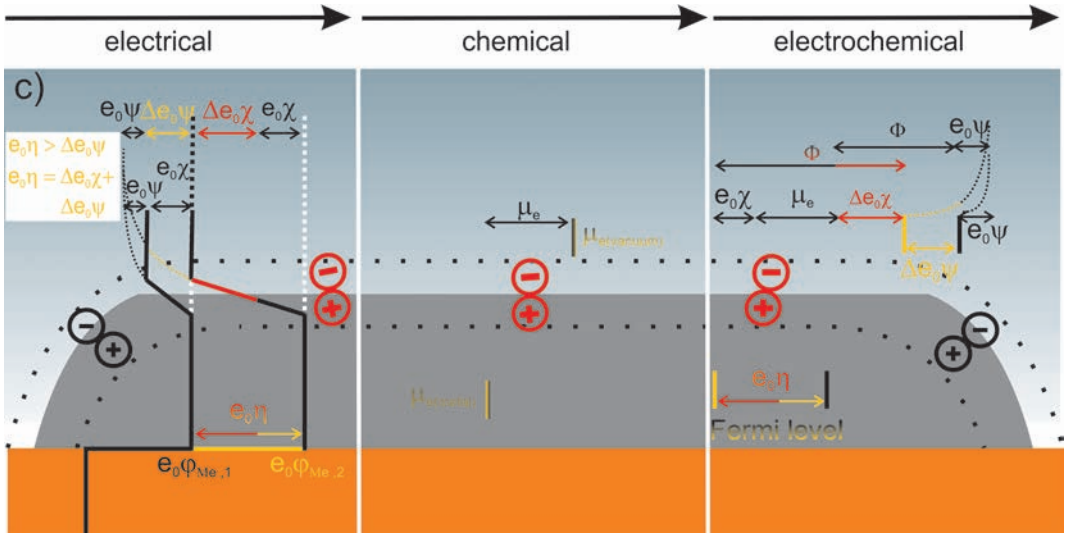

Figure 1.6: Potentials and energy levels of eletrons on the metal/vacuum interface with an applied electrochemical potential and spillover species.

Finally, the contribution of the applied overpotential η and therefore the Galvani potential φ and the Fermi level are distributed between the surface potential χ and the Volta potential ψ.

$$e_0\eta = e_0\Delta\chi + e_0\Delta\psi \text{ (pure electrical)} \tag{1.11}$$

$$e_0\eta = \Delta\Phi + e_0\Delta\psi \text{ (electrochemical)} \tag{1.12}$$

The distribution between both potentials is dependent on the nature (charge) of the spillover species and the surface concentration

of species which can accumulate on the catalyst during polarization which is mainly restricted by the surface sites of the catalyst. That means a very low number of available surface sites on the surface of the catalyst leads to a fast saturation with increasing overpotential (Fig. 1.7 a, red curve). In contrast a very high number of surface sites ensures a wide linear range of the surface coverage vs. overpotential behavior (Fig. 1.7 a, gray curve). Accordingly to this is the behavior of the work function which is linearly dependent on the spillover species coverage (adopting a parallel plate capacitor) in the case that there is a high number of available surface sites (Fig. 1.7 b, gray curve) or moving into a saturation in the case for a low number of available surface sites (Fig. 1.7 b, red curve). From the slope the charge of the spillover species can be obtained with z being the charge of the ions moving through the electrolyte and x being the charge of the spillover species (Fig. 1.7 c). In the case of YSZ the charge of the oxygen ions in the YSZ lattice is -2. Vayenas et al. have reported a 1:1 relation between the change of the work function and the overpotential measured by Kelvin probe which leads to a charge of the spillover species close to -2. Considering this, the 1:1 relation shows that the complete contribution of the overpotential is used for the increase of the surface potential χ and there is no contribution for the increase of the Volta potential. This means that the spillover species establish a very strong dipole moment at the surface of the catalyst resulting in a strong work function increase and at the same time an electrically overall neutral catalyst is obtained.

Further considerations of Fleig et al. [Flei05.2] and Metcalfe et al. [Metc01] included also the electrochemical contribution of a

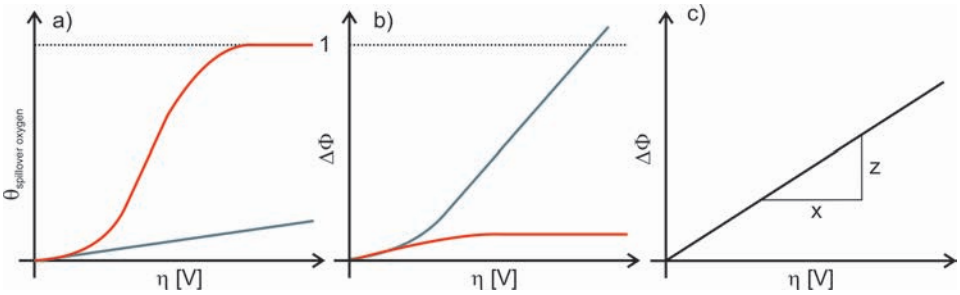

Figure 1.7: Coverage and work function as function of the overpotential: red = low amount of available surface sites, grey high amount of available surface sites. a) coverage, b) work function and c) determination of the spillover charge [according to Muto05].

spillover species at equilibrium conditions by assuming that the oxygen ions from the electrolyte (O^{2-}), the spillover ions $O^{\delta-}$ on the surface, the chemisorbed oxygen ions on the surface and the gas phase oxygen (O_2) are in local equilibrium. The resulting equation (1.13) for the overpotential during anodic polarization reveals that the contribution of the overpotential multiplied by the charge of an electron can be either used for the establishment of the dipole moment of the spillover species ($e_0\Delta\chi$, pure electrical contribution) or by increasing the chemical potential of the spillover species ($\Delta\mu_{O^{2-}}$, chemical contribution).

$$e_0\eta = e_0\Delta\chi + \Delta\mu_{O^{2-}} \tag{1.13}$$

(e_0: charge of an electron, η: overpotential, χ: surface potential, $\mu_{O^{2-}}$: chemical potential of spillover species)

The distribution between both terms ($e_0\Delta\chi$) and ($\Delta\mu_{O^{2-}}$) is strongly dependent on the surface coverage. $e_0\Delta\chi$ is linearly dependent on the surface coverage of spillover ions which can be seen from equation (1.14) resulting from the Helmholtz equation:

$$e_0\Delta\chi = \frac{Ne_0\mu(\theta_{O^{2-}} - \theta^0_{O^{2-}})}{\epsilon_0} \tag{1.14}$$

(e_0: charge of an electron, χ: surface potential, N: density of surface sites, μ: dipole moment of the oxygen ion, $\theta_{O^{2-}}$: surface coverage of spillover oxygen, $\theta^0_{O^{2-}}$: surface coverage of spillover oxygen in the initial catalyst state, ϵ_0: vacuum permittivity)

$\Delta\mu_{O^{2-}}$ is logarithmically dependent on the surface coverage of spillover ions according to the Langmuir isotherm:

$$\Delta\mu_{O^{2-}} = kT\ln\frac{\theta_{O^{2-}} \cdot \theta^0_*}{\theta_* \cdot \theta^0_{O^{2-}}} \tag{1.15}$$

($\mu_{O^{2-}}$: chemical potential of spillover species, k: Boltzmann constant, $\theta_{O^{2-}}$: surface coverage of spillover oxygen, θ^0_*: coverage of vacant site at initial catalyst state, θ_*: coverage state of vacant site, $\theta^0_{O^{2-}}$: surface coverage of spillover oxygen in the initial catalyst state)

According to the above mentioned cases (Fig. 1.6) the case $e_0\eta \approx e_0\Delta\chi$ results for intermediate coverages and enough accessible active sites for the spillover species. At low and high coverages (and/or low number of available surface sites) $\Delta\mu_{O^{2-}}$ becomes appreciable. At very low and very high coverages the contribution of $\Delta\mu_{O^{2-}}$ dominates over the contribution of $e_0\Delta\chi$ therefore $e_0\eta \approx \Delta\mu_{O^{2-}}$. To complete the considerations one also has to consider the lateral interactions between the spillover ions which are not negligible at higher coverages. Therefore, at equilibrium conditions the overpotential equals the sum of three terms:

$$e_0\eta = e_0\Delta\chi + \Delta\mu_{O^{2-}} + e_0\Delta V_{lat,O^{2-}} \quad (1.16)$$

(e_0: charge of an electron, η: overpotential, χ: surface potential, $\Delta\mu_{O^{2-}}$: chemical potential of spillover species, $\Delta V_{lat,O^{2-}}$: lateral interactions between spillover species on the surface)

In summary, the observation of the 1:1 relation is strongly dependent on the state of the catalyst and on the range of applied overpotential. To ensure the validation of the 1:1 relation the catalyst has to be in local equilibrium, it has to show enough active sites and the catalyst has to be at intermediate coverages to rule out contributions of $\Delta\mu_{O^{2-}}$ and $e_0\Delta V_{lat,O^{2-}}$.

Points of criticism of the Spillover mechanism of Vayenas et al. [Vaye01]

Many investigations have been conducted which support the existence of the spillover species, although the nature of this species has not been identified unequivocally.

1. In the case of oxygen the charge of the spillover species is not clear. The spillover species is denoted [$O^{\delta-}$- $Me^{\delta+}$] where δ has to be close to 2, because of work function measurements.
2. A discrimination between chemisorbed oxygen and spillover oxygen is problematic (see XPS and PEEM results).
3. A clear spectroscopic proof of the postulated species under typical reaction conditions is missing.
4. The 1:1 correlation between the overpotential and the work function change is only valid under very defined conditions (cf. chapter 1.3.1 and 1.4.1).

5. It is thermodynamically difficult to rationalize (deviation from local equilibrium) that oxygen arizinating from the electrolyte can behave differently to adsorbed oxygen from the gas phase, meaning the different oxygen species on the surface would "remember" where they originated from [Vaye90].

1.3.2 Chain reaction mechanism by Sobyanin et al. [Soby92 and Soby93]

Sobyanin et al. discussed the effect of electrochemical promotion on the basis of a chain reaction mechanism involving electrochemically generated oxygen species. The main focus of their work was to identify the different strength of the chemisorptive bond of oxygen species on the surface of the catalyst by applying an electrochemical potential [Soby92, Soby93]. Therefore they made an isotopic exchange experiment where they offered molecular ^{18}O and molecular ^{18}O on a catalyst with and without polarization of the catalyst. They observed the product formation of the isotopic exchange reaction taking place on the surface by MS. The isotopic exchange reaction is correlated to the binding strengh of the species on the surface. According to the spillover model by Vayenas et al. they expected a decrease of the bond strength of chemisorbed oxygen during anodic polarization and correspondingly an increase during cathodic polarization. However the strength of the chemisorbed oxygen remains unchanged during electrochemical polarization and thus the effect of electrochemical promotion can hardly be explained by a change of the strength of chemisorptive bonded oxygen.
Based on these findings, Sobyanin et al. proposed a new mechanism

to explain the non-faradaic behavior during electrochemical polarization. They suggested the formation of oxygen surface species with a very short lifetime under electrochemical polarization which react with the reaction gas in a chain mechanism [Soby93, Bely00]. They could show that this mechanism reproduces the experimental behavior and the kinetic properties for carbon monoxide oxidation on metal electrodes satisfactorily.
The first step is an ordinary catalytic reaction following the Eley-Rideal mechanism (equation 1.17 and 1.18).

$$2Z_O + O_2 \rightleftharpoons 2Z_OO \tag{1.17}$$

$$Z_OO + CO \rightarrow CO_2 + Z_O \tag{1.18}$$

(Z_O: catalytically active site on the gas-exposed surface, Z_OO: atomic oxygen species on a catalytically active site on the gas-exposed surface)

The initial step (under anodic polarization) is a current producing step and consists of spillover of oxygen ions from the electrolyte to a catalytically active site at the TPB (equation 1.19).

$$Z + O^{2-} \rightarrow ZO^- + e^- \tag{1.19}$$

(Z: electrochemically active site on the TPB, ZO^-: a charged monoatomic oxygen species on the electrochemically active site, O^{2-}: oxygen anion in the bulk of YSZ)

The chain propagation steps include conversion of ZO_2^- to ZO^- and back to ZO_2^- (Fig. 1.8). In the first step the charged monoatomic

oxygen species reacts with an atomic oxygen species on the catalytic active surface (equation 1.20). Afterwards the charged molecular oxygen species reacts with CO back to the charged monoatomic oxygen species and starts the reaction again (equation 1.21).

$$ZO^- + Z_OO \rightarrow ZO_2^- + Z_O \tag{1.20}$$

$$ZO_2^- + CO \rightarrow ZO^- + CO_2 \tag{1.21}$$

(ZO_2^-: charged molecular oxygen species on the electrochemically active site)

One possible chain termination step is a recombination of two charged monoatomic oxygen species forming an oxygen molecule (equation 1.22).

$$2ZO^- \rightarrow 2Z + O_2 + 2e^- \tag{1.22}$$

Points of criticism of the chain reaction mechanism by Sobyanin et al. [Soby92, Soby93]

1. The chain mechanism has been investigated only for a few different systems where only the CO combustion was investigated.
2. The introduced short-lived oxygen species in the chain mechanism are not spectroscopically proven.
3. The complete mechanism is only verified by phenomenological (kinetic) data.

All in all this description of a mechanism matches more the physical intuition than the utilization of a special spillover species. Whether

this mechanism contribute to the phenomenon of EPOC or not has to be shown by further measurements.

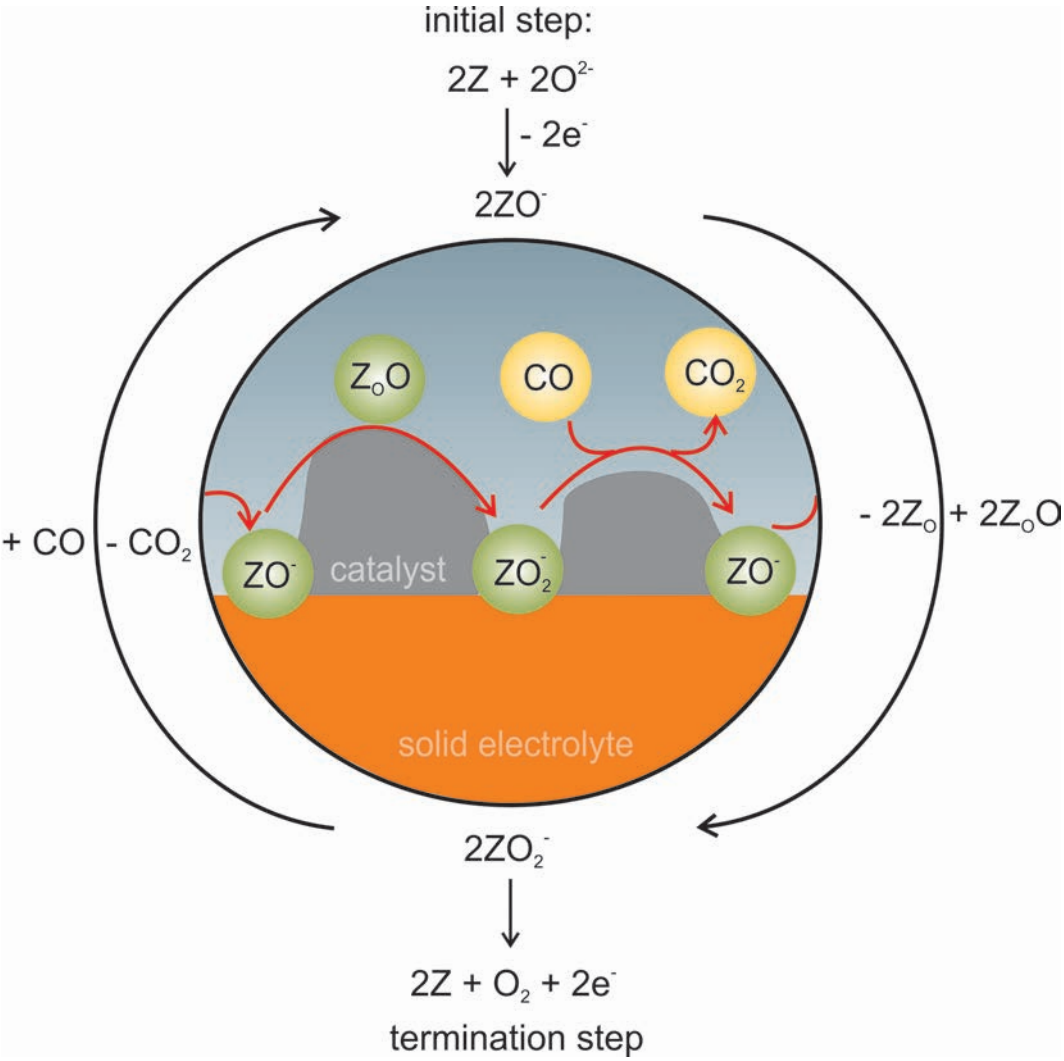

Figure 1.8: Chain mechanism for explanation of the non-faradaic behavior of metal electrodes during electrochemical polarization (Z is an electrochemically active site on the TPB, ZO^-/ZO_2^- is a charged monoatomic or molecular oxygen species on the electrochemically active site, Z_O is a catalytically active site on the gas-exposed surface and Z_OO is an atomic oxygen species on a catalytically active site on the gas-exposed surface).

1.3.3 Ignition mechanism by Imbihl et al. [Togh10, Togh10.2]

An alternative mechanism to explain the effect of electrochemical promotion was proposed in 2010 by Imbihl et al. [Togh10, Togh10.2]. They investigated the oxidation of ethylene on a Pt catalyst under UHV conditions (10^{-6} mbar to 10^{-5} mbar) with a differentially pumped quadrupole mass spectrometer for analysis of the reaction products and with photoelectron emission microscopy (PEEM) to image the work function under different applied electrochemical potentials with spatial resolution. As electrode system they chose a porous Pt electrode prepared by sputtering and annealing afterwards to achieve a high porosity on YSZ as solid electrolyte.

The experiments were performed at 350 °C, an oxygen partial pressure of $5{\cdot}10^{-5}$ mbar and a cyclically varying ethylene content between $1{\cdot}10^{-5}$ mbar and $4.5{\cdot}10^{-4}$ mbar. By increasing the ethylene partial pressure the reaction rate decreases and with decreasing ethylene content afterwards the reaction rate was still very low. The authors explained this hysteresis with the formation of a carbon surface layer (CH_x layer) on the surface of the catalyst which impedes the adsorption of oxygen. During anodic polarization the poisoning layer is removed by reaction of pumped oxygen ions with the carbon layer at the TPB resulting in the formation of active adsorption sites for oxygen from the gas phase finally leading to a drastic increase of reaction rate (Fig. 1.9). The ignition, e.g. the transition from a poisoned catalyst surface to an active catalyst can explain the non-faradaic behavior under electrochemical po-

larization. This mechanism is confirmed by PEEM measurements showing the movement of pumped oxygen ions from the TPB to the surface of the catalyst and accordingly the removal of the carbon layer. In addition to the spillover process from anodically pumped oxygen species, indicated by a darkening of the catalyst surface in the PEEM experiment, they observed small bright dots after a short period of polarization which were associated with the adsorption of oxygen on the carbon free oxygen sites [Neub04, Luer00, Luer06].

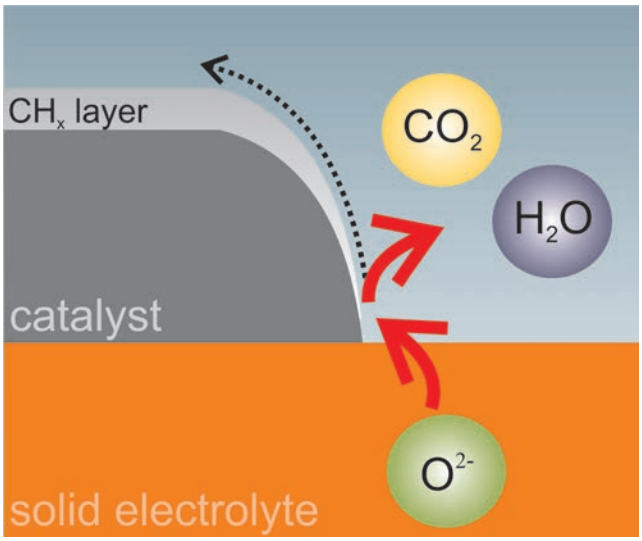

Figure 1.9: Ignition model by Imbihl et al.. The catalyst surface is poisoned by a carbon layer, which is removed under anodic polarization by reaction with the pumped oxygen ions at the TPB, finally leading to new active adsorption sites and therefore an increase in reaction rate.

Points of criticism on the ignition mechanism by Imbihl et al. [Togh10, Togh10$_2$]

1. The mechanism is working under atypical NEMCA conditions: The measurements were conducted under fuel rich conditions, meaning that the ratio of ethylene to oxygen was between 3 and 10. Furthermore, the total pressure was in a range of 10^{-2} mbar

compared to 10 mbar up to 1 bar which is typical for NEMCA conditions. Especially the utilization of fuel rich conditions is critical, because it will lead to a poisoning of the surface, which is not happening under typical NEMCA conditions.

2. The typical NEMCA curve progression (transient) is not obtained, instead a long activation even after stopping the polarization takes place. This behavior is attributed to a reconstruction of the surface.

3. The conducted kinetic investigations are mass transfer limited, because of an activation energy smaller than 1 $\frac{\text{kcal}}{\text{mol}}$, due to an open circuit rate, which is hardly changing between 568 K to 763 K.

4. The mechanism grounds on the formation of a carbon layer (CH_x) from the reactants. This mechanism is only valid for a reaction in which carbon species are involved, but not for other reactions. At the same time reactions that exhibit an electrophilic behavior, which means a rate increase by negative polarization, cannot be explained by this mechanism.

Overall the proposed mechanism of Imbihl et al. explains the obtained results properly, but by the choice of NEMCA atypical conditions the authors probably investigated a special case of electrochemical promotion which is not suitable to explain the general observed behavior. Accordingly, the model by Imbihl et al. was severely criticized by Vayenas [Vaye11].

1.4 Surface analysis techniques toward deeper understanding of EPOC

All proposed mechanisms for explanation of electrochemical promotion are based on changes of the surface of the catalyst by either migration of oxygen species (mechanism of Vayenas et al. and Sobyanin et al.) or removal of surface species (mechanism of Imbihl et al.). Therefore, an important criterion for an evaluation of the proposed mechanisms is the identification of the different discussed surface species with surface analysis techniques. The next part gives a short summary and a critical evaluation of the most important surface analytical techniques used in the field of electrochemical promotion.

1.4.1 Kelvin probe technique (KP)

The Kelvin probe is a technique used to measure changes in the work function of metals, semiconductors and liquids by using a vibrating reference electrode in plane-parallel orientation to the sample, thereby creating a capacitor. Probe and sample electrode are electrically connected and the potential between both ("contact potential") is set to zero by a compensating voltage source. This potential equals the difference in the work function of both electrodes. By knowledge of the work function of the probe electrode the work function of the sample can be calculated. In the case of EPOC, Kelvin probe measurements were performed to investigate changes of the work function during electrochemical promotion caused by migration of spillover oxygen species onto the surface of the catalyst. Changes of the work function due to electrochemical

promotion are one of the key elements in the proposed mechanism from Vayenas et al..

Although many work function measurements with application of an electrochemical potential have been reported, especially the correlation of work function and applied potential is controversially discussed. Vayenas et al. found experimentally that there is a wide linear range where the change of the work function equals the change of the applied potential at the working electrode which he calls the "1:1 relation":

$$e\Delta U_{\mathrm{WR}} = \Delta\Phi_{\mathrm{W}} \tag{1.23}$$

(e: charge of an electron, U_{WR}: electric potential difference between working and reference electrode, Φ_{W}: work function of working electrode)

The 1:1 relation has been experimentally as well as theoretically questioned.

The results of Kelvin probe measurements are quite sensitive and it is often difficult to obtain reliable data. In order to obtain reliable results different criteria have to be fulfilled in order to guarantee reproducible measurements [Neub04]:

1. The Kelvin probe has to be brought in an optimal position to the sample in order to measure the real work function.
2. The complete working electrode has to be in electrical contact, because otherwise electrostatic effects will falsify the measurement (parts of the electrode are not grounded).

3. Impurities have to be excluded, because they can migrate to the surface during polarization and therefore change the work function.

Measurements show that the fulfillment of the above mentioned criteria is difficult and the results depend strongly on the sample preparation. Confirmation of the 1:1 relation has been found over a range of 1 eV [Vaye90, Vern11] or even over a range of 4 eV [Popp99]. Therefore the sample preparation as well as the history of the sample has a huge influence on the results.

1.4.2 Photoelectron emission microscopy (PEEM)

In PEEM typically a D_2 discharge lamp or other light source is utilized in order to extract photoelectrons from the surface which are captured by a system of lenses and displayed by a phosphorus screen to see work function differences. Because of a relatively good spatial resolution ($\approx 1\ \mu$m) it has been used to image the spreading of the spillover oxygen from the electrolyte onto the surface of the catalyst by different photoelectron intensities. The time dependent darkening of the catalyst surface upon polarization showed clearly a change to a higher work function which was interpretated as the movement from oxygen onto the catalyst [Luer06]. In order to obtain the diffusion coefficient of the spillover species the oxygen coverage has to be calculated from the PE intensities. In principle the PEEM intensities are convertible into local work functions which are linearly connected to surface coverage (cf. Helmholz equation). At very high oxygen coverage the linear dependence is not valid,

leading to coverage values subject to errors. The resulting diffusion coefficient of $D_0 = (9.2 \pm 1.8) \cdot 10^{-4}$ $cm^2 s^{-1}$ at 670 K is 4-5 orders of magnitude higher than obtained from other methods analyzing the microscopic diffusion of oxygen on Pt (111) [Lewi68, Wint96, Bart00]. The high diffusion coefficient can only be explained by taking strong repulsive interactions between the oxygen spillover species into account, which may occur at high coverages as suggested by Vayenas et al..

1.4.3 X-ray photoelectron spectroscopy (XPS)

X-ray photoelectron spectroscopy allows to identify the chemical state of surface species according to their electron binding energy. The sample surface is irradiated by an X-ray source and the energy distribution of emitted photoelectrons is analyzed. XPS investigations of Pt/YSZ electrodes under vacuum conditions show a formation of a peak at 530.4 eV after introducing O_2 which is attributed to chemisorbed gas phase oxygen. By additional electrochemical polarization the maximum at 530.4 eV increases while at the same time a second maximum occurs which is shifted to lower binding energies of 528.8 eV to 530.0 eV depending on the sample and the experimental conditions. The appearance of a second peak has been interpreted differently in the literature. Vayenas et al. and others attributed the second peak to the population of another adsorption state which they interpreted as the spillover species [Vaye01].
However, other interpretations for the appearance are also possible. Imbihl et al. argue that some of the investigated Pt layers are very thin so that the underlying YSZ contributes and creates a sec-

ond peak. Secondly, some of the electrodes exhibit a bad electrical conductivity resulting from a Pt layer where not all particles are in electrical contact with each other, and therefore the electrode is not grounded properly, leading to artifacts. Furthermore, a very fast decay of the signals is obtained after stopping the polarization which is better explained by kinetic cleaning processes from the gas phase. Additionally, experiments without gas phase oxygen show that upon application of an anodic potential the pumped oxygen shows a maximum at 530.4 eV which equals the energy of chemisorbed oxygen. A relatively small shifted second maximum is also explainable by adatom interactions in denser adlayers resulting in bonding configuration changes, formation of chemical combounds and subsurface phases [Luer00].
Nevertheless the development of a second maximum has been reported in all investigations. Even that the largest part of the pumped oxygen during polarization is used to create the signal at 530.4 eV and only a small part is used for the development of a second peak is consistent with the theory of NEMCA, because at low coverages spillover oxygen transforms to chemisorbed oxygen.

1.4.4 Scanning photoelectron microscopy (SPEM)

Scanning photoelectron microscopy (SPEM) uses photons with an energy of a few hundred eV to eject core level photoelectrons. By the utilization of a synchrotron source and by scanning the sample surface a spatially resolved elemental distribution of the sample surface is obtained. Measurements show that the spillover species is identical to chemisorbed oxygen (304.2 eV), but that there develops

another population state after prolonged polarization which can be due to adatom interactions in denser adlayers resulting in changes in the bonding configuration, formation of chemical compounds or subsurface phases. Phase formation or the population of another adsorption state is most likely at high coverages [Luer00].

1.4.5 Thermal desorption spectroscopy (TDS)

Thermal desorption spectroscopy is a method to observe and identify molecules or atoms adsorbed on a surface by increasing the temperature of the surface and therefore slowly desorbing the molecules. The measurements are conducted in high vacuum and the molecules are identified by a mass spectrometer. In principle, different adsorption states of a species can be identified due to different binding energies. By introducing gaseous oxygen to a Pt catalyst a desorption peak is visible at 720 K to 740 K which is attributed to chemisorbed oxygen. In the absence of gaseous oxygen an anodic polarization of the catalyst leads also to a maximum at 720 K to 740 K, but an additional smaller peak at around 780 K appears after prolonged polarization. The additional peak is attributed to the stronger bonded spillover species, whereas the weaker bound state is attributed to chemisorbed oxygen obtained also under oxygen gas atmosphere. The occurrence of two adsorption states during polarization with a time or coverage dependent population is explained by the transformation of the chemisorbed species into spillover species at a point where the surface is almost saturated with chemisorbed oxygen and spillover oxygen can be present at the surface [Neop95, Neop98, Tsip99]. Further experiments with isotopically labeled oxygen (^{18}O)

under atmospheric pressure (Kats04, Kats04.2) support the results of the development of two distinct peaks, although isotopically labeled oxygen show a mixing of gas phase oxygen and the oxygen from the electrolyte.
Critics argue that the peak position itself is dependent on the crystal orientation of the metal planes as well as on coverage. The values can vary by up to 160 K, clearly showing that the nature of the oxygen cannot be attributed to a specific desorption temperature [Vatt08]. Additionally, contaminants can also be oxidized leading to higher O_2 TD peaks.

1.4.6 Scanning tunneling microscopy (STM)

Scanning tunneling microscopy is a technique utilizing a very thin conductive tip to scan the surface to be examined. By approaching the tip to the surface a bias between the sample and the surface is applied, resulting in tunneling of electrons from the surface. The tunneling current is dependent on the position of the tip, the applied bias and the electronic structure of the atom seated underneath the tip. Due to the very good lateral (0.1 nm) and depth (0.01 nm) resolution the imaging of single atoms is possible in optimal cases. Investigations [Arch06, Vaye06] at room temperature and atmospheric pressure with a Pt (111) single crystal on YSZ show the well known Pt (111)-(2 x 2)-O-adlattice, which is attributed to chemi- sorbed oxygen together with an overlapping Pt (111)-(12 x 12)-O-adlattice upon annealing of the sample. By a negative polarization of -1 V the Pt (111)-(12 x 12)-O-adlattice vanishes and reappears by a positive polarization of $+1$ V. Therefore the authors

attributed the Pt (111)-(12 x 12)-O-adlattice as being the spillover species. Despite the clear appearance and disappearance of an adlayer upon polarization the chemical nature of this adlayer has not been examined and is therefore unclear. Also comparable investigations [Arch06, Makr96] with a sodium conducting electrolyte (β-Alumina) show a similar Pt (111)-(12 x 12) adlattice upon polarization, which are attributed to sodium spillover ions. Therefore a contamination with sodium ions in the case of Pt/YSZ cannot be ruled out.

Supporter of the STM measurements also refer to theoretical work [Leiv08] which tries to explain the formation of the effective double layer and the accompanied adlattice structures by adding sodium or oxygen atoms to a Pt (111) layer. Although the results encourage the formation of the overlapping Pt(111)-(12 x 12)-Na-adlattice the formation of the Pt(111)-(12 x 12)-O-adlattice has not been investigated.

1.4.7 Isotope exchange measurements

Investigations with adsorbed isotopically labeled oxygen (^{18}O) on Pt/YSZ show that a mixing between ^{18}O from the gas phase and ^{16}O from the YSZ takes place during polarization by mediation of the spillover species [Kats04]. Additionally, measurements from Sobyanin et al. [Soby93] over Pt/YSZ show no increase in the binding strength of oxygen with the surface as proposed from Vayenas et al. ruling out a special oxygen species. Despite the measurements critics argue [Vern11] that under the chosen conditions of Sobyanin et al. (high vacuum and temperatures above 700 K) no NEMCA

effect has ever been reported.

1.4.8 Cyclic voltammetry (CV)

Cyclic voltammetry is a method to analyze the processes occurring at an electrode induced by a sweeping potential and is usually not considered as a surface analytical tool. Hereby, the appearance of peaks becomes visible reflecting oxidation and reduction processes at the electrode. Early studies [Kiuk57, Etse70, Gara11] conducted on Pt electrodes in contact with YSZ show besides the occurence of an oxidation peak for the formation of PtO_x in the anodic regime and the accompanied decomposition of this species in the cathodic regime the growth of a second peak in the cathodic regime after prolonged anodic pumping attributed to the spillover species. Another study [Muto09] investigating typical paste electrodes as well as porous and dense (111) Pt electrodes, shows the appearance of the second cathodic peak only for the paste electrodes. These paste electrodes are known to contain glass additives. Investigations by ToF-SIMS reveal a significant content of Si in these electrodes leading to the conclusion that the oxidation and reduction reaction of Si in these electrodes are causing the second cathodic peak.

1.4.9 Surface area calculation, turn over frequency calculation and the comparability of measurements

In order to evaluate and compare the characteristics and the performance of a catalyst the turn over frequency (TOF) is utilized. The turn over frequency is defined as the number of product molecules formed per second by each active site of the catalyst. It is depen-

dent on the type of catalyst (material, crystal orientation, defects), the temperature, the gas composition (reaction ratio, reactants, total pressure) and in the case of NEMCA also the potential between the active working and the counter electrode.

$$\mathrm{TOF} = \frac{r}{A} \tag{1.24}$$

(TOF is given in s^{-1}, r: rate in mol s^{-1}, A: number of active sites in mol)

The difficulty in determining the TOF is in most cases not the determination of the rate, but the counting of the active sites. By determining both factors accurately a comparison with other laboratories, the influence of different materials, crystallographic orientation and the influence of different preparation techniques is possible (e.g. impurities). In heterogeneous catalysis the determination of the active surface area is very difficult, especially by the utilization of solid thin films which are used in NEMCA investigations. The common way to measure the surface area of porous solid samples with sufficiently high surface area is the utilization of the Brunauer-Emmett-Teller (BET) method by which the surface area is determined from the amount of adsorbed gas on the surface. Especially for thin films with large area which are used in NEMCA experiments this method is not applicable. In order to overcome this problem Vayenas et al. introduced three different techniques to determine the surface area of Pt film electrodes on YSZ: the isothermal titration, current interruption and the galvanostatic transient technique.

All of these three techniques are supposed to determine the active

surface area which means the area accessible by gas adsorption. The active surface can therefore differ from the real surface area. All of these three measurements should be performed in the reactor where the NEMCA measurements are conducted and at the temperature where the NEMCA measurements are performed, because the adsorption of gas molecules is temperature dependent. The isothermal titration technique is the most straightforward method. By prolonged exposure of the catalyst by reactive gas (e.g. CO at low T) the surface is strongly covered with the reactive gas by almost one monolayer. Following introduction of oxygen leads to a reaction with the previously adsorbed molecules. The product molecule concentration can then be analyzed. The obtained amount of product molecules is therefore linearly dependent on the surface area and the surface area can be easily calculated. The surface area obtained by the other two methods originates from transient measurements taken the controversial spillover species into account.
These three methods are used throughout the NEMCA literature to determine the surface area and to calculate the TOF.
To exclude the influence of impurities, of different surface phases or deactivated surfaces (which activate during polarization) and therefore to be sure that higher TOFs are obtained because of polarization it is necessary to compare the TOFs obtained from the experiment with the literature.
Furthermore, due to the huge number of parameters, i.e. reaction conditions (gas mixture, pressure, temperature) and materials (metals, orientations, impurities, dopants) a comparison of even similar measurements is difficult.
In table 1.1 different measurements of ethylene oxidation under

similar conditions are summarized. As can be seen the TOFs differ more than one magnitude which is less based on the differences in the rate measurements, but due to the difficult and erroneaous estimation of the surface area.

Determination of the surface area and the TOF was also performed in the present study, but discarded due to strongly differing results (more than one order of magnitude).

Overall, the measurements from literature (see table 1.1) as well as the performed measurements in this study suggest that the methods introduced by Vayenas et al. are not suitable for the determination of the surface area and therefore for the determination of the TOF. Unfortunately, a comparison between the values obtained from the literature remains difficult and other methods have to be considered in order to estimate the TOF more accurately.

	catalyst	active area [mol]	method	r_0 TOF [s^{-1}]	r TOF [s^{-1}]	λ
this study	Pt	$4.00 \cdot 10^{-7}$	surface titration	1.00	1.20	1-1000
Stou81	Ag	$1.40 \cdot 10^{-7}$	surface titration	1.00	1.50	7
Bebe89	Pt	$4.20 \cdot 10^{-9}$	surface titration	3.47	50.00	74000
Yent92	Pt	$2.72 \cdot 10^{-8}$	surface titration	3.51	19.85	144
Plia96	Pt	$1.90 \cdot 10^{-7}$	surface titration	0.21	2.36	1974
Marw98	Pt	$3.80 \cdot 10^{-8}$	surface titration	7.00	5.50	-1032
Kout06	Pt	$1.60 \cdot 10^{-8}$	surface titration	1.00	31.00	116
Tsam09	Pt	$2.90 \cdot 10^{-8}$	current interruption	1.11	9.34	1060

Table 1.1: Comparison of surface areas and TOFs for ethylene oxidation from literature.

1.5 Electrochemical promotion with impact to technology

NEMCA research has made contributions to a better understanding of catalytic processes in heterogeneous catalysis. By the help of electrochemical promotion it is possible to influence the reactivity and selectivity of catalysts in situ by application of an electrochemical potential. Despite of its enormous potential a transfer from laboratory scale to industrial applications has not been succeeded yet. The reproducibility of the effect is poor and often depending on the state of the catalyst and the experimental conditions. Besides classic investigations of the effect on metal electrodes deposited on solid electrolytes an extension on aqueous solutions as electrolyte [Anas93, Neop94] and molten salt electrolyte systems [Petr00] has been studied. The reactions where electrochemical promotion may play a role are manifold and contain oxidation and reduction reaction from organic as well as from inorganic species. Especially reactions which have an environmentally relevant influence are of particular interest for industry [Kats10]. This includes oxidation of hydrocarbons (CH_4) [Roch08], (C_2H_4) [Thur03], (C_3H_6) [Karo08], (C_3H_8) [Bill07], hydrogen [Labo07], alcohols [Tsia02] and CO [Luca08]. Furthermore, an enormeous potential of electrochemical promotion is seen by the supporter of the NEMCA theory by the acceleration and control of slow reaction processes which are of importance for industry. A prominent example is the ammonia synthesis. Yiokari et al. [Yiok00] managed to improve the ammonia synthesis significantly on a commercial catalyst by electrochemical promotion. At the present time, the catalytic synthesis

of ammonia in the Haber-Bosch process is a very important process. In this study the conventionally used catalyst (Fe promoted with K_2O, CaO and Al_2O_3, supplied by BASF) was placed on a proton conducting solid electrolyte. By this setup a non-faradaic behavior with ρ values of 12 and more could be obtained. The rate increase has been attributed to the supply of H^+ ions to the catalyst surface which lower the work function of the surface and therefore cause an enhancement of the chemisorption of the electron acceptor N and a weaker binding of the electron donors H and NH_3 takes place. Further interesting applications of electrochemical promotion in environmental technology are for the purpose to avoid environmental pollutants and allow the production of clean energy sources. A prominent example is the reduction of NO_x in the automobile exhaust treatment which has been the focus of numerous studies [Dora07, Lint08]. A first effort to transfer NEMCA to an industrial scale has been executed by a cooperation of BASF, Ecole Polytechnique Federale de Lausanne (EPFL) and the University of Patras by the development of the first monolithic electropromoted reactors (MEPRs) [Balo04, Tsip05, Balo06, Soue08]. Unfortunately, this first effort was not successful and the MEPRs did not show high lambda values.

In the field of fuel cell research the concept of NEMCA has also been applied. Salazar et al. [Sala06] reported the electrochemically promoted olefin isomerization reaction in a polymer electrolyte membrane fuel cell. Additional investigations showed the importance of electrochemical promotion for the use in fuel cells [Ploe97, Ploe00, Sapo07, Sapo07.2, Balo04, Balo06].

Besides the manifold of potential applications of electrochemical

promotion, practical aspects have to be considered for an industrial use. A major aspect is the production of applicable catalysts. Up till now thick catalysts with thicknesses in the μm range have been used in research, which have been mainly deposited by pastes. The big disadvantage of these electrodes is the low utilization of material (metal dispersion below 0.01 %) [Tsip09]. For an application on the industrial scale, the utilization of material has to be improved which can be achieved by the use of thin catalyst films or dispersed catalysts. A major step has already been taken by Marwood et al. [Marw98]. They dispersed the catalytic active Pt on electronically conductive gold, which has been brought onto a solid electrolyte. By this setup they obtained ρ values of 3 and Λ values in the magnitude of 10^3. Another example has been shown by Neophytides et al. [Neop94, Neop96] who used dispersed Pt on graphite electrodes in an aqueous alkali solution to catalyze the hydrogen oxidation.

Despite of some promising examples the practical usage of electrochemical promotion is still far away from industrial use. This is due to the fact, that the focus has been mainly drawn to the understanding of the effect und less on commercialization. In the recent years a transformation from the laboratory purpose to industrial applications and the therefore demanded research of production processes and plant construction has been started. Relevant examples are shown in the following reviews of Anastasijevic and Tsiplakides [Anas09, Tsip09]. Despite the optimism, not all aspects of the electrochemical promotion are fully understood and some aspects are still controversial. In industry, mostly highly dispersed catalysts are used which cannot be easily promoted. To promote

them, they have to be brought on an ion conductive substrate in order to allow a change of the work function which alters the reaction conditions. Furthermore the polarization of small particles deposited on a substrate material is difficult to achieve. Due to the fact that the particles are not in electrical contact with each other a polarization by a simple attachment of a wire is impossible. In this case a polarization has to be done wirelessly by an electric field caused by additional electrodes which are not participating in the catalytic reaction. A realization of such a complex system appears to be very difficult on an industrial scale. Besides the need for a uniform and homogeneous current distribution the flow distribution of gases has to be optimized due to the blocking and deflecting of the gas flow by the ion conductive substrates. The future will show if the challenges to overcome the technical aspects can be solved and which area of application can be developed in this way.

Chapter 2

Experimental Part

2.1 The preparation of metal thin film electrodes

This chapter focuses on the preparation and characterization of different metal thin film electrodes on yttria-stabilized zirconia as solid electrolyte. These types of electrode systems are of general interest not only from a scientific point of view (e.g. electro-catalytic processes, heterogeneous catalysis, kinetic investigations) but also in relation to practical applications (e.g. solid oxide fuel cells, oxygen sensors, ceramic capacitors or superconductors). One of the best studied model electrode system in solid state electrochemistry is the system Pt(O_2)/YSZ. Fischer, Mutoro and Pöpke have successfully established the preparation of dense and de-wetted Pt films on YSZ single crystals by pulsed laser deposition (PLD) for the investigation of structural, morphological and kinetic properties on the characteristics of model type thin film platinum electrodes [Beck07, Muto08, Beck11]. But due to the fact that platinum is expensive, a lot of research effort is related to replace platinum in a lot of applications with cheaper metals. Often silver is discussed as a substituent as it is considerably cheaper. However, silver causes

different problems like a lower activity in reduction reactions and a lower melting point and in consequence problems with de-wetting and evaporation processes at high working temperatures. In the present study the influence of different metal films with different microstructures on the electrocatalytic oxidation of carbon monoxide and ethylene has been investigated. The different metal thin film electrodes were chosen corresponding to the current research issues. The first part of this chapter focuses on the preparation and characterization of well defined single crystalline platinum model electrodes on YSZ (111) with different morphologies and three phase boundary lengths for the investigation of kinetic parameters (e.g. platinum oxide formation) and their influence of the electrocatalytic oxidation reaction of carbon monoxide and ethylene. The second part deals with the preparation of platinum, palladium and silver model electrodes on polycrystalline YSZ in order to obtain insights in the different oxygen storage mechanisms (e.g. platinum oxide formation at the Pt/YSZ interface and oxygen storage in the bulk of Ag electrodes) with solid electrochemical mass spectrometry (SEMS) under high vacuum conditions.

2.2 Metal thin film model electrodes on YSZ (111)

2.2.1 Dense metal thin films on YSZ (111)

Dense and gas-tight Pt electrodes on YSZ (111) single crystals prepared by PLD are one limiting case of model electrodes. They provide a small, well-defined three phase boundary length together with a large interface contact area. The TPB is the region be-

tween the electronically conducting electrode, the ion conducting electrolyte and the gas phase. During electrochemical polarization of metals with low permeability for oxygen, the oxygen in- or excorporation is restricted to this region, therefore, its characteristics are important for any electrochemical investigation. Dense Pt electrodes with a small TPB length provide very low exchange currents (i) meaning that these electrodes show a high polarisability, which, in turn, influences the efficiency for the electrocatalytic oxidation of carbon monoxide or ethylene according to Vayenas [Vaye01]. One should note that the interface region between Pt and YSZ is also the location where platinum oxide formation may primerily occur, therefore dense Pt model electrodes with large interface regions are the ideal electrode type for the investigation of the oxygen storage mechanism [Pöpk11.2]. A detailed description of the preparation conditions and the characterization of dense thin film Pt electrodes is given in the literature [Beck07, Muto08 and Beck11]. The PLD and annealing parameters for the dense Pt electrodes used in this work are summarized in table 2.1.

Pulse energy	300 mJ
Repetition rate	10 Hz
Background gas	Argon
Background pressure	10^{-2} mbar
Substrate temperature	400 °C
Substrate-target-distance	4.5 cm
Film thickness	500 nm - 1 μm

Table 2.1: PLD parameter for dense Pt metal films on YSZ single crystals.

The Pt films were prepared on YSZ (111), (100), (110), (311) orientated single crystals and on (0001) orientated sapphire substrates. For all substrates nearly single crystalline metal films were observed after annealing in air at 750 °C for 48 hours with a heating and cooling rate of 2 °C/min. A detailed study of the influence of the different substrate orientations and preparation conditions on the film growth is given in G. Beck, C. Bachmann,*Oxygen removal at grain boundaries in platinum films on YSZ*, Solid State Ionics, 262, (2014), 508-511.

The morphology of the metal films was investigated by scanning electron microscopy (SEM) (Fig. 2.1 a and b). The orientated growth of the Pt films on YSZ was proven by X-ray diffraction (XRD) as demonstrated in Fig. 2.1 c. Electron backscatter diffraction (EBSD) and X-ray pole figure measurements were used for texture investigations and the determination of the fraction of twins and other grain boundaries as well as the grain size [Beck14].

In addition to Pt electrodes, dense Ag and Pd electrodes were also prepared. The preparation conditions were the same as in the case of Pt, only the substrate temperature during the deposition process was reduced to 200 °C and there was no need for an annealing step afterwards. A detailed description of the preparation and characterization of Ag and Pd dense thin film electrodes is given in G. Beck, C. Bachmann, *Microstructural changes due to anodic polarisation of palladium and silver films on YSZ*, Solid State Ionics, 263, (2014), 80-86.

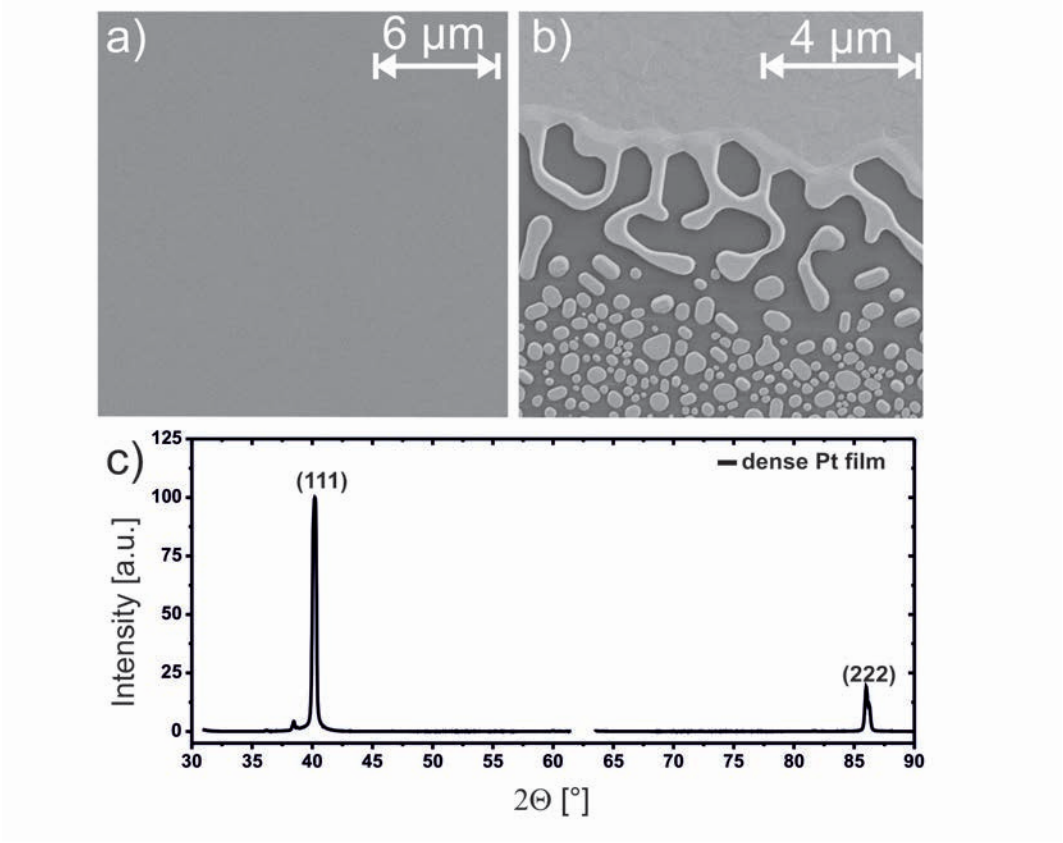

Figure 2.1: SEM image of the surface (a), the TPB region (b) and XRD pattern (c) of a typical dense Pt film on YSZ (111). The Pt film is very flat after heat treatment and no grain structures are visible (a). The TPB seems macroscopically linear but the higher magification (b) shows a jagged structure. However, the TPB length can be moderately precise estimated. The XRD pattern (c) shows only the (111) and (222) platinum reflexes meaning that the Pt film is (111) orientated.

2.2.2 De-wetted metal thin films on YSZ (111)

De-wetted Pt electrodes were used because dense gas-tight electrodes are temperature-stable, but the problem is an altering of the morphology during electrochemical polarization. Under anodic polarization oxygen ions are continuously pumped to the Pt/YSZ interface leading to blister formation, cracks or delaminations [Pöpk11]. These changes affect the electrochemical response due to changes of the TPB length and interface area. Therefore, an electrode sys-

tem with an increased TPB length and the same well-characterized properties like the dense Pt films (e.g. crystallinity, orientation etc.) was target of the next preparation step. De-wetted electrodes have the advantage that they provide a high TPB length and interface region and as a consequence they show a better stability during electrochemical polarization. The well-defined structure of de-wetted electrodes allows a good estimation of the relation of TPB length to interface region. But unfortunately the small film thickness, which is necessary for the preparation process limits the application possibilities to a temperature range of up to 400 °C. Higher temperatures cause an advance of the de-wetting process finally leading to isolated nanoparticles.
The PLD parameters for the preparation of de-wetted electrodes are given in table 2.2. A very thin Pt film with a thickness of 50 nm - 150 nm is deposited on a YSZ (111) single crystal. The de-wetting of the Pt film was caused by a high substrate temperature (900 °C) and accordingly a high mobility of Pt atoms during the deposition process.

Pulse energy	300 mJ
Repetition rate	2 Hz
Background gas	Argon
Background pressure	10^{-2} mbar
Substrate temperature	900 °C
Substrate-target-distance	4.5 cm
Film thickness	50 nm - 100 nm

Table 2.2: PLD parameter for de-wetted Pt metal films on YSZ single crystals.

The SEM images (Fig. 2.2 a and b) show a homogenous Pt network. The images were used to determine the TPB length, which was normally between 300 m - 600 m. The de-wetted Pt films on YSZ (111) were characterized by XRD and show an epitaxial growth with a single crystalline orientation of (111) (Fig. 2.2 c). A detailed study of the morphology and structure of the de-wetted electrodes as well as an investigation of the de-wetting process for platinum, palladium and silver films is given in G. Beck, C. Bachmann, R. Bretzler, R. Kmeth, *Thermal stability of platinum, palladium and silver films on yttrium-stabilised zirconia*, Thin Solid Films, 573, (2014), 164-175.

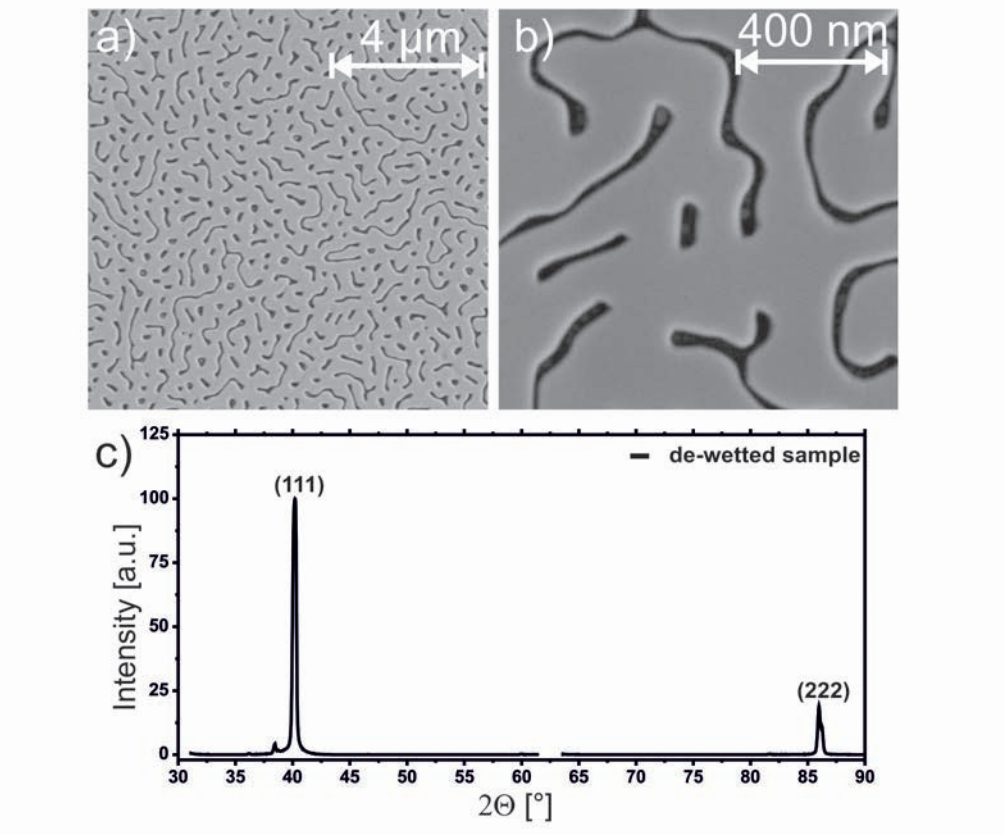

Figure 2.2: SEM images (a and b) of a typical structure of a de-wetted Pt electrode on YSZ (111). The electrode is characterized by a very uniform porosity and large TPB length. The XRD pattern (c) shows a (111) orientation.

2.2.3 Lithography of metal thin films on YSZ (111)

The rate for the oxygen exchange reaction on $Pt(O_2)$/YSZ electrodes depends on the TPB length [Opit10]. In consequence, the oxygen excorporation at the TPB is expected to be the rate determining step for the electrocatalytic oxidation of carbon monoxide and ethylene. Most of the studies in the literature were performed on porous Pt paste electrodes. These electrodes are the best way to reflect a real industrial system, but contaminations and lack of information on the system-determining factors like TPB length, interface region and surface area make the interpretation of experimental results and the reproducibility often impossible. To achieve a better understanding of the influence of the TPB length on the electrocatalytic oxidation of carbon monoxide and ethylene, dense single crystalline Pt electrodes with different TPB length were prepared by a lithograph process. The experimental realization of the sample preparation was carried out in a joint project with M.Sc. J. NEUMEIER during his bachelor and master thesis [Neum10, Neum13].

The lithographic process used for the preparation is schematically depicted in Fig. 2.3. Firstly, a dense Pt film is deposited on a YSZ or sapphire single crystal (b) followed by spin coating of the photoresist (c). After a softbake step (100 °C for 120 s) the photomask is aligned and the photoresist becomes exposured (d) and developed (e). The resist pattern is transferred into the underlying layer by an ion beam etching process (f and g). The final operation in the lithographic process is the resist strip (h).

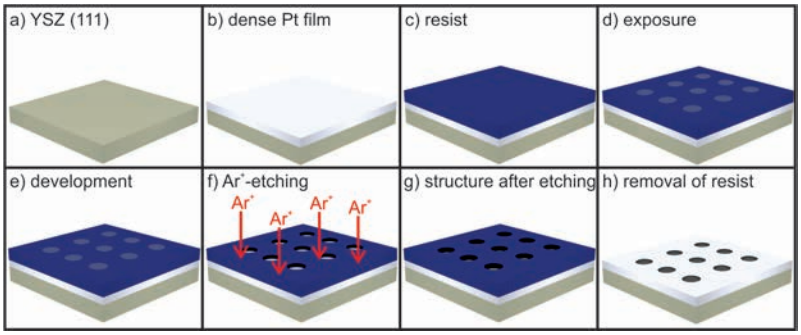

Figure 2.3: General scheme of the steps in the lithographic process for preparation of dense Pt films with defined TPB lengths.

The morphology and the tightness of the films were investigated with SEM (Fig. 2.4a). The annular edge profile (Fig. 2.4b) is caused by the harsh etching process and leads to a reduction of the specified TPB length. However, the contact area between Pt and YSZ is well defined and the real TPB length can be determined by SEM. The (111) orientation of the grown Pt film was demonstrated by XRD (Fig. 2.4c).

2.3 Metal thin film model electrodes on polycrystalline YSZ

For the kinetic measurements under high vacuum (HV) conditions the preparation of metal thin films was carried out on polycrystalline YSZ substrates. Single crystalline YSZ substrates tend to a fast reduction under reduced oxygen partial pressures and were thus not appropriate for the use in HV experiments. In contrast, polycrystalline YSZ shows slower reduction rates because of grain boundaries as kinetic barriers for oxygen ion conductivity [Jane99]. The PLD parameters for the preparation of Pt and Ag electrodes on polycrystalline YSZ are given in table 2.3.

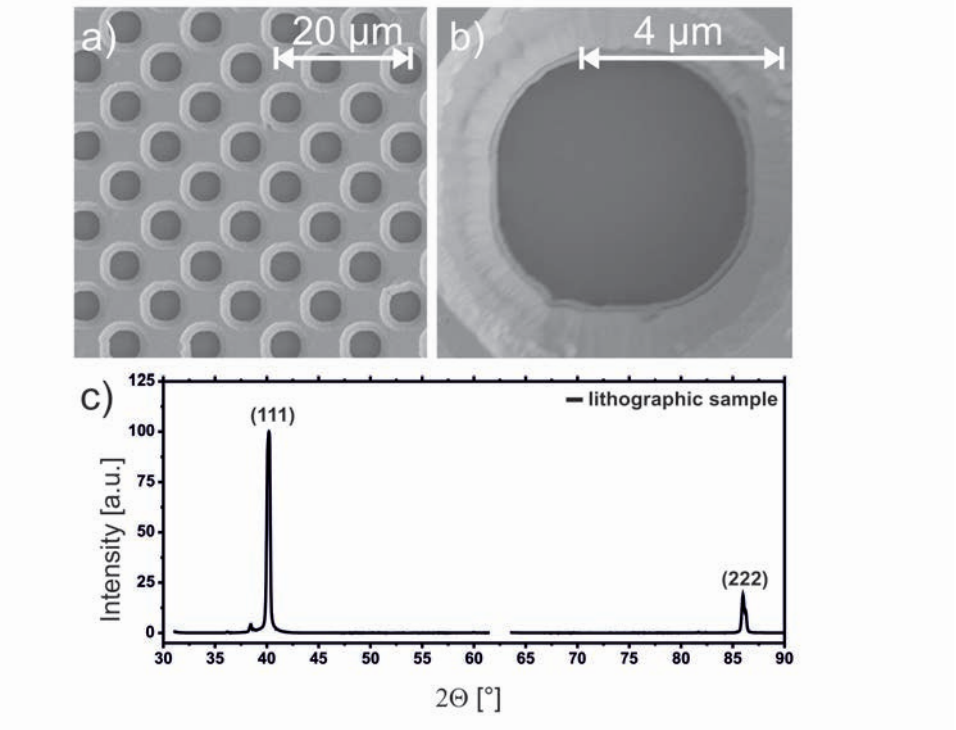

Figure 2.4: The SEM images of a typical Pt electrode prepared by a lithographic process show that the electrode is tight and provides a well-defined TPB length (a and b). The XRD pattern (c) shows a highly textured film with (111) orientation.

Pulse energy	300 mJ
Repetition rate	5 Hz (Ag), 10 Hz (Pt)
Background gas	Argon
Background pressure	10^{-2} mbar
Substrate temperature	200 °C (Ag), 700 °C (Pt)
Substrate-target-distance	4.5 cm

Table 2.3: PLD parameter for Pt and Ag metal films on polycrystalline YSZ.

In contrast to the single crystals the polycrystalline YSZ substrates are not as well polished which causes a higher porosity of the deposited metal film. The prepared metal films are not gastight as can be seen by the small holes in the SEM image (Fig. 2.5 a and b) and the TPB length is neither defined nor verifiable. Detailed information for the film growth of metal films on polycrystalline

YSZ substrates are given in G. Beck, C. Bachmann, *Microstructural changes due to anodic polarisation of palladium and silver films on YSZ*, Solid State Ionics, 263, (2014), 80-86 and G. Beck, C. Bachmann, *Oxygen removal at grain boundaries in platinum films on YSZ*, Solid State Ionics, 262, (2014), 508-511.

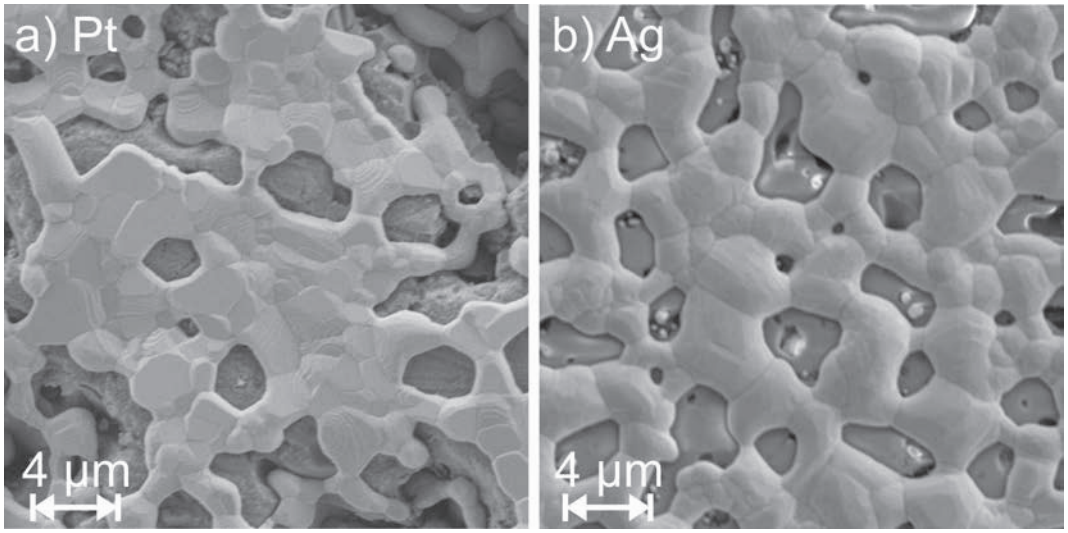

Figure 2.5: The SEM images of a typical Pt electrode (a) and a typical Ag electrode (b) on polycrystalline YSZ.

Chapter 3

Results and Discussion - Part 1: Experiments under High Vacuum Conditions

The phenomenon of electrochemical promotion has been mainly investigated and observed near ambient pressure and has been subject to controversy ever since. Especially in the measurements conducted under ambient pressure in this study (see chapter 4) the current mechanistic concepts of the NEMCA effect are questioned. In order to get more insight into the microscopic processes taking place during polarisation investigations under high vacuum conditions have been performed. These high vacuum measurements can be split into two different types of measurements: on the one hand surface analytical techniques were applied to model electrodes to help to explain the controversial results and to identify the nature of the postulated spillover species. On the other hand a complete set of EPOC measurements has been performed to investigate the reactive processes taking place at the catalyst/electrolyte interface during polarisation. Previous investigations were mainly performed

without reactive gases and therefore not able to monitor and quantify the EPOC effect under controlled conditions. Especially the use of isotopically labeled oxygen and HV conditions to discriminate faradaic from non-faradaic processes, which is very expensive and difficult under ambient pressure conditions, is reported for the first time.

3.1 Investigation of the oxygen exchange kinetics and electrochemical promotion of CO oxidation over Pt/YSZ electrodes under high vacuum conditions

3.1.1 Introduction

NEMCA investigations of model type reactions have been conducted mainly under ambient pressure conditions with partial pressures of reaction gases in the range of 10 mbar to 100 mbar, being balanced by mostly helium to atm. pressure. The obtained results are often questionable and especially the proposed mechanism by Vayenas [Vaye02] has been discussed controversially [Togh10, Togh10.2]. In order to shed more light on the complex processes taking place during electrochemical polarization of a catalyst, the use of model type electrodes and high vacuum conditions is essential. Imbihl et al. have been one of the first research groups to utilize a high vacuum chamber setup equipped with PEEM and a mass spectrometer in order to conduct NEMCA investigations [Popp99]. They developed a new model explaining the NEMCA effect, but unfortunately it was later revealed that their data were incorrect

[Togh10, Togh10.2]. Recently, Harbich et al. developed a high vacuum system capable of performing very precise and accurate EPOC measurements by performing electrochemical measurements under high vacuum conditions while monitoring the reaction products on-line. The setup consists of a micro reactor equipped with a gas analyzer quadrupole mass spectrometer (QMS) to investigate solid state cells. This new method is called solid electrochemical mass spectrometry (SEMS) [Falg10, Falg10.2] by the authors.
In order to get more insight into processes taking place during NEMCA measurements the SEMS system has been given as a loan from the work group of Dr. Wolfgang Harbich, EPFL Lausanne, Switzerland. The system has been brought to Gießen, and platinum as well as silver model electrodes have been investigated.
In this part of the thesis, the electrochemical measurements were carried out over Pt/YSZ electrodes to investigate the oxygen exchange reaction using solid electrochemical mass spectrometry technique (SEMS) under high vacuum conditions. In addition, the electrochemical promotion on the platinum catalyst was studied using isotopically labeled $^{18}O_2$ and $C^{16}O$ reactants at elevated temperatures. Based on the experimental results, a dynamic model of the oxygen exchange process at Pt/YSZ electrodes is proposed and its effect on the electrochemical promotion performance is discussed.

3.1.2 Experimental Part

Solid Electrochemical Mass Spectrometry Setup

The setup consists mainly of two parts, a micro reactor, which includes the electrochemical cell and the analyzing system consisting

of a sniffer device to collect the ions emitted from the catalyst and the mass spectrometer to detect and analyze the ions collected from the sniffer. A detailed scheme of the configuration is shown in Fig. 3.1.

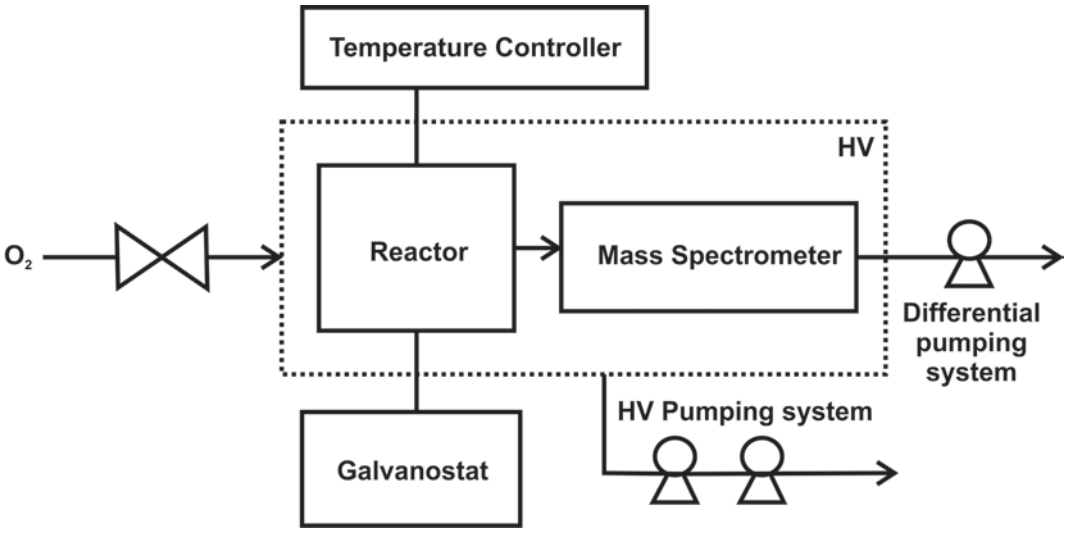

Figure 3.1: Configuration of the Solid Electrochemical Mass Spectrometry System.

The micro reactor is composed of two copper blocks (Fig. 3.2). The sample is fixed in the middle of the reactor by ceramic paste (Ceramabond 668, T-E-Klebetechnik) dividing two compartments for the reaction gases on the working side (working electrode) and the reference site (counter electrode and reference electrode). Each compartment exhibits 6 holes to ensure free circulation of gases in the whole reactor. Two of these holes were isolated with ceramic capillary tubes and used for electrical connection of the cell and the thermocouple positioned close to the catalyst. Another two of the holes are equipped with stainless steel pipes to supply the reaction gases. Additionally, a hole in the working compartment perpendicular to the cell is used for passing the emitting ions to the sniffer

device. The micro reactor is heated by a ceramic heater (Tectra Boraelectric standard 2D heater). The utilized micro reactor has been designed in Gießen in order to fit the dimensions of the electrochemical cell produced and commonly used in Gießen. All other parts of the setup as well as principal calculations necessary for the interpretation of the measurements are shown in detail elsewhere [Falg10].

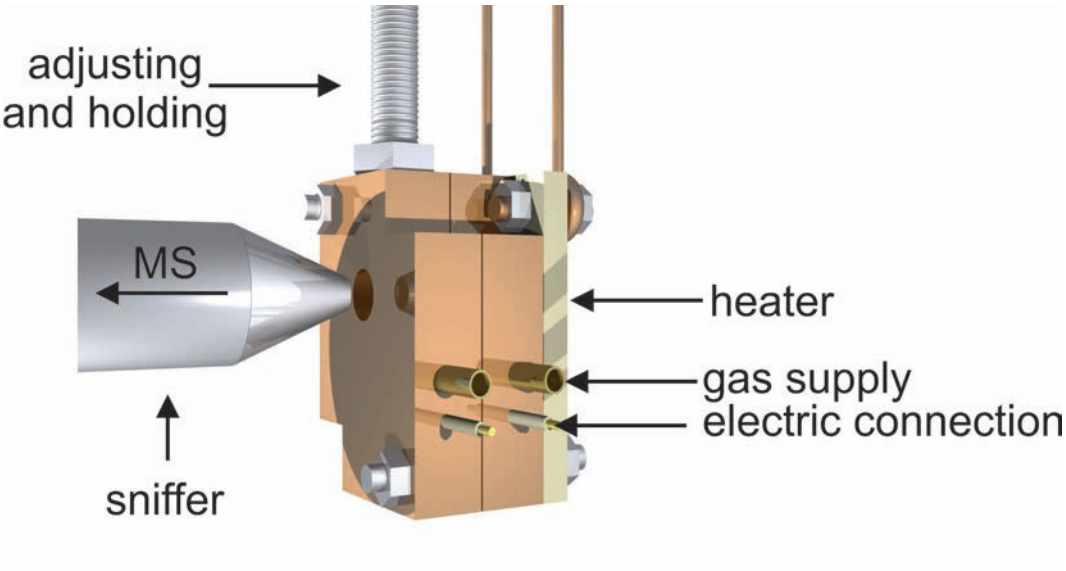

Figure 3.2: Schematic sketch of the used micro reactor.

Sample preparation

For investigations under HV conditions polycrystalline YSZ substrates have been proven to be highly advantageous compared to single crystalline substrates. Preliminary measurements with single crystalline substrates have shown a fast degradation of the cell performance due to strong reduction phenomena of the YSZ [Jane99]. Therefore, the use of polycrystalline substrates was favored and used throughout the measurements.

Rectangular platinum electrodes with a geometrical size of 6 mm x 3 mm were deposited on polycrystalline zirconia (stabilized by 8.5 mol% Y_2O_3) pellets (Frialit, Friatec Cooperation) by pulsed laser deposition (PLD). A detailed description of the PLD process is given in chapter 2.3. The as-prepared samples were sintered at 750 °C for 3 h in argon to stabilize the morphology. The thickness of the electrodes after calcination, as determined by profilometry using an Alpha-Step instrument (Alpha-Step IQ, KLA Tencor), was between 400 nm and 500 nm. The surface morphology and composition were investigated by high resolution scanning electron microscopy (SEM, Merlin, Zeiss) (Fig. 3.3).

For electrochemical measurements, a gold counter electrode (Du Pont 5771 Conductor paste) was coated on the opposite side of the YSZ pellet in a symmetrical face to face arrangement ensuring a homogeneous potential distribution. Additionally, a gold reference electrode was coated next to the counter electrode. The electrochemical measurements were carried out using solid electrochemical mass spectrometry (SEMS) under high vacuum conditions with a background pressure of 10^{-12} bar. More details on the setup are given in [Falg10]. The galvanostastic and potentiostatic steps were applied to the cell using a potentiostat (Gamry Instruments Reference 600) while the gaseous products were monitored by an online quadrupole mass spectrometer (QMS, Pfeffer, Prisma200). When needed, the reactive gases (Carbon monoxide ($C^{16}O$ (5.0)) and isotopically labeled oxygen (^{18}O (3.0)) were fed into the micro reactor via leak valves and capillary stainless steel gas lines for the electrochemical promotion (EP) investigation. The operating temperature was kept between 300 °C and 550 °C.

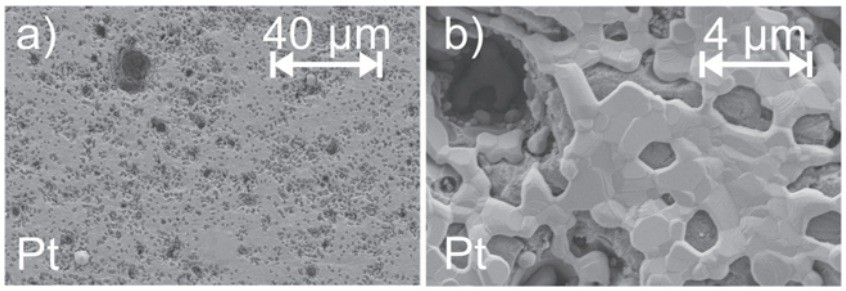

Figure 3.3: SEM images of polycrystalline Pt electrodes.

3.1.3 Results

Investigations of the Pt/YSZ interface

In order to identify the processes taking place at the Pt/YSZ interface during electrochemical polarization different electrochemical investigation methods have been applied.

- In the absence of reactive gas chronopotentiometric measurements have been conducted at 400 °C.
- In the absence of reactive gas galvanostatic measurements have been conducted at 400 °C.

Chronopotentiometric measurements were performed while the rate of oxygen evolution ($r_{32_{O_2}}$) was monitored in situ by QMS. The variable parameters during the investigations were the anodic limit, the cathodic limit and the scan rate. Due to the difficult interpretation of the results of the cathodic limit and scan rate measurements the focus is drawn on the measurements with a change of the anodic limit.

To identify the processes taking place during a cyclovoltammetric (CV) measurement a superposition of the CV data and the MS data is suitable [Falg10]. The corresponding measurement for a CV with limits of -200 mV to 850 mV and a scan rate of 50 $\frac{\text{mV}}{\text{s}}$ is shown

in Fig. 3.4. The CV shows 2 redox couples. The first one is found (1 and 5 in Fig. 3.4, red) between 300 mV and 400 mV and the second one (2 and 4 in Fig. 3.4, red) between 400 mV and 550 mV. The first redox couple is assigned to the oxidation and reduction of platinum at the Pt/YSZ interface (process 1 and 5).

$$\mathrm{PtO_{(Pt/YSZ)}} + 2\mathrm{e^-} \underset{1}{\overset{5}{\rightleftharpoons}} \mathrm{Pt} + {}^{16}\mathrm{O^{2-}} \tag{3.1}$$

The second redox couple is assigned to the oxidation and reduction of platinum at the Pt/gas interface (process 2 and 4).

$$\mathrm{PtO_{(Pt/gas)}} + 2\mathrm{e^-} \rightleftharpoons \mathrm{Pt} + {}^{16}\mathrm{O^{2-}} \tag{3.2}$$

Furthermore, at around 500 mV oxygen evolution sets in which will be mainly located at the TPB (process 3).

$${}^{16}\mathrm{O^{2-}} \rightleftharpoons \frac{1}{2}{}^{16}\mathrm{O_2} + 2\mathrm{e^-} \tag{3.3}$$

Interestingly, the oxygen evolution signal shows a strong hysteretic behavior. Oxygen formed at the TPB could stay at the platinum surface as chemisorbed oxygen, which evolves during the backward scan (process 4 and 5).

$$\text{"Pt} - \text{O"} \rightleftharpoons \frac{1}{2}{}^{16}\mathrm{O_{2(gas)}} + \mathrm{Pt} \tag{3.4}$$

A better overview over the relationship between pumped oxygen during a CV and the oxygen evolution signal can be seen from

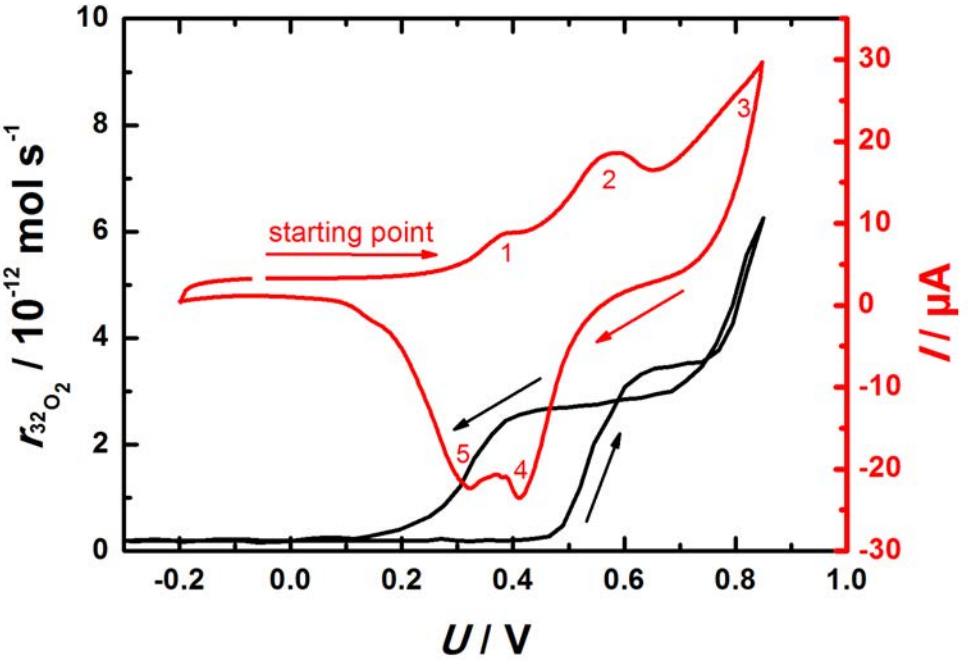

Figure 3.4: Potential dependent CV-MS measurement of a Pt/YSZ sample at 400 °C.

Fig 3.5. The figure shows the superposition of the CV and the oxygen evolution signal. It can be seen that oxygen evolution sets in when process 2 takes place. In the backward scan when the reversal point (no net current applied, around 15 s) is reached oxygen is still evoluted till process 4 and 5 are completed (around 25 s).

In order to get more information about the processes the anodic limit was changed between 600 mV and 850 mV while keeping the cathodic limit constant (Fig. 3.6, top). In the forward scan a change of the peak positions to lower values can be explained by a slight change of the morphology during measurements. More interestingly is the influence of the anodic limit on the backward scan. By increasing the anodic limit the peak heights increase substantially while a slight shift to more negative potentials is visible.

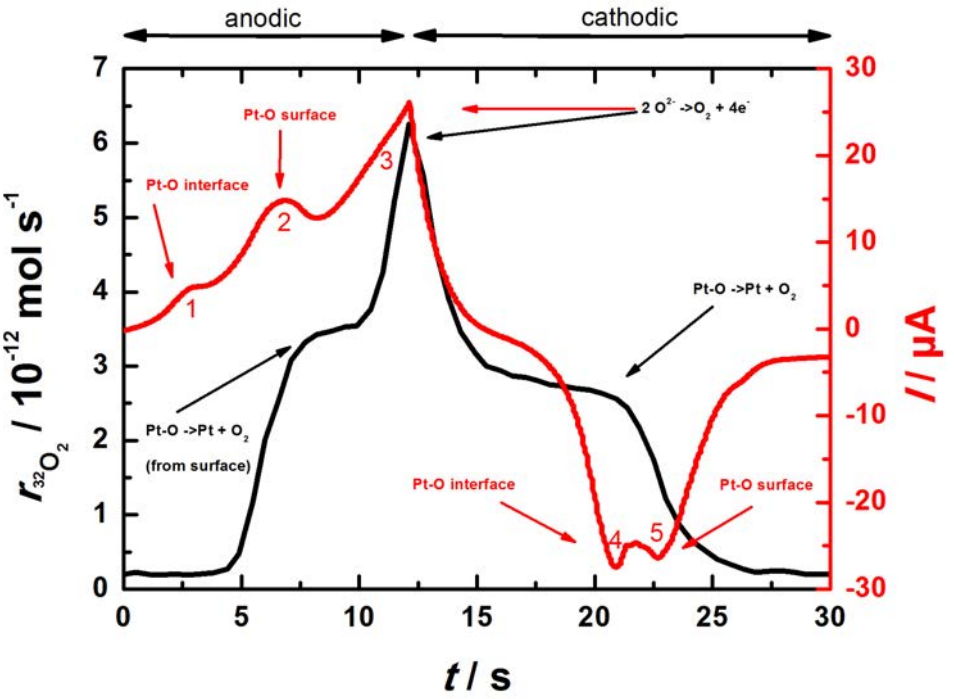

Figure 3.5: Time dependent CV-MS measurement of a Pt/YSZ sample at 400 °C.

In order to quantify the charge and therefore the amount of reduced platinum the peaks have been integrated. The relationship between charge and the anodic potential limit can be seen in Fig. 3.6, bottom. The amount of charge is relatively low ($\approx$ nC) indicating a very limited formation of oxide at the Pt/YSZ interface.

CP-MS measurements in the absence of CO

In order to obtain more information about reactions 1 - 4, chronopotentiometric measurements coupled with the MS signal (CP-MS measurements) were performed. The CP-MS measurements consist of the application of a constant current while monitoring the potential as well as the oxygen evolution signal. A typical CP-MS measurement during the application of +10 μA (anodic current) for 60 s is shown in Fig 3.7.

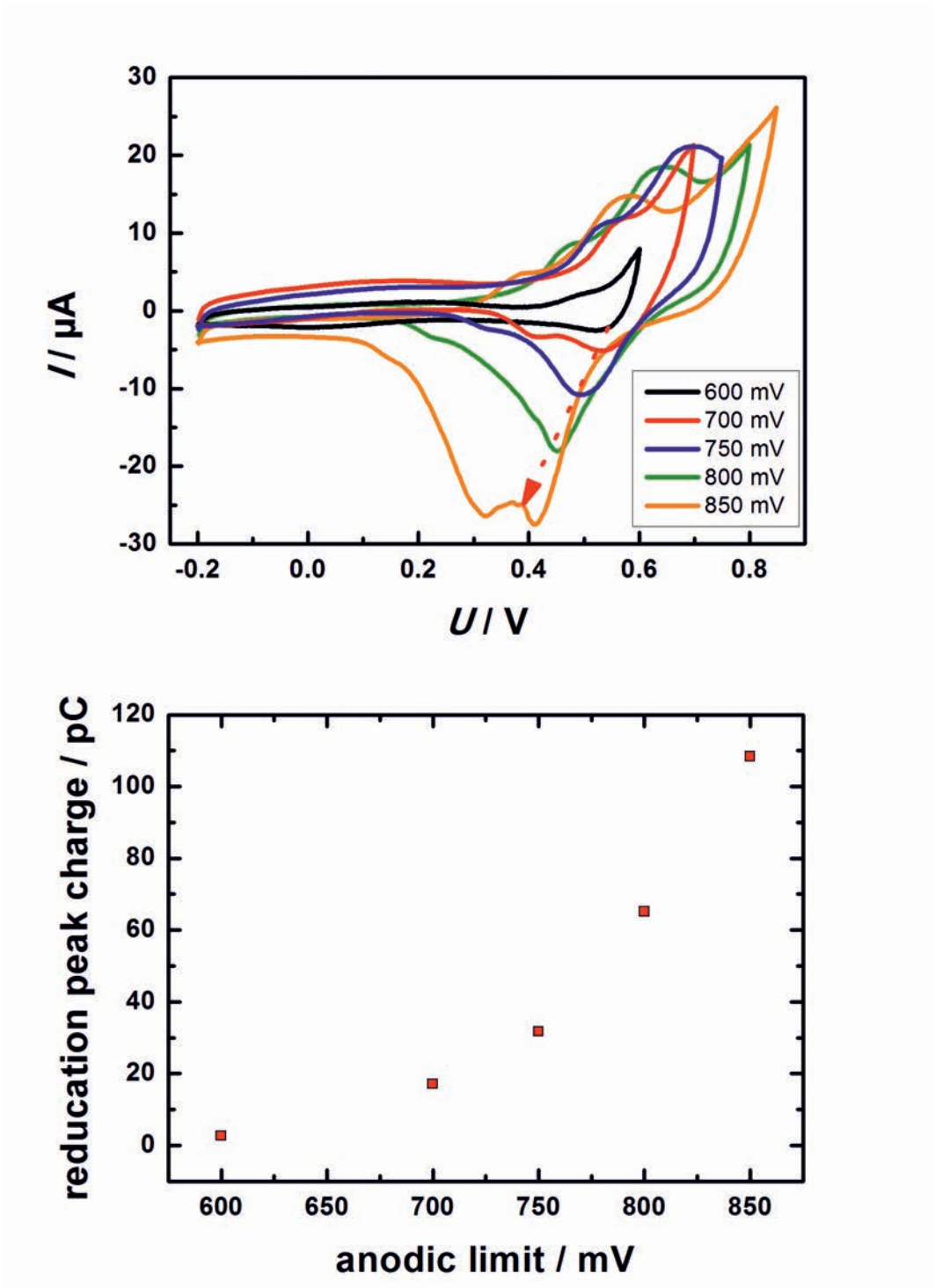

Figure 3.6: CV measurements for different anodic limits (top) and the charges within the reduction peaks of CV with different anodic peak limits (bottom) for a Pt/YSZ sample at 400 °C.

The progress of the measurements can be divided into 4 different domains:

Domain I (0 s - 10 s): Upon current application a strong increase in the potential is visible which is leading to a plateau state. No oxygen evolution takes place. This process is assigned to the reduction of previously formed YSZ at the Pt/YSZ interface.

$$Zr^{16}O_2 + 2\delta e^- \rightleftharpoons Zr^{16}O_{2-\delta} + \delta\,{}^{16}O^{2-} \tag{3.5}$$

Domain II (10 s - 30 s): This domain is marked by a point of inflection in the potential and MS response which is corresponding to 2 processes taking place. At the beginning PtO formation (process 1 and 2) is predominant while at the end oxygen evolution (process 3) becomes more favorable.

Domain III (30 s - 60 s): In this domain the potential has almost reached a steady state while the oxygen evolution rate is rapidly increasing. This process is determined by oxygen evolution (process 3).

Domain (IV): The polarization has ended (current interruption) and the potential is slowly decreasing, while oxygen evolution is still present for more than 1 minute. This process is determined by the reduction of PtO (process 1 and 2) and the accompanied oxygen evolution reaction (process 3). There is also a contribution of process 4.

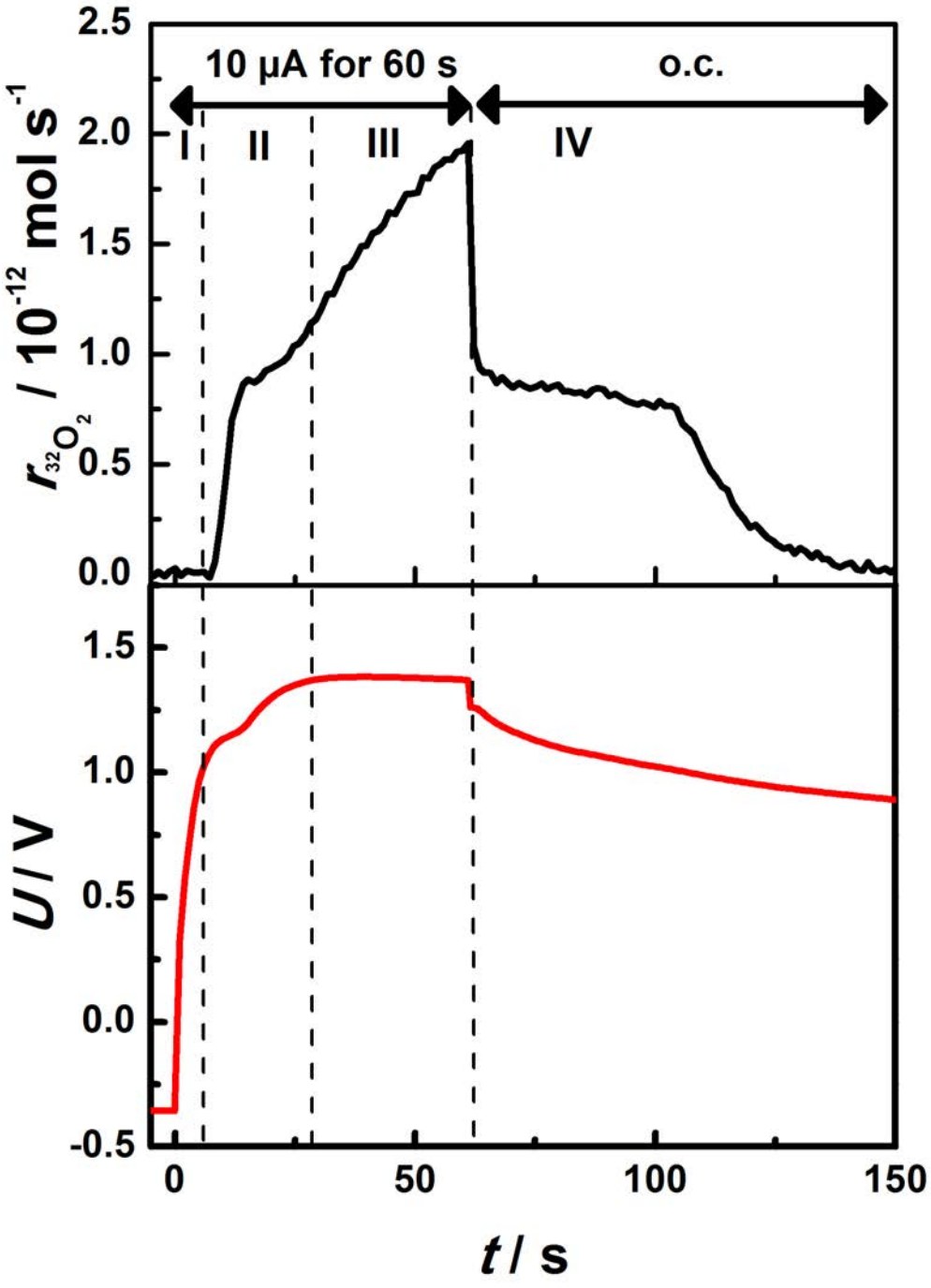

Figure 3.7: CP-MS measurement in the absence of CO with an applied current of 10 μA fo 60 s for a Pt/YSZ sample at 400 °C.

Fig 3.8 shows the influence of different applied currents on the CP-MS curves. The anodic steps are performed at 400 °C for 60 s with currents varying between 4 μA and 12 μA. Different features can be seen from the graphs: Domain I and II are shortened with increasing current. The oxygen evolution sets in earlier with increasing currents. Furthermore, the plateau region at around 1.2 V is shortened. The duration of oxygen evolution in domain IV is increased with increasing current, but surprisingly the rate of oxygen evolution is scarcely changed by the current. This indicates that the release of oxygen after stopping the polarization is controlled by the structure of the Pt/YSZ interface rather than the current. It is assumed that not only oxygen at the Pt/YSZ interface (cf. equation 3.2 and 3.4) is released, but also reaction 3.1 takes place releasing oxygen, which is moving towards the TPB, finally being evoluted.

To confirm this assumption measurements with different holding times at 400 °C with 2 μA have been conducted. Fig. 3.9 shows that by increasing the holding time the duration of the oxygen evolution signal after stopping the current increases. Furthermore, the rate of oxygen evolution after polarization is independent of the holding time and remains at a constant value, which underlines the assumption of structure dependent evolution.

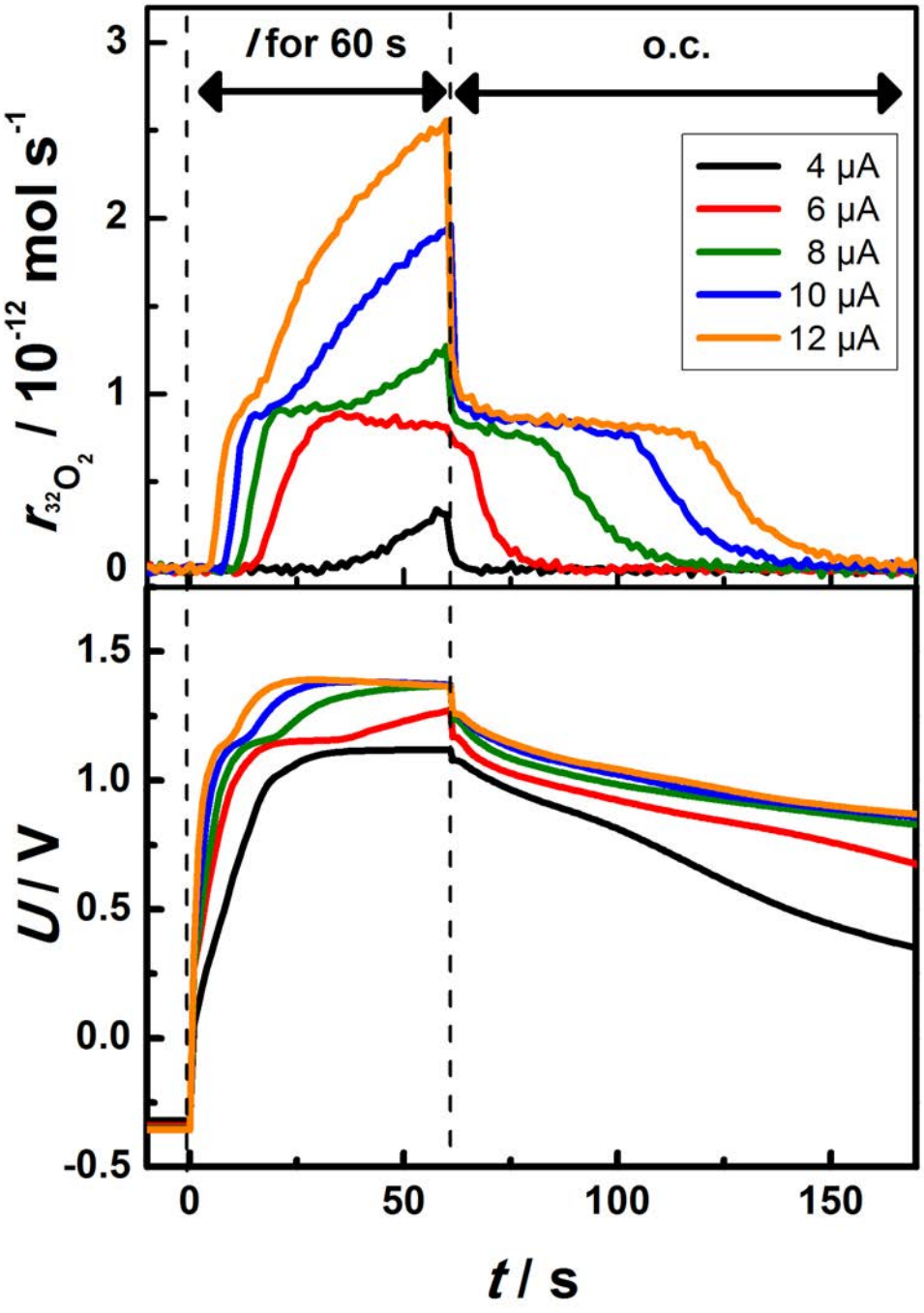

Figure 3.8: CP-MS measurement in the absence of CO with different applied currents for 60 s for a Pt/YSZ sample at 400 °C.

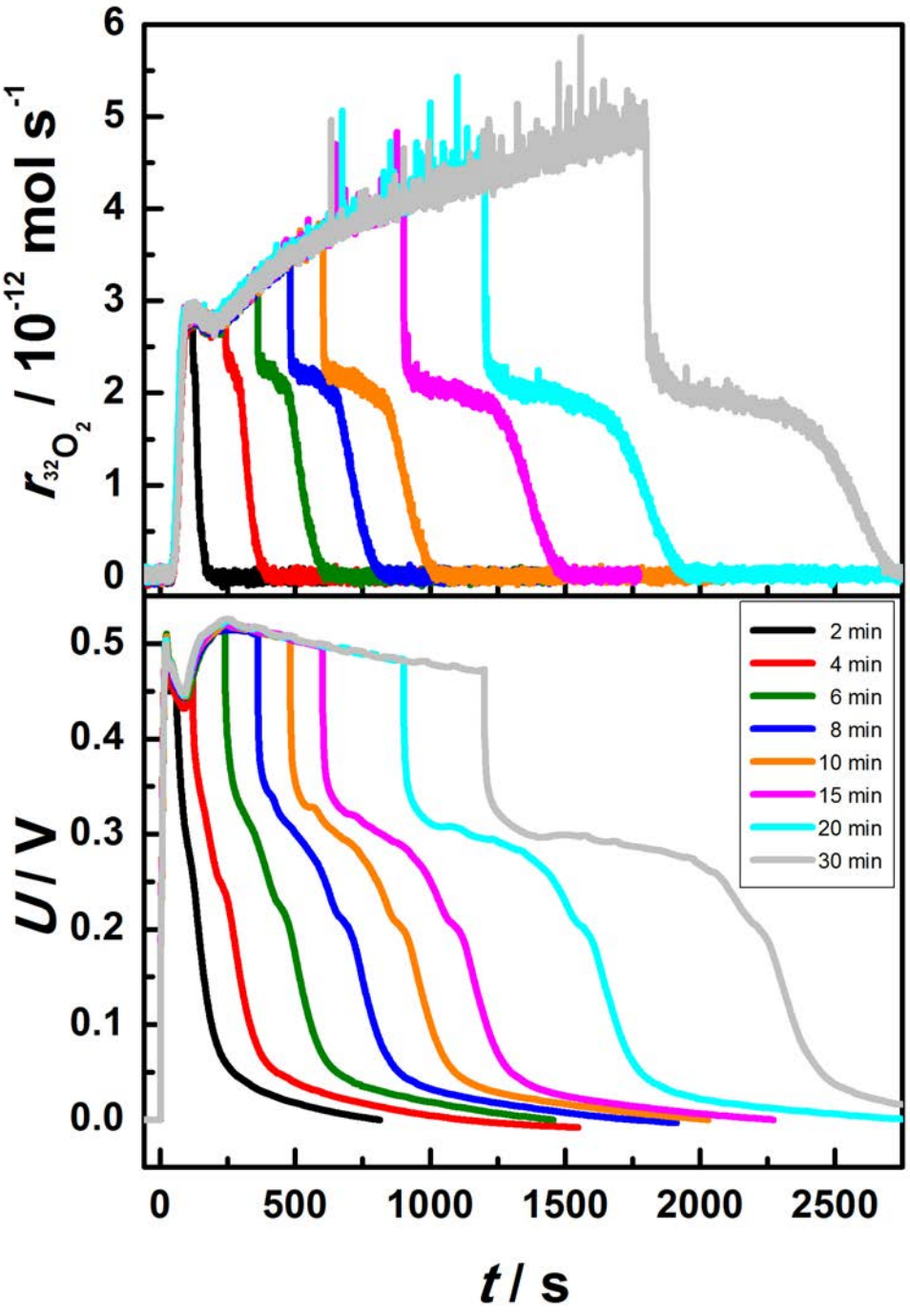

Figure 3.9: CP-MS measurement in the absence of CO with different applied holding times for 2 μA for a Pt/YSZ sample at 400 °C.

CP-MS measurements in the presence of CO

CP-MS measurements have been conducted in the presence of CO ($1{\cdot}10^{-6}$ mbar) at 400 °C. Due to the presence of CO an additional reaction is taking place at the catalyst surface during polarization:

$$C^{16}O + {}^{16}O^{2-} \rightarrow {}^{44}CO_2 + 2e^- \tag{3.6}$$

In Fig. 3.10 a measurement with 4 μA for 300 s is shown. In the beginning of the polarization the potential increases strongly and the CO_2 formation sets in at a potential of around 800 mV ($\approx$ 25 s after polarization). By a further increase of the potential ($\approx$ 1200 mV) the oxygen evolution sets in ($\approx$ 50 s after polarization). The different set-in times indicate that the electrochemical CO_2 formation (3.6) and the oxygen evolution (3.3) are potential-dependent. The CO_2 rate and the potential reach a steady state while the oxygen evolution increases after reaching a short plateau state. After polarization the oxygen signal drops till a new steady state is reached with a same trend seen in the potential. The CO_2 formation appears almost unaffected. After 200 s the oxygen signal drops to 0 while a peak in the CO_2 signal is visible before the CO_2 signal also slowly drops to 0.

Equivalent to the experiments done under high vacuum conditions without the presence of CO, different currents for a fixed time as well as different holding times were applied for a fixed current.

Fig. 3.11 shows the influence of different currents on the electrochemical CO oxidation. Besides the characteristics already explained for the 4 μA measurement there are a few important new features. The offset of the oxygen evolution signal and the CO_2

signal increase with decreasing current. After stopping the polarization the oxygen evolution rate and the CO_2 signal decrease to a plateau state which extension depends on the current. Interestingly, both plateaus for oxygen evolution and CO_2 formation have constant values independent of the current indicating a material dependent evolution (Fig. 3.9 different holding times).
The influence of different holding times on the electrochemical CO oxidation is shown in Fig. 3.12. An increase in the holding time also enlarges the plateau regime for the oxygen evolution signal as well as for the CO_2 signal.

CP-MS measurements in the presence of CO and $^{18}O_2$

CP-MS measurements have been conducted in the presence of CO ($1{\cdot}10^{-6}$ mbar) and $^{18}O_2$ ($5{\cdot}10^{-6}$ mbar) at 300 °C. Due to the presence of CO additional reactions take place at the catalyst surface.

$$C^{16}O + \frac{1}{2}{}^{16}O_2 \rightarrow {}^{46}CO_2 \tag{3.7}$$

$$C^{16}O + \frac{1}{2}{}^{18}O_2 \rightarrow {}^{48}CO_2 \tag{3.8}$$

Reaction (3.8) is very unlikely due to the unfavoured oxygen exchange with CO and contributes only in a minor way. Therefore, it is neglected in the examination.
In Fig 3.13 a measurement with 10 μA for 300 s is shown. At

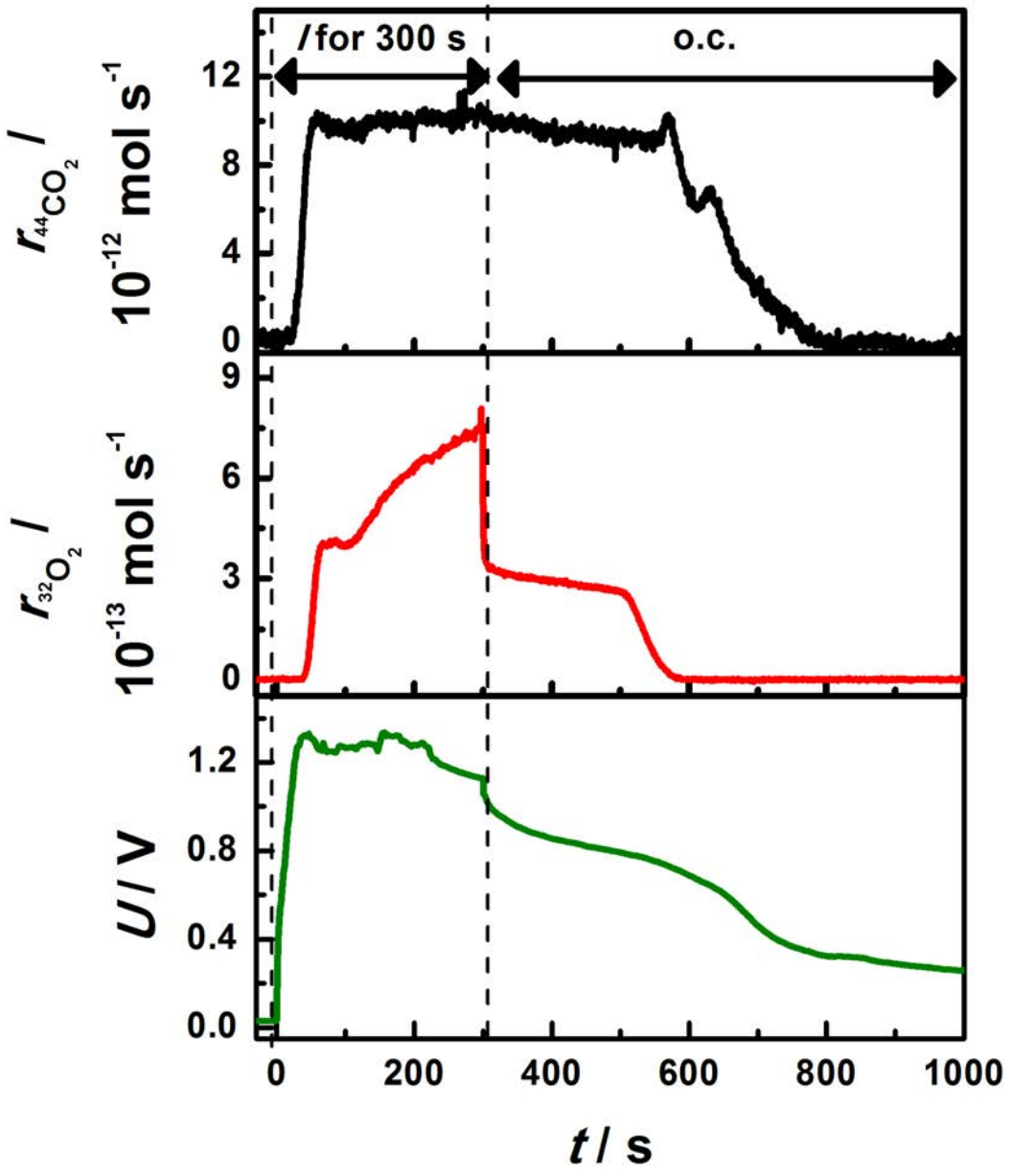

Figure 3.10: CP-MS measurement in the presence of CO with an applied current of 4 μA for 300 s for a Pt/YSZ sample at 400°C.

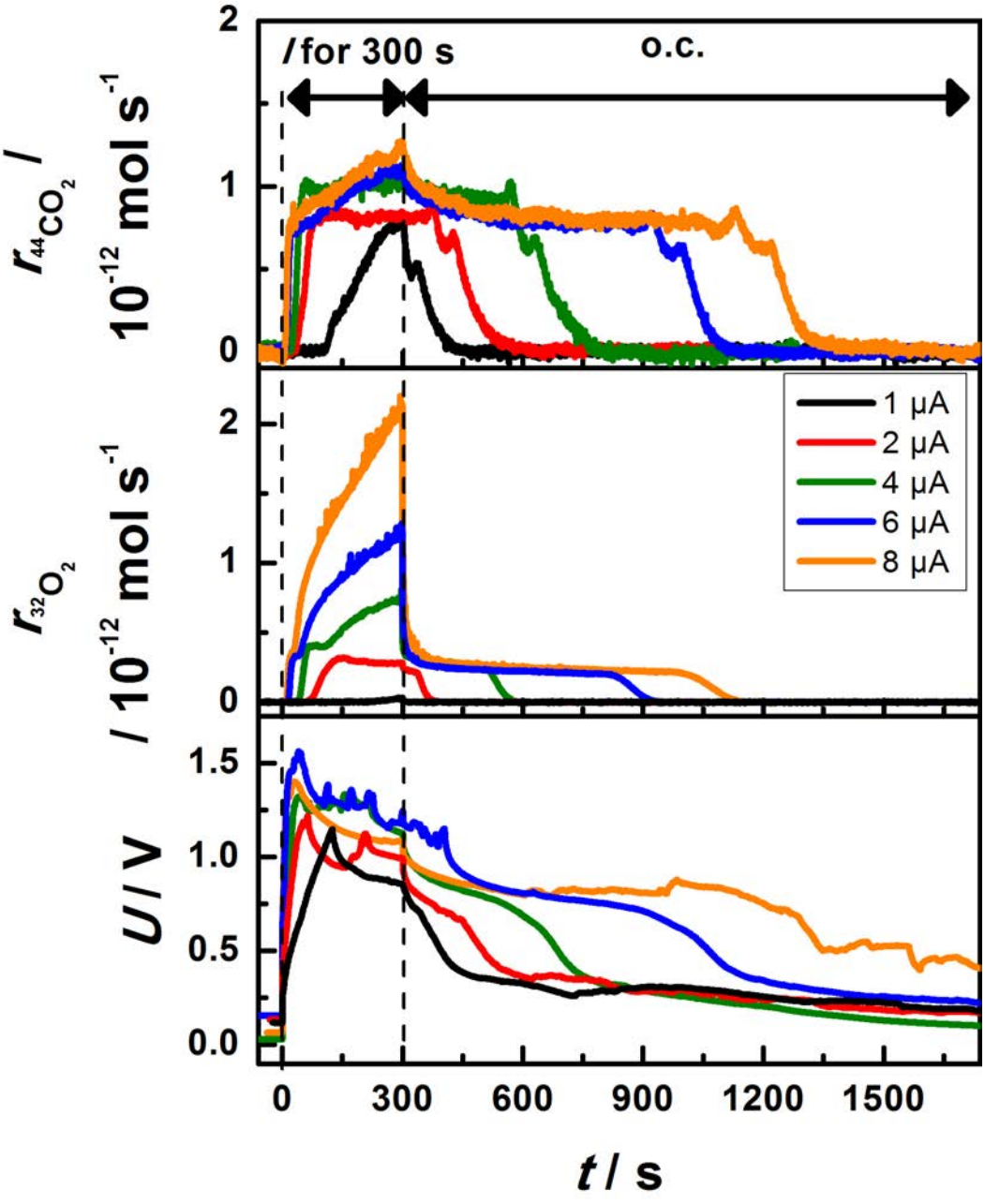

Figure 3.11: CP-MS measurement in the presence of CO with different currents for 300 s for a Pt/YSZ sample at 400°C.

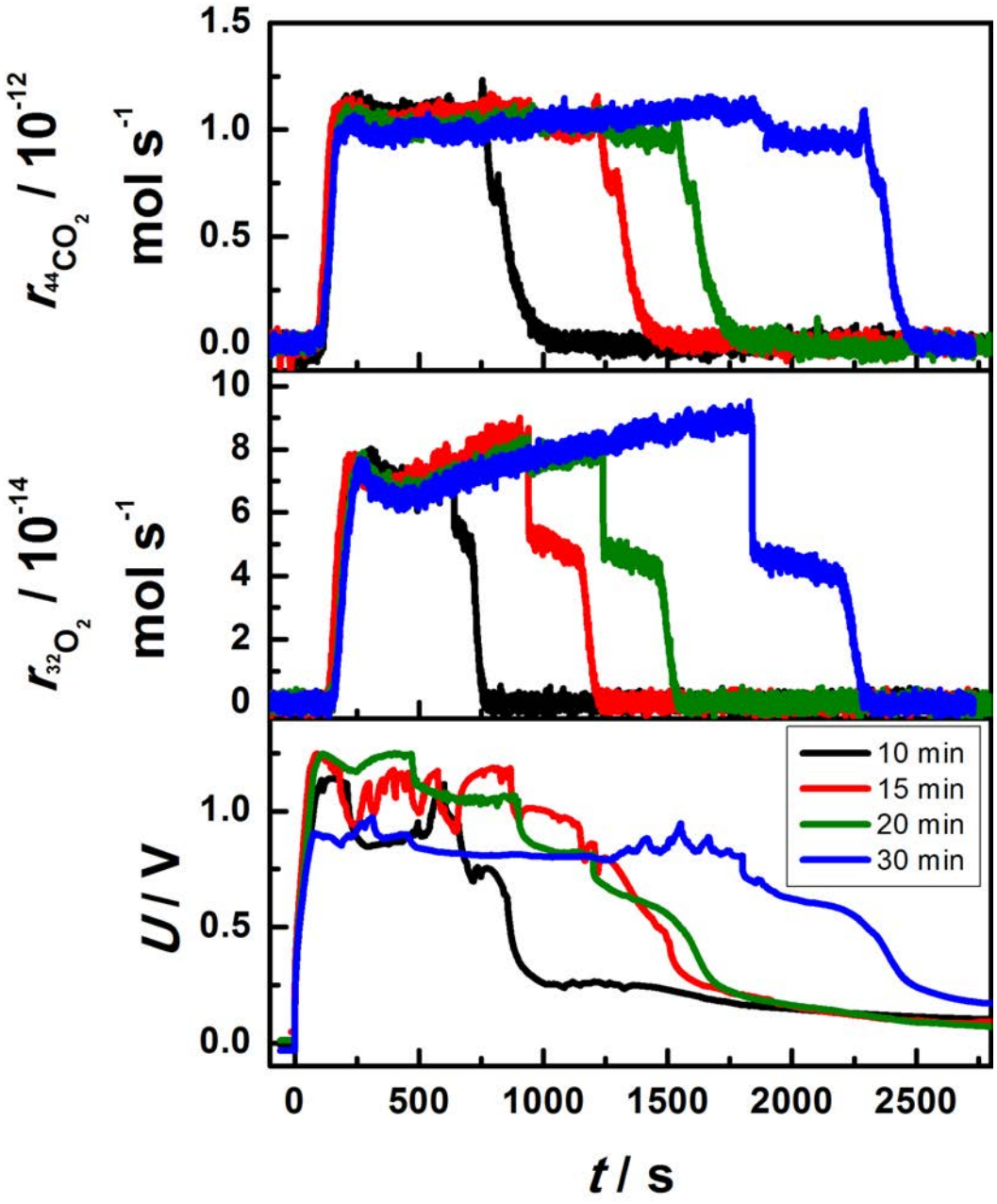

Figure 3.12: CP-MS measurement in the presence of CO with different holding times of 4 μA for a Pt/YSZ sample at 400°C.

300 °C a steady state rate of $^{46}CO_2$ formation of $1.76 \cdot 10^{-10}$ $\frac{\text{mol}}{\text{s}}$ takes place (process 6). In the beginning of the polarization the potential increases strongly and stabilizes at 0.4 V. At the same time the oxygen evolution reaches a steady state of $1.7 \cdot 10^{-10}$ $\frac{\text{mol}}{\text{s}}$. Simultaneously, process 5 sets in and the formation rate of $^{46}CO_2$ increases. Upon current interruption the potential as well as the oxygen evolution rate decreases within one minute, while process 5 and 6 need much longer to reach their initial states.

Comparable to the investigations performed for the electrochemical CO oxidation, different holding time measurements at a constant current of 10 μA (Fig.3.15) and different current measurements for a constant polarization time of 300 s at 400 °C and the above mentioned partial pressures have been performed (Fig. 3.14).

By increasing the applied current during polarization the potential increases as well as the amount of CO_2 from the electrochemical CO oxidation (process 5) and the amount of CO_2 from the gas phase reaction (process 6) at steady state. After stopping the polarization the potential and the oxygen evolution signal return within seconds to their original value and no appreciable current dependence is visible. The electrochemical CO_2 formation and the catalytical CO_2 formation need much more time to return to their initial values and a strong correlation with the applied current is visible. By increasing the current the CO_2 rates remain longer on a higher value.

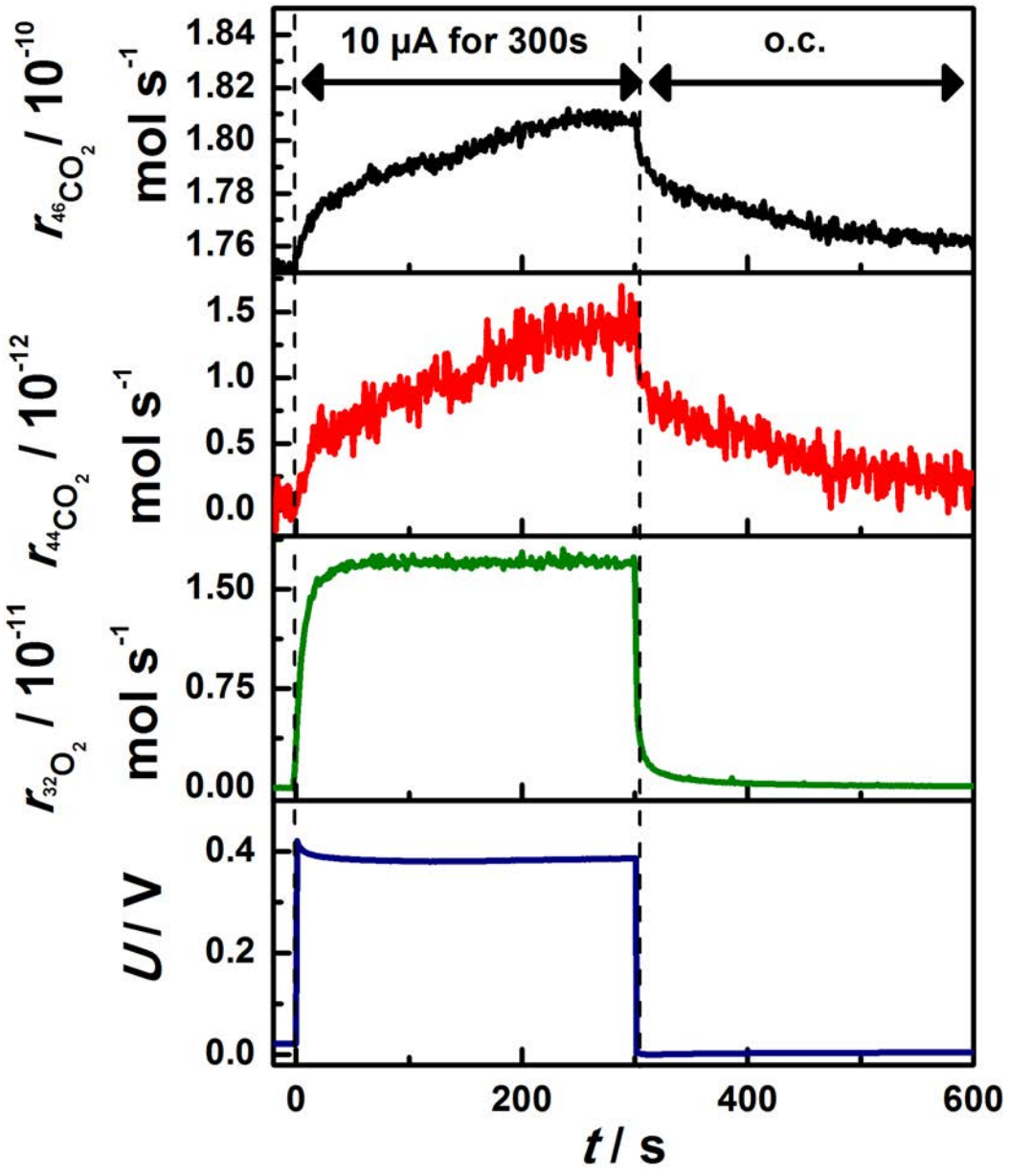

Figure 3.13: CP-MS measurement in the presence of CO and $^{18}O_2$ with an applied current of 10 μA for 300 s for a Pt/YSZ sample at 400 °C.

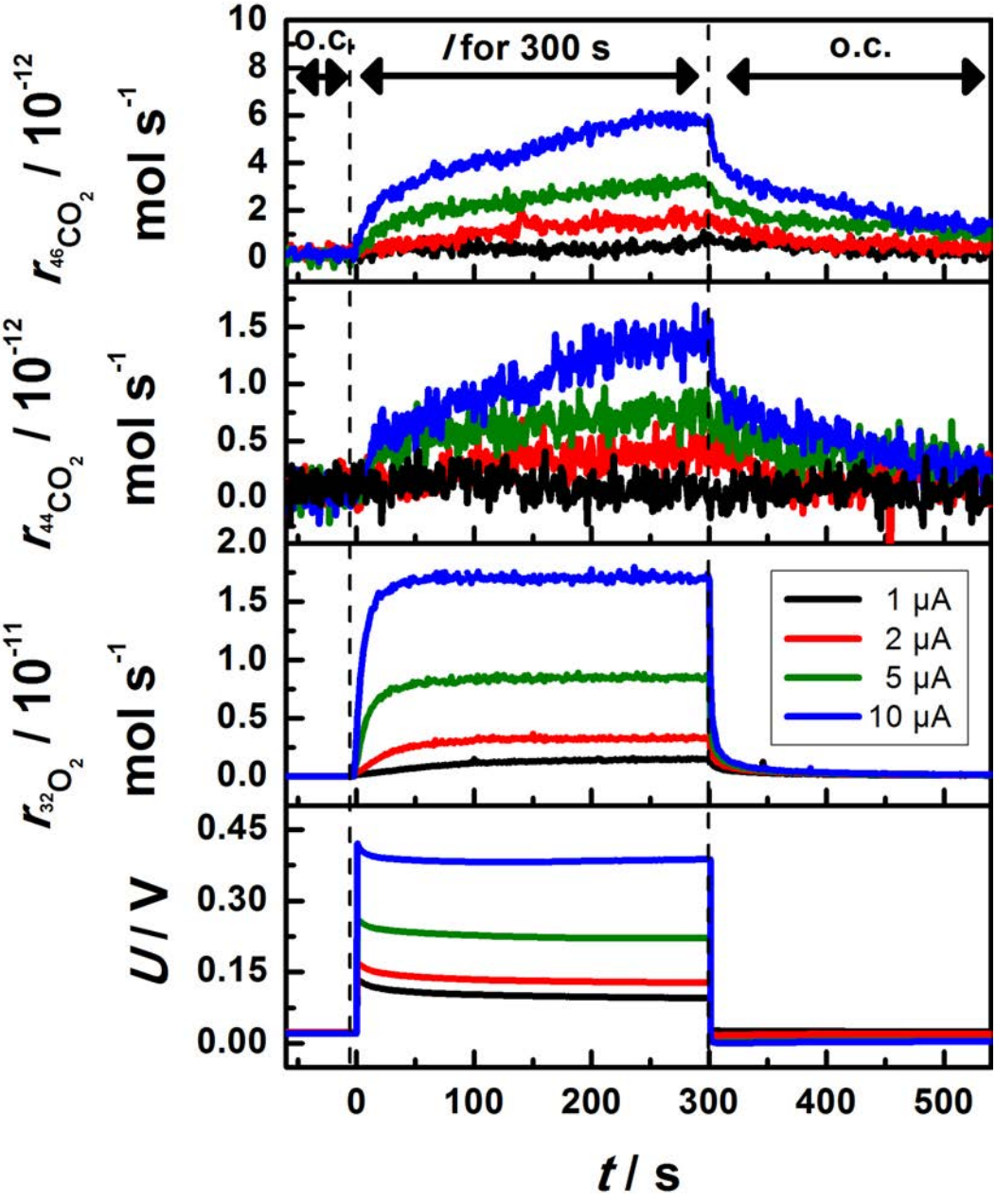

Figure 3.14: CP-MS measurement in the presence of CO and $^{18}O_2$ with different currents 300 s for a Pt/YSZ sample at 400 °C.

Varying the holding time has a similar impact on the behavior of the cell as the change of the current has (Fig. 3.15). By increasing the holding time the behavior of the potential and the oxygen evolution seems almost unaffected while a strong correlation between the persistent effect of formation of both CO_2 and the holding time is visible.
The faradaic efficiency and the enhancement ratio, which characterize the NEMCA effect, can be easily calculated from the terms:

$$\Lambda = \frac{r_{CO_2} - r^0_{CO_2}}{\frac{I}{zF}} \tag{3.9}$$

$$\rho = \frac{r}{r_0} \tag{3.10}$$

For the use of isotopically labeled oxygen ($^{18}O_2$) different definitions have to be used:

$$\Lambda = \frac{r_{C^{16}O_2} + \Delta r_{C^{16}O^{18}O}}{r_{C^{16}O_2}} = 1 + \frac{r_{C^{16}O^{18}O}}{r_{C_{16}O_2}} \tag{3.11}$$

$$\rho = \frac{r_{C^{16}O_2} + r_{C^{16}O^{18}O}}{r_{C^{16}O^{18}O}} \tag{3.12}$$

The values for the different currents and different holding time measurements are shown in table 3.1:

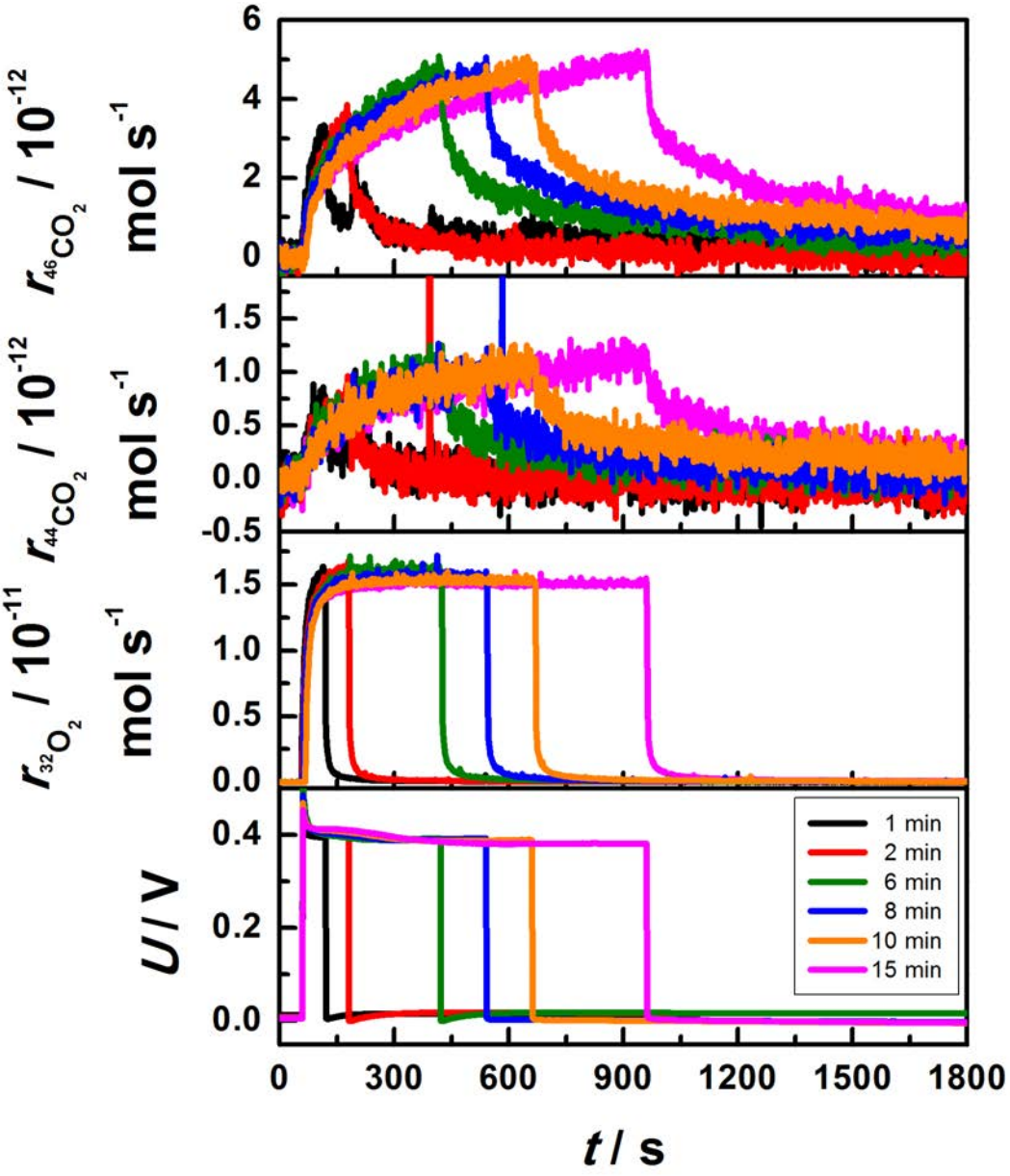

Figure 3.15: CP-MS measurement in the presence of CO and $^{18}O_2$ with different holding times for 10 μA for a Pt/YSZ sample at 400 °C.

I [μA]	Λ	ρ
1	3	1
2	5	1.01
5	5.3	1.02
10	5	1.04
10 (holding time)	5.2	1.04

Table 3.1: Λ and ρ values for different currents for a Pt/YSZ interface at a partial pressure of $1{\cdot}10^{-6}$ mbar CO and $5{\cdot}10^{-6}$ $^{18}O_2$ at 400 °C.

3.1.4 Discussion

By coupling MS and CV measurements it can be shown that at a low anodic potential of around 300 mV platinum is oxidized at the Pt/YSZ interface while a second peak is visible at a potential of 600 mV which is assigned to the oxidation of the platinum surface due to the fact that oxygen evolution is taking place at a similar potential. A further increase of the potential leads to a third peak and a strong oxygen evolution signal which is the reason for an assignment of the peak with the formation of gaseous oxygen. The hysteretic oxygen signal in the backward scan implies that an oxygen reservoir has been built up in the forward anodic scan. The reduction of the platinum in the backward scan has been quantified for different anodic limits and shows relatively low charges in the pC range, which implies that only very thin films ($\approx$ 1ML) of oxide has been formed in the anodic branch.

The results have been further elucidated and quantified by CP-MS measurements. In the absence of reactive gas ZrO_2 is reduced, PtO_2 is formed at the Pt/YSZ interface (3.1) and at the surface (3.2) and oxygen evolution (3.4) takes place during anodic polarization. Surprisingly, oxygen evolution maintains after polarization which is

explained by the decomposition of previously formed oxide mainly at the Pt/YSZ interface (3.1). The oxygen evolution signal is almost independent of the current and the holding time indicating a release of oxygen through the TPB [Pöpk11.2, Pöpk11.3, Pöpk13]. In the presence of CO an additional electro-oxidation reaction takes place (3.6). Interestingly, the CO electro-oxidation sets in before the oxygen evolution takes place and persists longer than the oxygen evolution signal upon current interruption. Both effects indicate a lower potential necessary for the electro-oxidation of CO than for the oxygen evolution signal.

In the presence of CO and $^{18}O_2$ an increase in the formation of $^{44}CO_2$ and $^{46}CO_2$ during polarization indicates that two processes (3.6 and 3.7) take place. An increase in the $^{44}CO_2$ results from the electrooxidation of the CO and the steady state rate depends directly on the applied current. In contrast, the increase in the $^{46}CO_2$ rate cannot be directly explained by the applied current. An increase in the $^{46}CO_2$ rate coud occur if the binding strength of the reactants CO and O_2 are changed and therefore the product formation is enhanced. This is commonly explained by the formation of an effective double layer which changes the work function of the catalyst and also the binding strength of the reactants (see explanation by Vayenas [Vaye01]). Additionally the surface oxygen activity and therefore the $^{46}CO_2$ rate depends on the surface coverage which is strongly influenced by the anodic polarization.

The values show a slightly non-faradic behavior, although the enhancement ratio is very close to 1. Additionally, an exchange of $^{18}O_2$ with the lattice oxygen is possible, therefore also explaining an increase of $^{46}CO_2$ during polarization.

Furthermore, especially in the high vacuum pressure range a falsification of the rate by an application of a current can easily happen. Due to the anodic pumping of oxygen ions, oxygen is built out at the catalyst and therefore increasing the total pressure measured in the MS. An increased total pressure signal leads to increased MS signals pretending too high rates. Although this effect should be weak, in evaluating the low NEMCA values, this influence should be kept in mind.
Nevertheless, the results show a clear picture of the processes taking place at Pt/YSZ interface in the presence and absence of reactive gas. Especially by the use of isotopically labeled oxygen a discrimination between gas phase oxygen and electro-oxidation is feasible.

3.2 Investigation of the oxygen exchange kinetics and electrochemical promotion of CO oxidation over Ag/YSZ electrodes under high vacuum conditions

3.2.1 Introduction

The oxygen exchange reaction at $Me(O_2)$/YSZ electrodes can occur at different reaction sites of the electrode system, and each reaction site involves different reactions and rate determining steps which all contribute to the overall electrochemical reaction in the cell. For most applications a fast oxygen exchange between the gas phase and the electrode is important. In electrode systems with low oxygen bulk diffusivity in the metal phase the oxygen exchange reaction takes place in the vicinity of the TPB and the electro-

chemical performance is directly related to the TPB length. The prototype example for such a system is the electrode $Pt(O_2)/YSZ$ [Opit10, Opit10.1, Opit12, Luer06].

Platinum has a low solubility for oxygen, and thus, the oxygen reduction and oxidation take place at the TPB. To improve the electrode performance it can be of advantage to enlarge the electrochemically active reaction region to the entire electrode surface. Therefore, catalytically active metals or mixed conducting oxides with high oxygen solubility and diffusivity are often used in practice. In this case oxygen will be supplied by bulk diffusion through the volume of the electrode. The electrode $Ag(O_2)/YSZ$ can be regarded as a prototype system, where the electrode performance is primarily controlled by the oxygen exchange reaction at the inner two-phase boundary Ag/YSZ [VanH94, Kont91, Jime97, Knej94].

In this part of the work, the electrochemical measurements were carried out over Ag/YSZ electrodes to investigate the oxygen exchange reaction using solid electrochemical mass spectrometry technique (SEMS) under high vacuum conditions. In addition, the electrochemical promotion on the silver catalyst was studied using isotopically labeled $^{18}O_2$ and CO reactants at elevated temperatures. Based on the experimental results, a dynamic model of the oxygen exchange process at Ag/YSZ electrodes is proposed and its effect on the electrochemical promotion performance is discussed.

3.2.2 Experimental Part

Sample preparation

The preparation of the silver electrodes follows the same procedure as that of the platinum electrodes. Accordingly, rectangular silver electrodes with a geometrical size of 6 mm x 3 mm were deposited on polycrystalline zirconia (stabilized by 8.5 mol% Y_2O_3) pellets (Frialit, Friatec Cooperation) by PLD. A detailed description of the PLD process is given in chapter 2.3. The as-prepared samples were sintered at 550 °C for 5 h in argon to stabilize the morphology. The thickness of the electrodes after calcination, as determined by profilometry using an Alpha-Step instrument (Alpha-Step IQ, KLA Tencor), was around 1 μm. The surface, morphology and composition were investigated by SEM and EDX (Fig. 3.16, down). The crystal structure was examined by X-ray diffraction (Fig. 3.16, up).

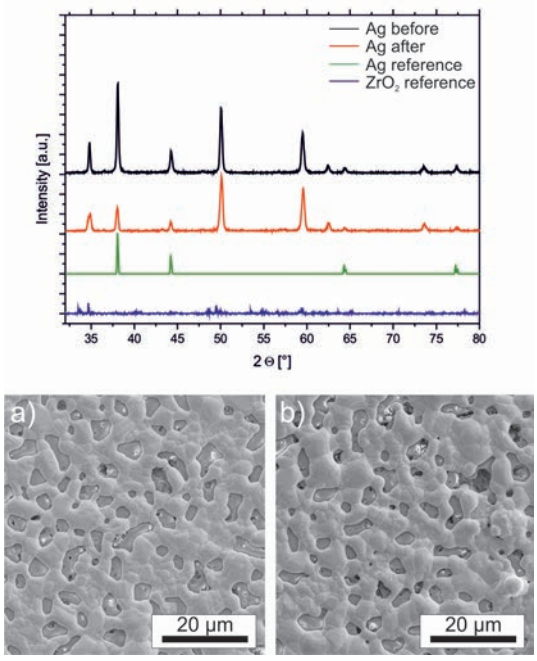

Figure 3.16: XRD (top) and SEM (bottom) investigation of an Ag electrode on polycrystalline YSZ before (a) and after (b) heat treatment.

Electrochemical Measurements

For electrochemical measurements, a gold counter electrode (Du Pont 5771) was coated on the opposite side of the YSZ pellet in a symmetrical face-to-face arrangement ensuring a homogeneous potential distribution. The electrochemical measurements were carried out using solid electrochemical mass spectrometry (SEMS) under high vacuum conditions with a background pressure of 10^{-12} bar. Furthermore, the same conditions and equipments were used as for the platinum measurements (cf. 3.1.2). The galvanostastic/potentiostatic steps were applied to the cell using a potentiostat (Gamry Instruments Reference 600) while the gaseous products were monitored by an online quadrupole mass spectrometer (QMS, Pfeiffer, Prisma 200). When needed, the reactive gases (carbon monoxide ($C^{16}O$ 5.0) and isotopic labeled oxygen ($^{18}O_2$ 3.0) were fed into the micro reactor via leak valves and capillary stainless steel gas lines for the EP investigation. The operating temperature was kept between 300 °C and 550 °C.

3.2.3 Results

Anodic polarization in the absence of CO

A constant current of 10 μA was imposed to the Ag/YSZ/Au cell at elevated temperature (background pressure of 10^{-12} bar), such that the anodic potential was applied to the Ag/YSZ electrode. Oxygen evolution was observed by MS as shown in Fig. 3.17.
During anodic polarization of the Ag electrode, $^{16}O^{2-}$ ions migrate from the cathode through the YSZ lattice to the anode causing YSZ reduction at the cathode (as oxygen supply to the cathode

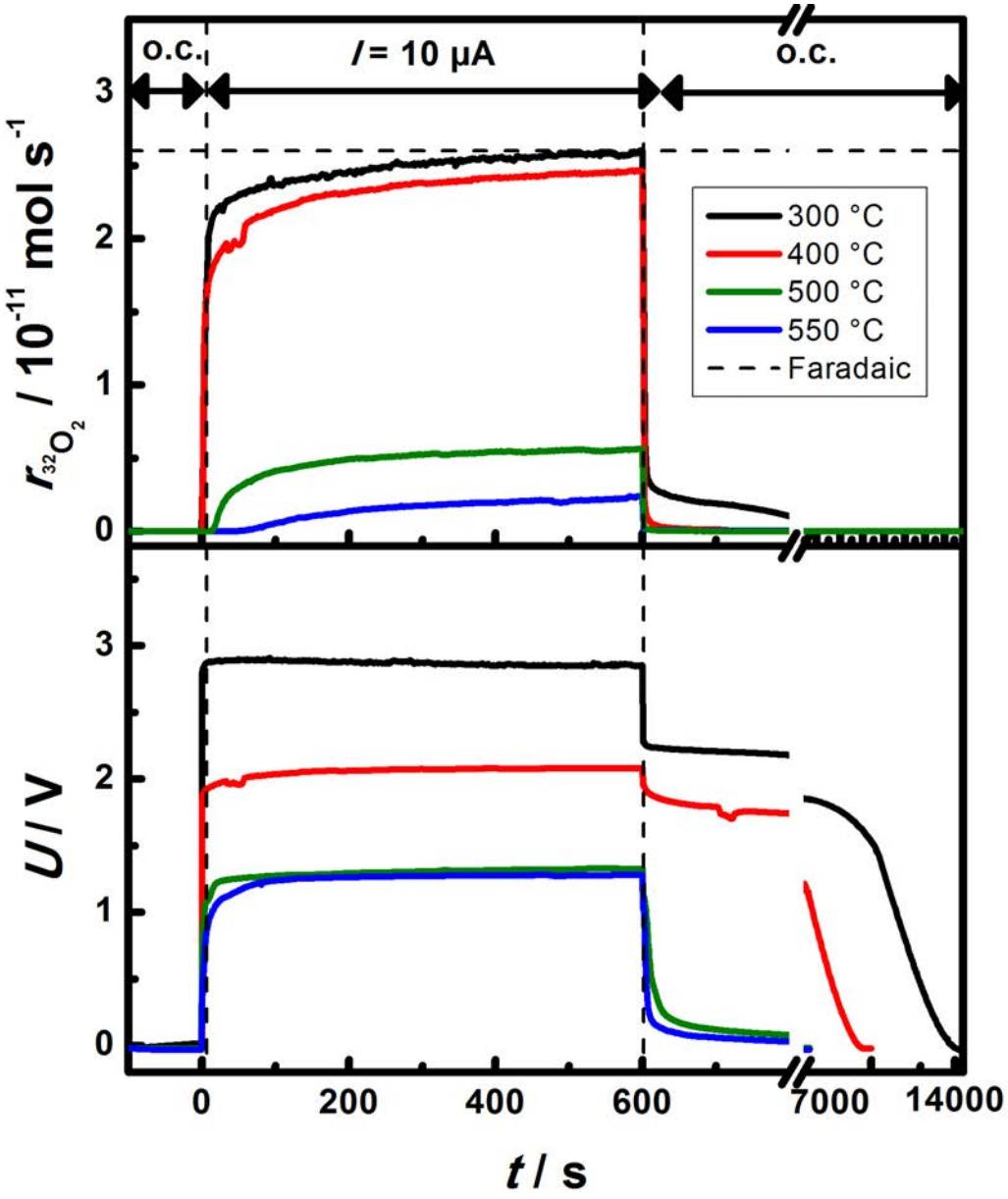

Figure 3.17: Oxygen evolution rate from an Ag/YSZ electrode after application of an anodic current of 10 μA for 10 minutes at different temperatures. The oxygen signal and the potential between working and counter electrode (U) are monitored during electrochemical polarization.

is limited by the low $p(O_2)$) and oxygen evolution at the anode (equation 3.13 and 3.14).

$$Zr^{16}O_2 + 2\delta e^- \rightarrow Zr^{16}O_{2-\delta} + \delta^{16}O^{2-} \tag{3.13}$$

$$^{16}O^{2-} \rightarrow \frac{1}{2}{}^{16}O_2 + 2e^- \tag{3.14}$$

Interestingly, it is found that the steady-state rate of oxygen evolution decreases with increasing operation temperature. At 300 °C, the rate of oxygen evolution is stabilized at $2.6{\cdot}10^{-11}$ $\frac{\text{mol}}{\text{s}}$ very close to the theoretical value of the faradaic rate (indicated by a dashed horizontal line in Fig. 3.17). With increasing temperature, the rate decreases down to $0.25{\cdot}10^{-11}$ $\frac{\text{mol}}{\text{s}}$ at 550 °C, being almost one order of magnitude lower than at 300 °C. The cell voltage, necessary to drive the applied current, decreases from 2.8 V at 300 °C to 1.5 V at 550 °C. Upon current interruption, an oxygen desorption plateau is observed for 200 s at 300 °C which then slowly returns to the background value while the oxygen rates drop within few seconds at higher temperatures. The open circuit potential (OCP) after electrochemical polarization shows an even more pronounced difference as a function of temperature. At 300 °C the large OCP of about 2 V needed about 4 hours to reach its initial value whereas at 400 °C the time to reach steady state is reduced to less than 2 hours. Above 400 °C the OCP reaches its original start value within seconds.

This initial experiment clearly demonstrates that less oxygen evolves directly into the gas phase with increasing temperature. During anodic polarization the pumped oxygen can either be dissolved

(stored) in the Ag electrode or evolve into the gas phase. Oxidation of silver can be excluded, as the known silver oxides decompose already at lower temperatures [Mich03]. For the quantification of this effect we define the electrochemical efficiency for oxygen evolution (equation 3.15) and the electrochemical efficiency of storage (equation 3.16) by:

$$\eta_{O_2} = \frac{Q_{O_2}}{Q_{total}} \tag{3.15}$$

$$\eta_{O_{Ag}} = \frac{Q_{O_{Ag}}}{Q_{total}} = 1 - \eta_{O_2} \tag{3.16}$$

with Q_{O_2} being the amount of charge which is calculated from the amount of $^{16}O^{2-}$ ions used for oxygen evolution (calculated by the area under the oxygen evolution curve) and Q_{total} being the total amount of charge pumped by $^{16}O^{2-}$- ions during the polarization step (integrated current). η_{O_2} and $\eta_{O_{Ag}}$ have been evaluated from the steady state values for the oxygen flux after application of different currents for 10 minutes at 300 °C and 500 °C.

Fig. 3.18, left shows the calculated efficiencies for 300 °C for different applied currents. Oxygen evolution is always favored, but as the applied current and therefore the overpotential increases, oxygen evolution becomes even more dominant, meaning that the efficiency for oxygen storage in silver is more distinct at low currents. This behavior can be explained by the overpotential which is needed for the oxygen evolution process. The incorporation into silver is favored over the oxygen evolution at 500 °C (Fig. 3.18,

right), but the ratio of the efficiencies is reduced by increasing potential meaning that oxygen evolution becomes more distinct at higher currents.

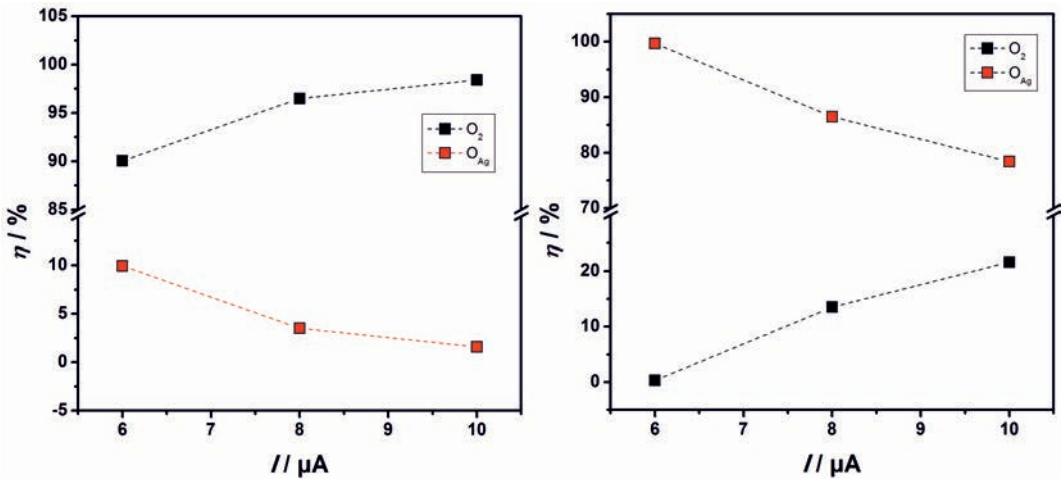

Figure 3.18: Charge efficiencies for oxygen evolution and oxygen storage at Ag/YSZ electrodes at 300 °C (left) and 500 °C (right).

In order to investigate the formation of the oxygen desorption plateau upon current interruption we applied a current of 10 μA for different holding times at two different temperatures (300 °C and 500 °C). For 300 °C, (Fig. 3.19, left) shows that by increasing the holding time the maximum oxygen evolution steady state flux increases, whereas the potential remains almost constant at 3.2 V. Upon current interruption the plateau is well visible and increases significantly with longer duration of holding time. Simultaneously, the potential response OCP after current interruption also shows a dependence on the holding time. With longer holding time the OCP needs more time to reach its initial start value.

The measurements at 500 °C show, in contrast to the ones at 300 °C, no extended plateau, neither in the oxygen signal nor in the OCP recorded after current interruption (Fig. 3.19, right).

Even after very long holding times the signals return to their initial values in minutes after current interruption, indicating a different oxygen storage mechanism compared to lower temperatures.

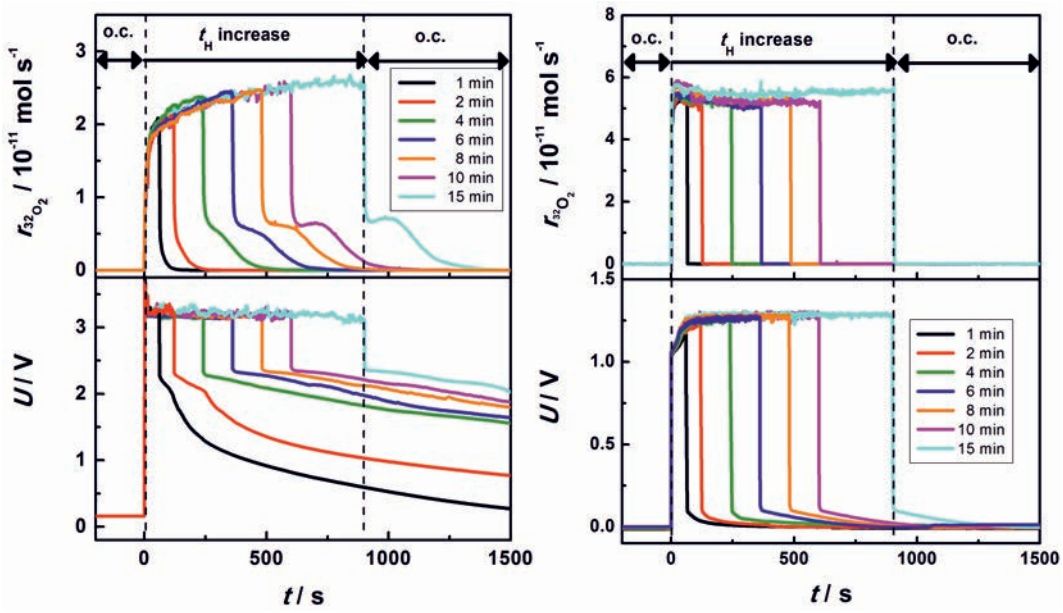

Figure 3.19: Oxygen evolution and potential response of a Ag/YSZ electrode for the application of 10 μA with different holding times at 300 °C (left) and 500 °C (right).

In order to shed more light on the storage mechanism for oxygen in the Ag electrode we take a closer look at a possible oxide formation. Thermodynamic considerations for Ag and AgO_x show that oxide formation is favored at high oxygen partial pressures and low temperatures. At the experimental conditions selected in this study (high vacuum conditions and a temperature range between 300 °C and 550 °C), Ag is thermodynamically stable, but a strong local increase in the oxygen partial pressure at the TPB and Ag/YSZ interface due to electrochemical polarization could drive oxide formation, as recently reported for the system Pt/YSZ [Pöpk11, Pöpk12, Pöpk13, Falg10, Falg10.2]. Additionally, surface oxides could be

more stable than bulk oxides. Because of the instability of the silver oxides under high vacuum conditions at high temperature decomposition of any oxide should take place directly after stopping the electrochemical polarization. The observed plateau formation upon current interruption at 300 °C which is also visible in the open circuit potential is an indicator for storage of oxygen species during the electrochemical polarization either via oxide formation and the subsequent decomposition of previously formed oxide, or via bulk diffusion of oxygen into silver. With increasing holding time the plateau also stretches, indicating a larger quantity of oxide being formed with longer polarization time. The maximum rate of oxygen flux in the plateau region is limited to $6{\cdot}10^{-12}$ $\frac{\text{mol}}{\text{s}}$ indicating a release of the oxygen from the decomposed oxide mainly across the TPB of the system. According to literature [Lawl74, Cabr49], mainly relying on Wagner´s theory of metal oxidation, the oxide growth follows the well known parabolic rate law, indicating a diffusion controlled mechanism. Fig. 3.20 shows the amount of oxygen in mol released after polarization related to the square root of the polarization holding time showing an almost linear behavior as predicted in literature, clearly pointing to diffusion-controlled oxide formation at the Ag/YSZ interface at 300 °C. At higher temperatures no plateau is visible indicating negligible oxide formation. Therefore, it appears to be reasonable to rule out oxide formation at higher temperatures, but rather to consider oxygen dissolution in silver as storage mechanism. This is plausible due to increased oxygen solubility in silver at elevated temperatures.

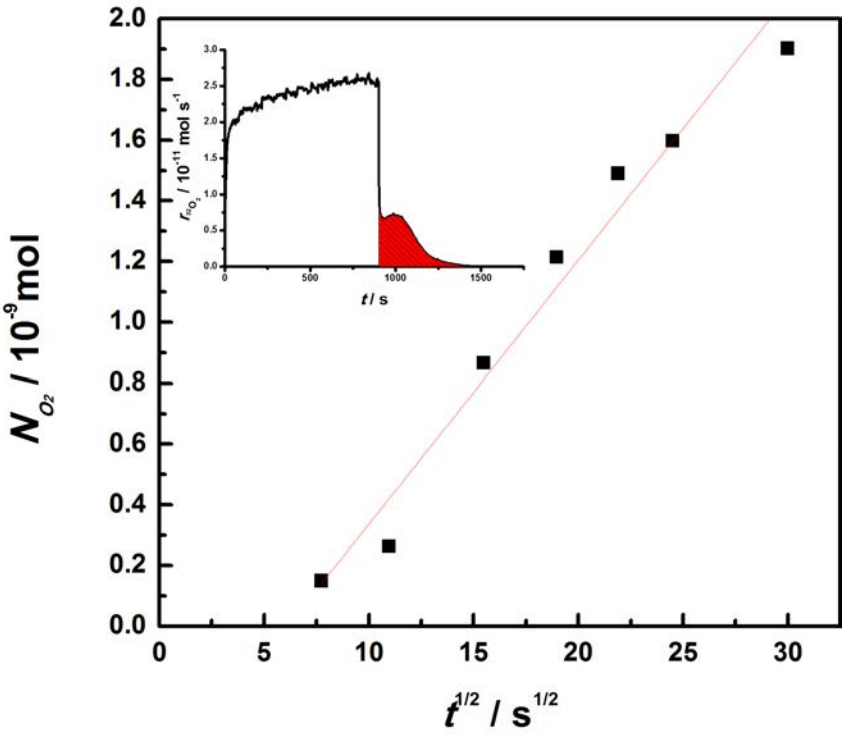

Figure 3.20: Amount of released gaseous oxygen after current interruption for different holding times at 300 °C vs. the square root of the polarization holding time. The amount of released oxygen is calculated from the area of the plateaus in Fig 3.19.

Anodic polarization in the presence of CO

Fig. 3.21 presents the transient effect of an applied current of 10 μA at 300 °C in the presence of CO ($3.5{\cdot}10^{-5}$ Pa). During electrochemical polarization the $^{16}O_2$ and CO_2 signals increase meaning that a part of the pumped oxygen is used for the electrochemical oxidation of CO to CO_2 (equation 3.17).

$$C^{16}O + {}^{16}O^{2-} \rightarrow C^{16}O_2 + 2e^- \tag{3.17}$$

There is a difference of approximately 5 seconds between the onset of CO_2 production and $^{16}O_2$ production upon polarization. Additionally, in the first seconds the CO_2 signal reaches a maximum before decreasing to a steady state value when the $^{16}O_2$ production increases.

This behavior indicates a much lower onset potential for the electrochemically driven CO_2 formation than for the oxygen generation. Only when the potential is high enough, the O_2 evolution sets in as a parallel process competing with the electrochemical CO oxidation, decreasing the CO_2 rate until a new steady state rate is reached. Upon current interruption the O_2 signal decreases to the open circuit value within seconds whereas the CO_2 signal needs approximately 2 minutes to return to the open circuit rate. This slow decrease of the CO_2 rate indicates that a part of the anodically pumped oxygen is stored in the electrode system, which is slowly released after current interruption and can still be used for electrochemical CO oxidation explaining the long time till the OCP is reaching its initial start value.

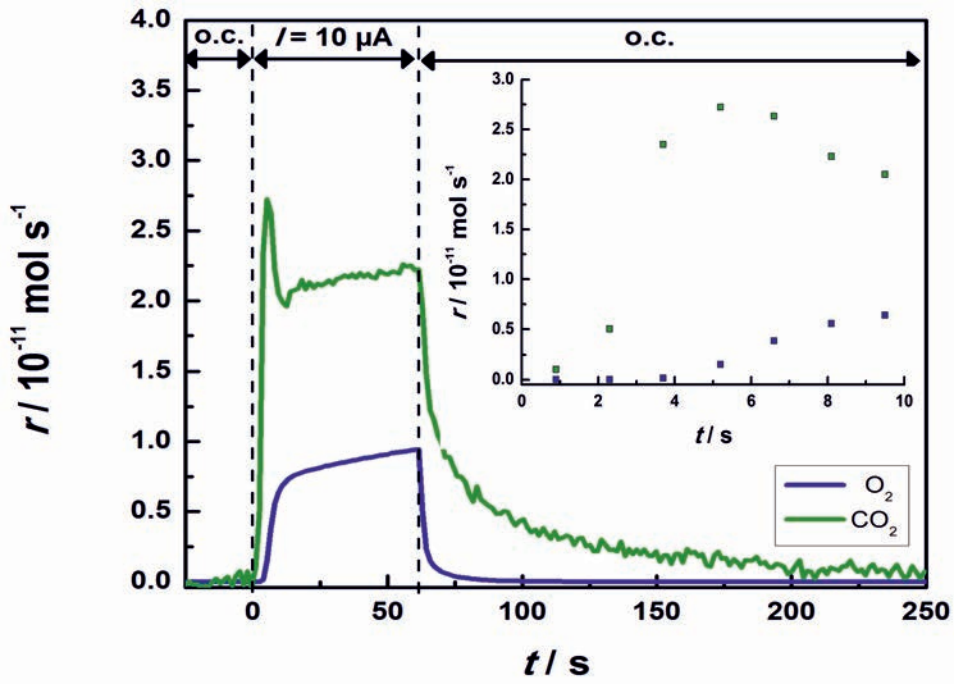

Figure 3.21: MS response during polarization of 10 μA for 60 s in the presence of $3.5{\cdot}10^{-5}$ Pa CO at 300 °C.

Anodic polarization in the presence of reactive gas (CO and $^{18}O_2$)

In the presence of a reactive gas ($C^{16}O$ ($4.46{\cdot}10^{-6}$ Pa) and $^{18}O_2$ ($3.79{\cdot}10^{-5}$ Pa)) the Ag electrode acts as catalyst for CO combustion. Once this catalytic effect is superimposed by an additional electrochemical oxygen pumping, two parameters are useful for the quantification and interpretation of electropromotion effects, i.e. the rate enhancement ratio ρ and the faradaic efficiency Λ [Vaye88, Vaye90, Vaye02].

$$\rho = \frac{r_{CO_2}}{r^0_{CO_2}} \tag{3.18}$$

$$\Lambda = \frac{(r_{CO_2} - r^0_{CO_2})}{\frac{I}{2F}} \tag{3.19}$$

where r_{CO_2} and $r^0_{CO_2}$ present the electropromoted and the initial open circuit rate of CO combustion expressed in $\frac{mol}{s}$ and F is Faraday's constant. The catalytic open circuit rate (r_{CO_2}) is about $8.4{\cdot}10^{-11}$ $\frac{mol}{s}$ at 300 °C. By increasing the temperature the catalytic rate increases to $15.3{\cdot}10^{-11}$ $\frac{mol}{s}$ at 500 °C.

Upon application of 10 μA a 1.11-fold increase in the catalytic rate is observed at 300 °C and an almost similar value of 1.13 at 500 °C (Fig. 3.22 top). The faradaic efficiency at 300 °C is 4.34 and 2.35 for 500 °C, showing a more efficient promotion at lower temperatures. Looking at the mass signal of $C^{16}O_2$ (44 amu) (Fig. 3.22 middle) it can be seen that the rate increase during electrochemical polarization is nearly the same for both temperatures indicating a temperature independent process limitation, which was also confirmed for other temperatures, although at higher temperatures oscillations set in, indicating a periodic release of stored oxygen.

This observation implies that the electrochemical oxidation of CO takes place mainly at the TPB. Therefore, the transient reaction under polarization can be easily divided into two processes, i.e. a faradaic process and a non-faradaic one:

$$C^{16}O + \frac{1}{2}{}^{18}O_2 \rightarrow C^{16}O^{18}O \tag{3.20}$$

Simultaneously to the increase of the mass 44 signal ($C^{16}O_2$) and the mass 46 signal ($C^{16}O^{18}O$), the oxygen signal (Fig. 3.22 bottom) also increases showing a similar behavior as observed in the measurements performed without reactive gas.

Upon current interruption all signals return to their initial state within 30 s, except the mass 46 ($C^{16}O^{18}O$) signal at 300 °C, indi-

cating only a small persistent electropromotion effect.

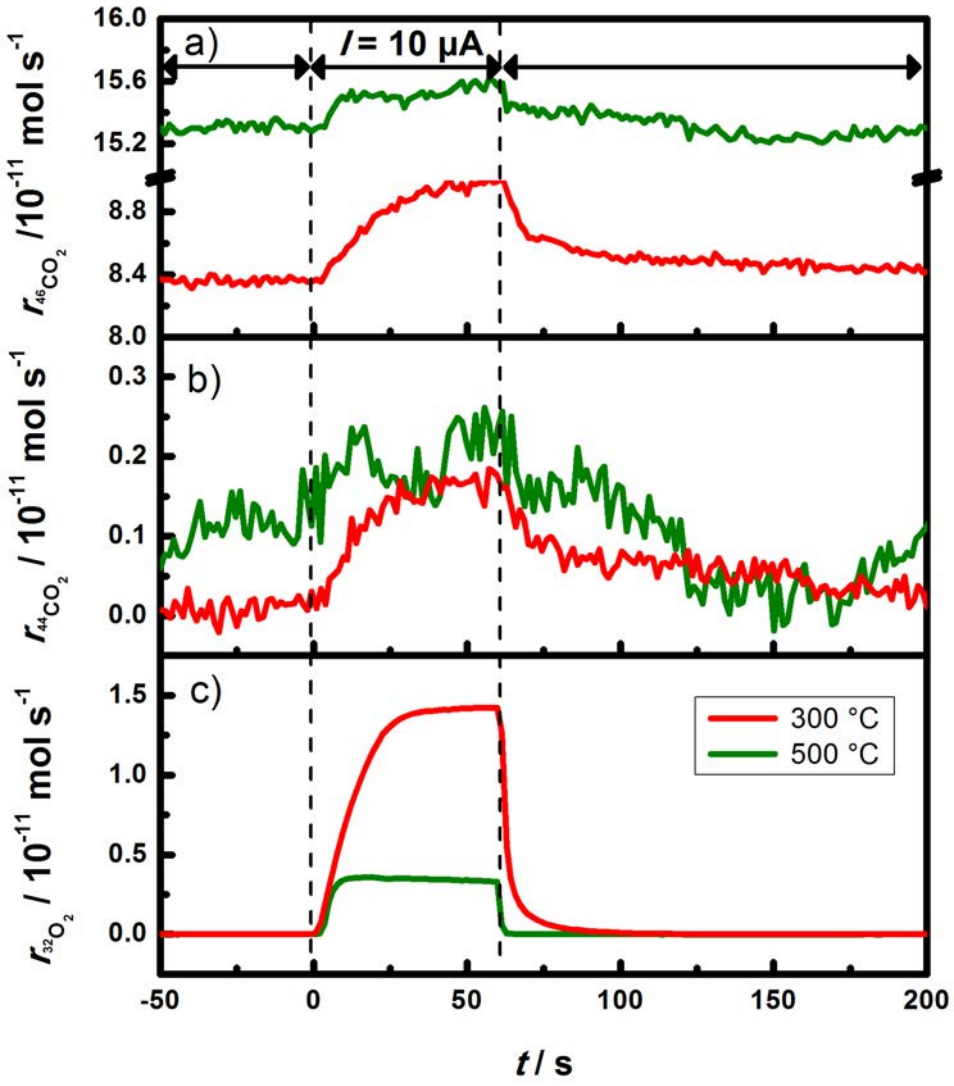

Figure 3.22: MS response during polarization of 10 μA for 60 s in the presence of $4.46{\cdot}10^{-6}$ Pa CO and $3.79{\cdot}10^{-5}$ Pa $^{18}O_2$ at 300 °C and 500 °C.

In agreement with literature the observed electropromotion effect is higher at lower temperatures [Pöpk13]. In general, the electropromotion effect is explained by migration of pumped oxygen onto the surface of the catalyst (spillover) which facilitates the surface reaction by forming a double layer of negatively charged oxygen ions and a positive charge in the metal ($O^{\delta-}$ + $Me^{\delta+}$) [Vaye02]. At

higher temperatures a part of the pumped oxygen is dissolved in Ag and less oxygen is available to form the effective double layer, i.e. the electropromotion becomes smaller. We emphasize that this explanation is a concept which still awaits its ultimate proof, and there is an ongoing discussion on the validity of the spillover concept.

The longer time which is needed by the mass 46 ($C^{16}O^{18}O$) signal at 300 °C to reach its initial start value after current interruption can be explained by storage of pumped oxygen which is released after current interruption and maintains the double layer for a certain period of time.

3.2.4 Discussion

Oxygen incorporation into silver during electrochemical polarization can be achieved in different ways: The arriving oxygen ions can either be discharged at the TPB, dimerize and move towards the Ag surface finally desorbing from the surface as $^{16}O_2$ (Fig. 3.23a), or they can be stored at the Ag/YSZ interface (Fig. 3.23b). Additionally, oxygen can dissolve as atomic oxygen in the Ag lattice (Fig. 3.23c).

$$\mathrm{Ag} + {}^{16}\mathrm{O}^{2-}_{(\mathrm{YSZ})} \rightarrow Ag + {}^{16}O_{(Ag/YSZ)} + 2e^{-} \tag{3.21}$$

$$\mathrm{Ag} + {}^{16}\mathrm{O}^{2-}_{(\mathrm{YSZ})} \rightarrow \mathrm{Ag} + {}^{16}\mathrm{O}_{(\mathrm{Ag})} + 2\mathrm{e}^{-} \tag{3.22}$$

$$\mathrm{O}^{2-}_{\mathrm{YSZ}} \rightarrow \mathrm{O}_{\mathrm{TPB}} + 2\mathrm{e}^{-} \rightarrow \mathrm{O}_{\mathrm{surf}} + 2\mathrm{e}^{-} \tag{3.23}$$

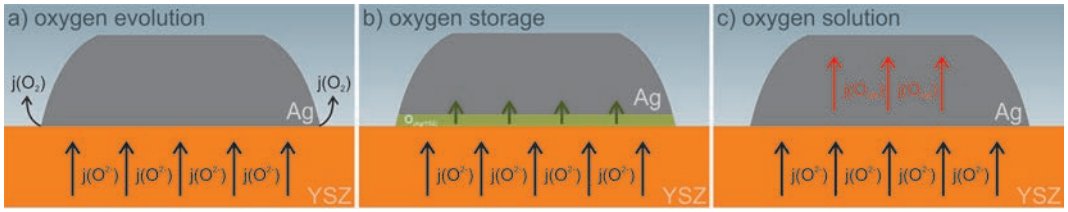

Figure 3.23: Possible paths for the oxygen flux upon anodic polarization. Depending on temperature oxygen ions can be discharged mainly at the TPB and be desorbed as O_2 (a), they can be stored at the interface Ag/YSZ (b) or dissolved in the silver lattice as atomic oxygen (c).

At 300 °C in the absence of reactive gas a part of the anodically pumped oxygen ions are stored at the non-gas exposed area at the Ag/YSZ interface (Fig. 3.24a, (eq. 3.21)), the remaining oxygen ions are discharged at the TPB forming $^{16}O_{2(g)}$ (Fig. 3.24a (eq. 3.14)) or move towards the surface (Fig. 3.24a (eq. 3.23)). Upon current interruption the previously stored oxygen species are mainly releasing oxygen at the TPB which can be detected in the MS by formation of a plateau after current interruption (Fig. 3.24b (eq. 3.23) and (eq. 3.14)). In presence of CO the pumped $^{16}O^{2-}$ ions in the first seconds of electrochemical polarization are used for electrochemical CO oxidation (Fig. 3.24a (eq. 3.17)) as well as for the storage of the oygen species (Fig.3.24a (eq. 3.14)). At a certain potential the oxygen evolution reaction starts reducing the CO_2 formation to a lower steady state value. After interrupting the electrochemical polarization the stored oxygen species are released and migrate to the surface and react with the CO adsorbed on the electrode surface (Fig. 3.24b (eq. 3.17)).

In the presence of $C^{16}O$ and $^{18}O_2$ the silver electrode acts as catalyst for CO oxidation. By application of a positive (anodic) current between working and counter electrode the pumped $^{16}O^{2-}$-ions are

stored at the Ag/YSZ interface hidden at a non-gas exposed area (Fig. 3.24a (eq. 3.21)) or move towards the surface of the electrode mainly through the TPB. Therefore, the oxygen ions can either enhance the catalytic reaction rate (increase in $C^{16}O^{18}O$ signal (46)) by promoting the surface (effective double layer), Fig.3.24 a(eq. 3.23)), they can be partially consumed by reaction with CO (increase in $C^{16}O_2$ signal (44)) (Fig. 3.24a (eq. 3.17)) and they can be directly desorbed as molecular oxygen, especially at 500°C (increase in $^{16}O_2$ signal (32), Fig. 3.24a (eq. 3.14)). Upon current interruption the stored oxygen is released and the resulting oxygen moves to the electrode surface, maintaining the decomposing double layer while becoming slowly consumed (Fig. 3.24a (eq. 3.23)). At 500 °C in the absence of reactive gas during polarization the oxygen ions migrate to the electrode, are discharged and mainly dissolved as oxygen atoms into the lattice of the Ag electrode. To a smaller extent they are discharged and desorbed as $^{16}O_2$ or move towards the surface, as indicated by a promotion effect in the presence of CO. Upon current interruption no oxygen is released from the system due to the high bulk oxygen storage ability of the electrode. In the presence of CO and $^{18}O_2$ the conversion of CO is much higher than at 300 °C. During polarization the oxygen ions either move to the electrode, discharge and desorb to the gas phase or dissolve into the silver lattice. Due to the high temperature a surface oxide formation or formation of an effective double layer is not favored, most of the oxygen is dissolved which explains the weak electropromotion effect. Upon current interruption all signals decrease to their open circuit state in seconds due to the disability to release stored oxygen.

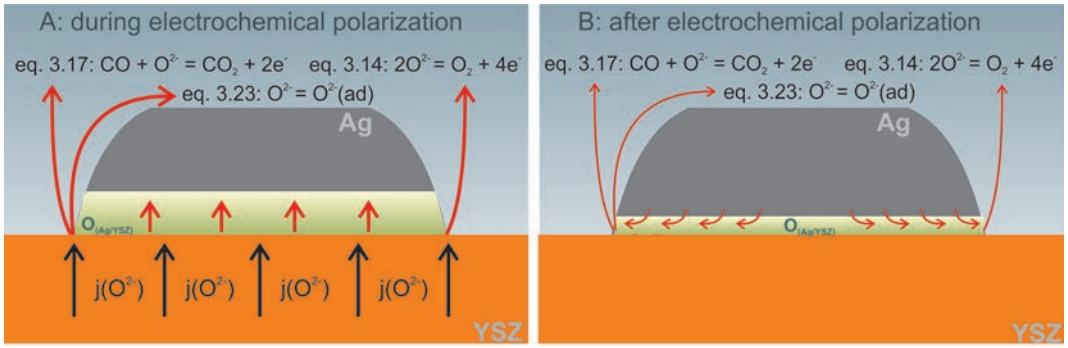

Figure 3.24: Oxygen storage during polarization (a) and oxygen release upon current interruption (b) in the presence of reactive gas at low temperature (300 °C): a) The pumped oxygen is stored at the Ag/YSZ interface and released mainly at the TPB reacting with CO from the gas phase (a), migrating on the surface (b) and desorbing O_2 to the gas phase. 8b) Upon current interruption the stored oxygen at the Ag/YSZ interface decomposes maintaining the processes shown in 8a) in a weakened form.

Chapter 4

Results and Discussion - Part 2: Experiments under ambient reaction conditions

Measurements under high vacuum conditions show a relatively small NEMCA effect with lamda values slightly higher than one and therefore a nearly faradaic behavior. In order to give clear evidence of the NEMCA related behavior of different model type electrodes, typical measurements under ambient pressure conditions with reaction gases in the low mbar range have been conducted. Prior to the electrochemical investigations kinetic measurements were performed to characterize the samples and to explore the correlation between the TPB length and the kinetic behavior of the samples. Therefore, samples with different TPB length have been prepared and the influence of different ratios of p(CO) and $p(O_2)$ was examined.

4.1 Investigation of the kinetic behavior of different model type electrodes under reaction conditions

4.1.1 Introduction

The first part of this chapter deals with the investigation of the catalytic kinetics at model Pt thin film electrodes with different TPB lengths.

Typical catalysts are complex materials and their catalytic behaviour is associated with structural or chemical parameters. Hence, the characterisation of the resulting systems is difficult and the optimisation of the activity and selectivity towards desirable products is challenging. In the last few decades the development of well-defined model systems has allowed the better understanding of reaction mechanisms and kinetics at a microscopic level. Model catalysts can bridge the gap between the microscopic structure on the one hand and the reaction kinetics on the other. This problem is known as the material gap [Freu01].

Nevertheless, the selection of the appropriate model system is still challenging. Model systems should be able to describe the complex structural or chemical features of a real catalyst surface avoiding the complexity of the real system and yet at the same time it should be possible to perform reaction rate measurements. The field is advancing fast but confined to work mainly on unsupported single crystals, like Pt. Moreover, early studies were focused on work under ultra-high vacuum conditions, however most catalytic reactions are performed under atmospheric pressure or even at higher pres-

sure [Henr98]. In recent years there has been significant interest in working with model catalysts at atmospheric or near-atmospheric pressure in order to better understand reaction mechanisms [Gao12, Hend05, West13, Libu05]. Clearly real catalysts (and certainly real noble metal catalysts) tend to be supported. Work on model supported catalysts has focussed on systems where the catalyst is supported on a material which is intended to remain inactive such as alumina (Al_2O_3). However, it is very common for catalysts to be supported on materials that can in some way participate in the reaction. In the case of platinum various active support materials have been used such as reducible oxides like CeO_2 and TiO_2 [Chen10, Lin08]. In such cases there are many possible ways the oxide support could participate in the reaction and mechanisms can be complex [Lin08, Daus90]. These complexities can make experimental design and data interpretation difficult. In order to reduce this complexity here we employ yttria-stabilised zirconia (YSZ, 8mol %) and Al_2O_3 as support materials. Although YSZ exhibits oxygen ion conductivity it has poor electronic conductivity [Larr11]. This results in an oxide that is very difficult to reduce in the bulk. Hence, we might expect YSZ to interact with the catalyst but without the complexity associated with many other support materials. In case of an Al_2O_3 support there should be no contribution to the rate from the support surface under the conditions employed here and furthermore the Al_2O_3 should not modify the active Pt catalyst in any way. It is clear that if we wish to study model-supported catalysts we must control and investigate the role of the length of the three-phase boundary between the support, the catalyst and the gas phase.

Here we use PLD to fabricate dense and well-adhered Pt films on both YSZ and Al_2O_3 surface, i.e. Pt (111)/YSZ (111) and Pt (111)/Al_2O_3 (0001) samples with 9 mm x 9 mm area. These fully covering films are then further treated by a subtractive lithographic technique. Additionally partially dewetted Pt films have been produced by PLD. As a result we obtained TPBs between $3.6{\cdot}10^{-2}$ m ($4.5{\cdot}10^{2}\frac{m}{m^2}$) and 400 m ($4.9{\cdot}10^{6}\frac{m}{m^2}$) (macroscopically determined). The role of the length and the nature of the TPB on the kinetics of the patterned Pt (111) single crystal catalysts for carbon monoxide oxidation were then studied as a function of temperature and partial pressures of oxygen and carbon monoxide at atmospheric pressure. The fact that carbon monoxide oxidation kinetics is so susceptible to the oxygen chemical potential of the Pt surface makes it an ideal system to study [Chen13, Berl88].

The following investigations have been conducted in a long-term research visit in the working group of Prof. Dr. Ian Metcalfe (School of Chemical Engineering and Advanced Materials, University of Newcastle) in cooperation with Dr. Evangelos Papaioannou in Newcastle upon Tyne. A detailed description of the utilized apparatus can be found elsewhere [Poul07]. The own work includes the sample preparation and characterization of the used model electrodes, the realisation of the kinetic measurements and analysis and discussion of the results.

4.1.2 Results and discussion

Sample characterization

In this study lithographic electrodes with different TPB lengths have been investigated, 1 m, 4 m and 16 m ($1.2{\cdot}10^4 \frac{m}{m^2}$, $4.9{\cdot}10^4 \frac{m}{m^2}$ and $2{\cdot}10^5 \frac{m}{m^2}$). The TPB length is obtained by a different amount of holes in the Pt film with a fixed edge length of 5 μm (Fig. 4.1, a-c). The overall change in surface area is small (24 % less for 16,2 m in comparison to 1 m). Additionally, a second type of electrode was prepared. By increasing the deposition temperature and decreasing the amount of pulses during the PLD process partially dewetted electrodes (Fig. 4.1, d) with thicknesses between 50 nm and 130 nm are obtained. A detailed description of the sample preparation and the lithographic process is given in chapter 2.

The average macroscopic TPB length was estimated from the SEM pictures and in the case of the dewetted sample using the software Adobe Photoshop (version CS4 extended). The TPB lengths were 1 m, 4 m and 16 m for the lithographically prepared samples and approximately 400 m ($4.9{\cdot}10^6 \frac{m}{m^2}$) for the dewetted sample. The macroscopic l(TPB) can be estimated from the number of holes ($50{\cdot}10^3$, $200{\cdot}10^3$ and $800{\cdot}10^3$ holes approximately for the 1 m, 4 m and 16.2 m l(TPB) samples, respectively) in a square arrangement with approximate hole diameter of 4.9 μm (it should be noted that the macroscopically observable l(TPB) is not necessarily the same as the microscopic l(TPB); Gauckler et al. [Gaucc11] have shown the importance of grain boundaries, grooves and voids in the electrode in the electrical polarisation of a Pt/YSZ system). Two more Al_2O_3-supported Pt films were prepared with $3.6{\cdot}10^{-2}$

m ($4.5{\cdot}10^2 \frac{m}{m^2}$) and 1 m ($1.2{\cdot}10^4 \frac{m}{m^2}$) l(TPB) for the lithographically prepared samples and approximately 400 m ($4.9{\cdot}10^6 \frac{m}{m^2}$) for the dewetted sample. The $3.6{\cdot}10^{-2}$ m ($4.5{\cdot}10^2 \frac{m}{m^2}$) l(TPB) Al_2O_3-supported Pt film did not contain any holes and the macroscopic l(TPB) was similar to the geometric perimeter of the Pt film.

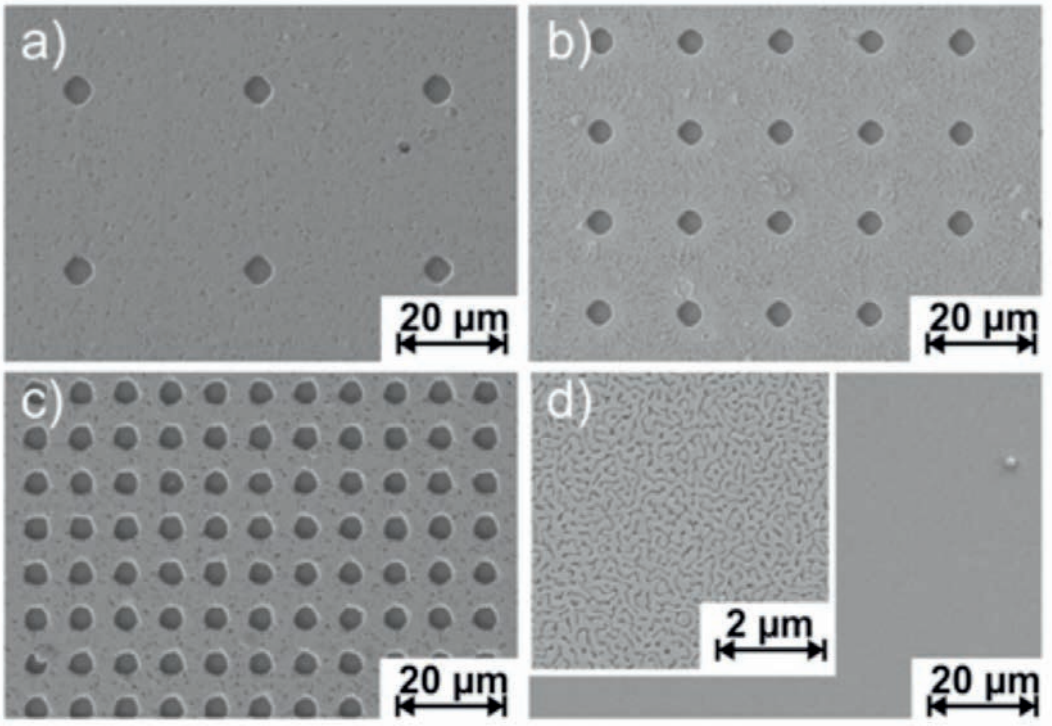

Figure 4.1: SEM images of electrodes with different TPB length: a) 1 m, b) 4 m, c) 16.2 m d) 400 m.

Atomic force microscopy (AFM) was used to further characterise the surface of the Pt films as well as the walls of the holes in the film. AFM experiments were conducted on an Agilent 5500 AFM microscope in air. Images were obtained in contact mode using nitrogen doped silicon tips with a force constant of 0.02-0.77 $\frac{N}{m}$. Typical scan rates were in the range of 0.5 - 1 kHz and 512 by 512 pixel resolution. Image processing was performed using version 5.1.6 of the Scanning Probe Image Processor (SPIP) software (Im-

age Metrology, Lyngby, Denmark). The AFM topographic images (Fig. 4.2) show a platinum wall exhibiting pile up and imperfections, unavoidable defects of the fabrication process.

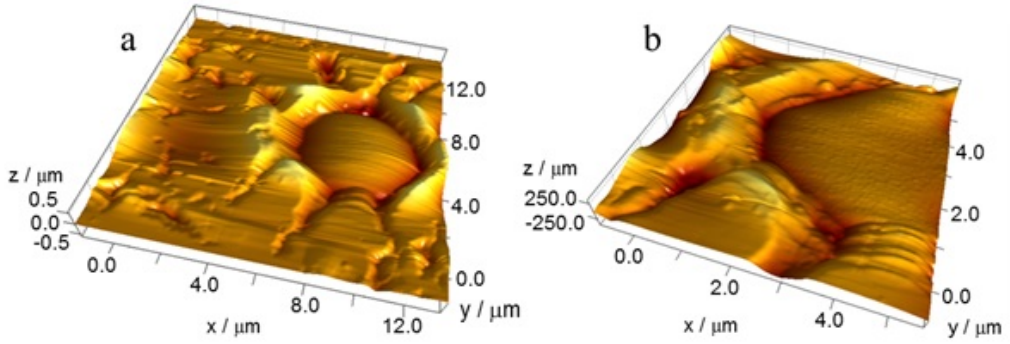

Figure 4.2: AFM image (a) of a hole and (b) the side walls of a hole of the Pt film (1m l(TPB)) deposited on YSZ.

All samples were characterized after the preparation process and before any experimental work with XRD showing single crystalline (111) orientation. XPS and SIMS measurements have been performed to exclude the influence of impurities during the preparation process.

It is worth mentioning that HRSEM micrographs and X-ray analysis obtained after the experiments showed no morphological changes and no change in the crystalline structure of the Pt film supported either on YSZ or Al_2O_3.

Experimental rig for kinetic evaluation

A continuous flow single chamber reactor with a total gas phase volume of 30 cm^3 was used for the catalytic experiments. The flow of gas to the reactor was controlled by electronic mass flow

controllers (MFCs). The gases used were 20% CO/He, 20% O_2/He and CP grade He (N5) provided by BOC Ltd. with typical flow rates at 150 $\frac{mL}{min}$. The flow rates were also measured at the outlet using a Varian digital flow meter (1000 series). Helium was used as a balanced gas throughout the experiments. All experiments were conducted under atmospheric pressure and flow rates are given at standard temperature and pressure (STP). The carbon dioxide (CO_2) concentration in the product stream was analysed using a X-STREAM-CO_2 analyser provided by Rosemount.
Reaction rates (r_{CO_2}) in terms of carbon dioxide production are calculated as shown in equation 4.1:

$$r_{CO_2} = Y_{CO_2} \cdot n^{\cdot} \cdot A^{-1} \tag{4.1}$$

where Y_{CO_2} is the measured carbon dioxide mole fraction at the gas outlet and $n^{\cdot}$ is the molar flow rate normalized by Pt area A. In this study we use the term superficial area to describe the area of the external facets of the dense Pt single crystal and the term pore wall area to define the area of the vertical walls inside the holes. The total Pt area is the sum of the superficial area and the pore wall area. Table 4.1 shows the superficial area, the pore wall area, the total Pt area and the moles of Pt corresponding to the total area for the samples used in this study. The minimum detection value for the X-STREAM-CO_2 analyser is 1 ppm CO_2 which corresponds in $1.1 \cdot 10^2$ $\frac{mol}{s}$. In order to be able to measure the reaction rate under known conditions the reactor was operated under conditions of differential conversion (20% conversion of carbon monoxide or less).

Support	TPB length (m)	Superficial Pt area ($10^{-5}m^{-2}$)	Pore wall Pt area ($10^{-5}m^{-2}$)	Total Pt area ($10^{-5}m^{-2}$)	Moles of Pt atoms** (10^{-10})
YSZ and Al_2O_3	400	5.76*	-	-	12.3*
YSZ	16.2	6.6	1.22	782	16.7
YSZ	4	7.79	0.303	8.09	17.2
YSZ and Al_2O_3	1	8.00	0.076	8.07	17.2
Al_2O_3	$3.6 \cdot 10^{-2}$	8.10	0	8.10	17.3

Table 4.1: Characteristic Pt surfaces and moles of Pt atoms used for the calculation of normalized rates and turnover frequencies. (*For the 400 m l(TPB) sample we used the area that calculated approximately from HRSEM micrograph via Photoshop software. The TOF calculation is based on this area. **Based on the total area.)

The kinetic behaviour of the samples in the carbon monoxide oxidation was firstly evaluated as a function of temperature. To study the effect of temperature the samples were heated in a gas mixture of 1.3 kPa of oxygen and 0.5 kPa of carbon monoxide from 150 °C up to 350 °C. The temperature was held during heating after each step of 20 °C, the holding time being varied between 1 h and 3 h depending on the time the reaction rate needed to become steady (the carbon dioxide production rate did not vary by more than ±5 % over 1h). The heating rate between the isothermal periods was 10 $\frac{^{\circ}C}{min}$.

Secondly, the rate dependence on $p(\mathrm{CO})$ and $p(\mathrm{O_2})$ was also examined. In these experiments $p(\mathrm{CO})$ is held constant and $p(\mathrm{O_2})$ is allowed to vary (oxygen kinetics) or vice versa (carbon monoxide kinetics) at 288 °C. Studying the influence of oxygen $p(\mathrm{CO}) = 0.5$ kPa was held constant and $p(\mathrm{O_2})$ was stepwise varied between 1.2 kPa and 13.5 kPa for the Pt samples with l(TPB) of 1, 4 and 16.2 m ($1.2{\cdot}10^4 \frac{m}{m^2}$, ($4.9{\cdot}10^4 \frac{m}{m^2}$) and ($2{\cdot}10^5 \frac{m}{m^2}$) and between 0.2 kPa and 13.5 kPa for the Pt sample with l(TPB) of 400 m ($4.9{\cdot}10^6 \frac{m}{m^2}$) with a varying step size of 0.6 kPa up to 4 kPa. In a second series of experiments $p(\mathrm{O_2}) = 0.64$ kPa was held constant and $p(\mathrm{CO})$ was stepwise varied between 0.5 kPa and 15 kPa with a varying step size of 0.6 kPa up to 2.8 kPa.

Temperature dependence of CO oxidation rate

Figure 4.3 shows the reaction rate of carbon dioxide formation (r_{CO_2}) as a function of temperature over the two different $\mathrm{Pt/Al_2O_3}$ samples with l(TPB) of $3.6{\cdot}10^{-2}$ m ($4.5{\cdot}10^2 \frac{m}{m^2}$) and 1 m ($1.2{\cdot}10^4 \frac{m}{m^2}$). The ratio of the pore wall Pt area to the total Pt area for the two samples is different. For the $3.6{\cdot}10^{-2}$ m ($4.5{\cdot}10^2 \frac{m}{m^2}$) l(TPB) sample this ratio is zero, i.e. there are no pore wall sites, while for the 1 m ($1.2{\cdot}10^4 \frac{m}{m^2}$) l(TPB) sample this ratio equals $9.4 \cdot 10^{-3}$ or is just below 1%. It can be seen that the minimum temperature for a measurable rate was around 310 °C for both samples. Below 300 °C no rate could be measured. The activity of $\mathrm{Pt/Al_2O_3}$ seems not to depend strongly on the number of sites in the pore wall available

and we tentatively conclude that reactivity of these pore wall sites are not different from the Pt (111) sites of the superficial area in kinetic terms (at least in the presence of an inactive support). This is consistent with the structure insensitive nature of CO oxidation over Pt/Al_2O_3 [Alli11]. Henceforth we normalize the reaction rates on a surface area basis considering that pore wall sites and superficial Pt (111) sites to be catalytically equivalent. The total Pt area is thus used in the normalization of the formation rates of carbon dioxide (r_{CO_2}). Even though the superficial Pt area differs between the two Pt/Al_2O_3 samples with different l(TPB) the total area of Pt remains similar. The rates of reaction (carbon dioxide formation) are also expressed in terms of turnover frequencies (TOF), which is defined as the number of carbon dioxide molecules produced per active site per second. Since the number of active sites is not strictly known, we calculate the total number of Pt surface atoms, z, and assume that there is one active site per surface Pt atom. Estimation of the number of Pt surface metal atoms is rather straightforward since the geometric surface area is known and the number density of surface atoms is known. We note that the dominant structural feature that differentiates the samples is the TPB length which of course resides next to the pore wall. In case of oxygen spillover using an active support caution should be used when interpreting the data as the pore wall active sites might behave differently than the superficial sites. This would be difficult to distinguish from the simple presence of interface.

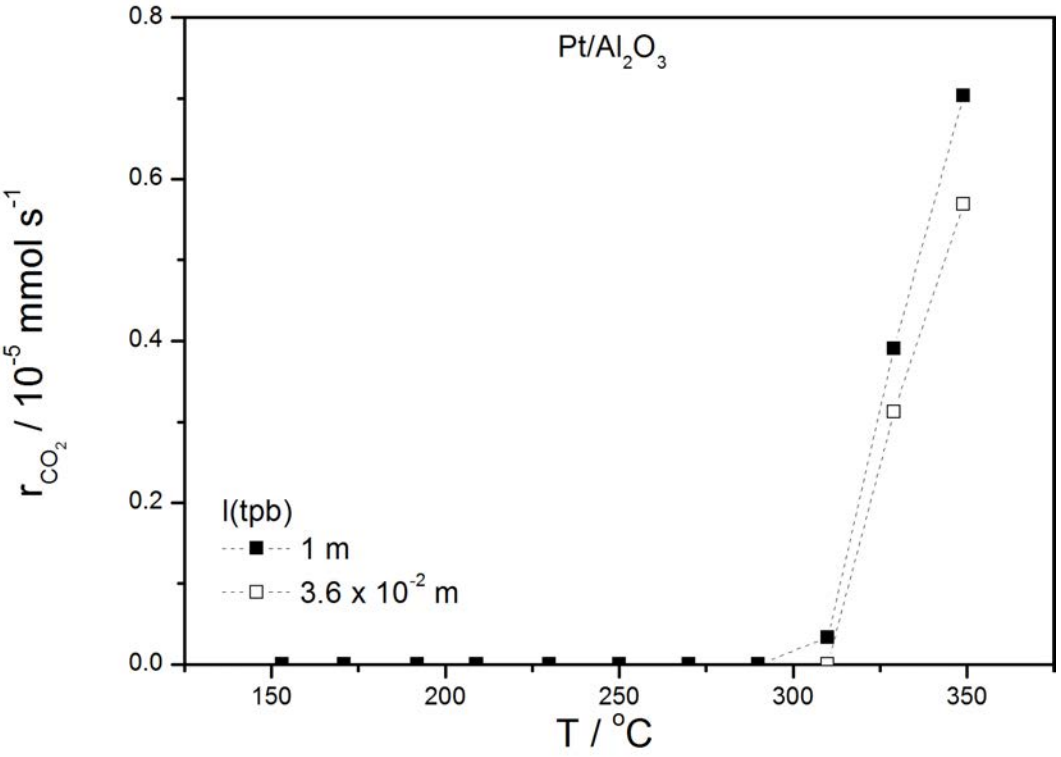

Figure 4.3: Effect of temperature on carbon dioxide formation rate (r_{CO_2}) over Al_2O_3 supported Pt samples with different l(TPB) ($3.6{\cdot}10^{-2}$ m and 1 m) in a feed gas mixture of $p(O_2)$ = 1.3 kPa and $p(CO)$ = 0.5 kPa. Total gas flow rate: 150 $\frac{mL}{min}$. The drawn dashed lines in the figure are only a guide to the eye.

Figure 4.4 shows the effect of temperature on the carbon dioxide formation rate (r_{CO_2}) and on the TOF values over four different Pt/YSZ samples with l(TPB) of 1 m ($1.2{\cdot}10^4 \frac{m}{m^2}$), 4 m ($4.9{\cdot}10^4 \frac{m}{m^2}$), 16.2 m ($2{\cdot}10^5 \frac{m}{m^2}$) and approximately 400 m ($4.9{\cdot}10^6 \frac{m}{m^2}$) and two Pt/Al_2O_3 sample with 1 m ($1.2{\cdot}10^4 \frac{m}{m^2}$) and approximately 400 m ($4.9{\cdot}10^6 \frac{m}{m^2}$) l(TPB). When Pt is supported by YSZ, facilitating spillover, an increasing l(TPB) appears to be correlated with higher reaction rates. The minimum temperature for a measurable rate for the lithographic samples was 225 °C approximately. Above this temperature the rate (r_{CO_2}) increases for the samples until the maximum operating temperature at 350 °C is reached. The Pt/YSZ

sample with 1 m ($1.2{\cdot}10^4 \frac{m}{m^2}$) l(TPB) showed a maximum rate of 0.33 $\frac{mmol}{m \cdot s^2}$ whereas the sample with a l(TPB) of 4 m ($4.9{\cdot}10^4 \frac{m}{m^2}$) and 16.2 m ($2{\cdot}10^4 \frac{m}{m^2}$) showed maximum values of 0.86 $\frac{mmol}{s \cdot m^2}$ and 1.10 $\frac{mmol}{s \cdot m^2}$, respectively. In contrast to the patterned samples the sample with l(TPB) of 400 m ($4.9{\cdot}10^6 \frac{m}{m^2}$) presents somewhat different behavior. The minimum temperature for a measurable rate is significantly decreased to 188 °C. A steep increase in the reaction rate between 210 °C and 220 °C and an almost linear increase in rate versus temperature above 220 °C is observed. The maximum rate was 2.07 $\frac{mmol}{s \cdot m^2}$ at 350 °C. We emphasize that the Pt/Al_2O_3 samples exhibited very low reaction rates compared to the Pt/YSZ samples.

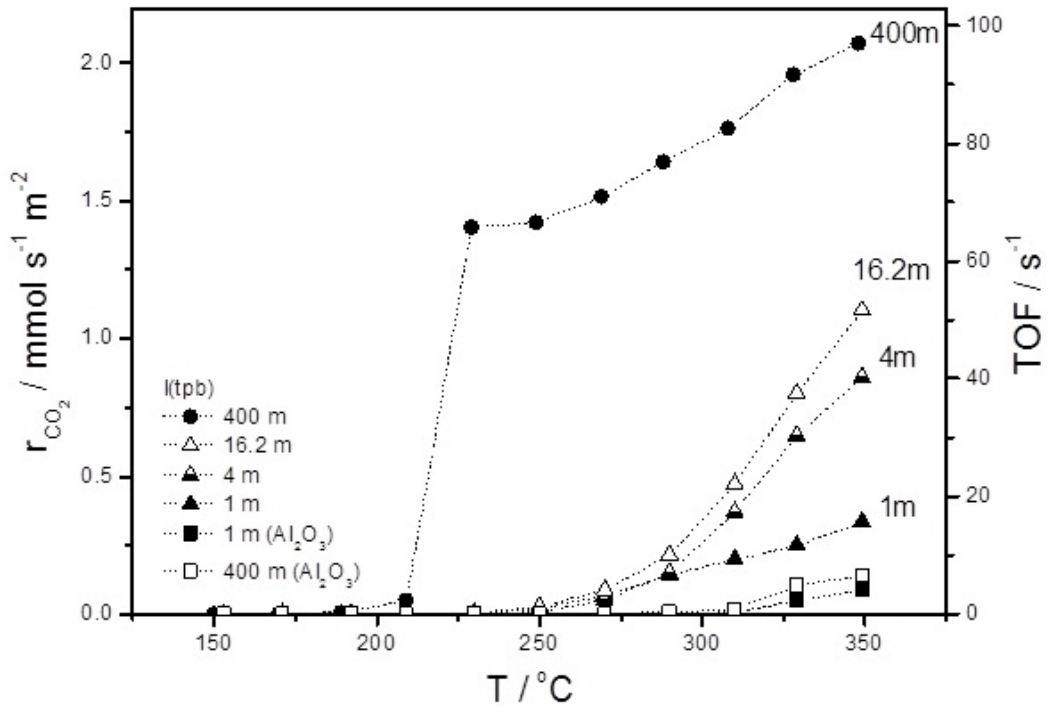

Figure 4.4: Temperature dependence of the CO oxidation rate over samples with different TPB length at an oxygen partial pressure of 1.3 kPa and a CO partial pressure of 0.5 kPa.

Oxygen kinetics with a constant CO partial pressure

Figure 4.5 shows the variation r_{CO_2} and TOFs with $p(O_2)$ at fixed p(CO) over four different Pt/YSZ samples with different l(TPB) and two Pt/Al_2O_3 samples with 1 m ($1.2{\cdot}10^4 \frac{m}{m^2}$) and approximately 400 m ($4.9{\cdot}10^6 \frac{m}{m^2}$) l(TPB) at 288 °C. For the YSZ-supported samples with l(TPB) higher than 1 m ($1.2{\cdot}10^4 \frac{m}{m^2}$) the carbon dioxide formation rate increases with increasing $p(O_2)$ undergoing a transition from a low rate to a high rate. The $p(O_2)$ required to achieve the step transition in rate here is lower for samples with a greater l(TPB). The onset of the higher catalytic activity state over the 400 m ($4.9{\cdot}10^6 \frac{m}{m^2}$) l(TPB) sample occurs at a very low $p(O_2)/p$(CO) ratio such that it is difficult to precisely comment on where the transition lies while the transition over the 4 m ($4.9{\cdot}10^4 \frac{m}{m^2}$) and 16.2 m ($2.5{\cdot}10^5 \frac{m}{m^2}$) l(TPB) samples occurs at $p(O_2)/p$(CO) ratios of approximately 13-16 (i.e. oxygen partial pressures of 6.6 to 8 kPa). The sample with l(TPB) of 400 m ($4.9{\cdot}10^6 \frac{m}{m^2}$), during the high catalytic activity state, exhibits a carbon dioxide formation rate that is insensitive to further increases in oxygen partial pressure for $p(O_2)/p$(CO) up to 12. The rate seems to decrease under highly oxidizing conditions. In the high catalytic activity state the catalytic rates are one order of magnitude greater than those observed before the rate transition for the samples with 4 m, 16.2 m and 400 m ($4.9{\cdot}10^4 \frac{m}{m^2}$, $2{\cdot}10^5 \frac{m}{m^2}$ and $2{\cdot}10^6 \frac{m}{m^2}$) l(TPB). In the high catalytic activity state the TOF values are up to 80 s^{-1} for the samples with 16.2 m ($2{\cdot}10^5 \frac{m}{m^2}$) and 400 m ($4.9{\cdot}10^6 \frac{m}{m^2}$) l(TPB) and up to 70 s^{-1} for the sample with 4 m ($4.9{\cdot}10^4 \frac{m}{m^2}$) l(TPB) (values taken at $p(O_2)/p$(CO) = 26). It is interesting to note that a

similar rate transition to a high catalytic activity state is not observed with the samples with 1 m ($1.2{\cdot}10^4 \frac{m}{m^2}$) l(TPB) where Pt is supported either on YSZ or Al_2O_3 and with the sample with 400 m ($4.9{\cdot}10^6 \frac{m}{m^2}$) l(TPB) where Pt is supported on Al_2O_3. However, this does not mean that a transition to a high catalytic activity state would not be seen at even higher $p(O_2)/p(CO)$.

For the YSZ-supported samples, the carbon dioxide formation rate increases with increasing $p(O_2)/p(CO)$ ratio undergoing a transition from a low rate to a high rate. Similar rate transition to a high catalytic activity state is not observed with the Al_2O_3 supported samples.

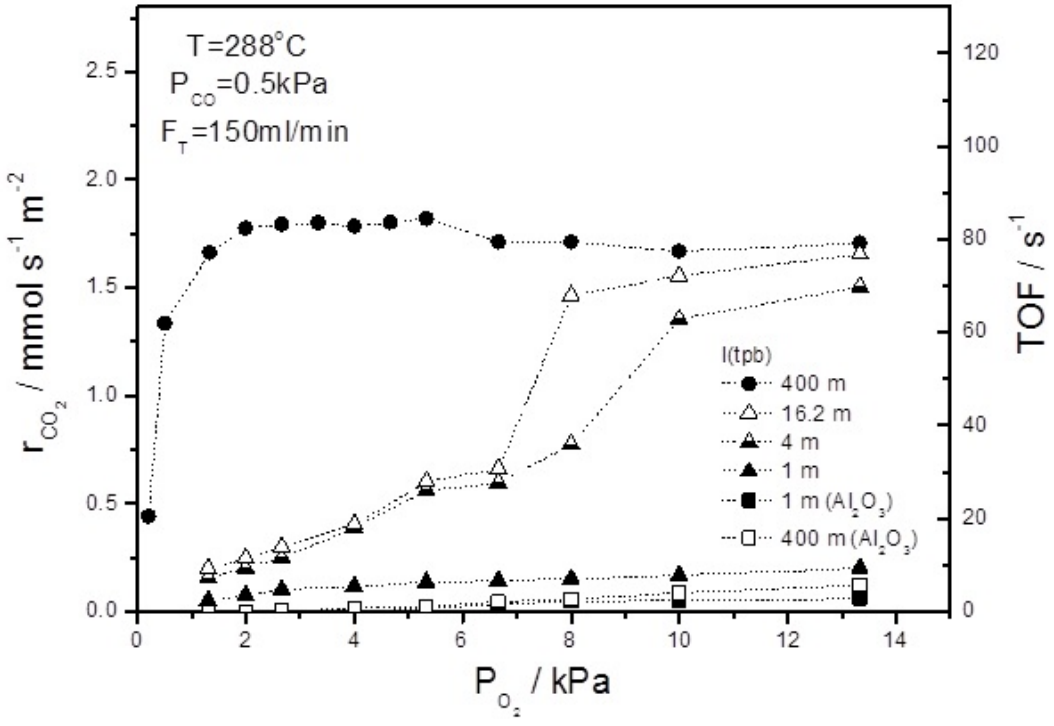

Figure 4.5: Oxygen kinetics for CO oxidation at a $p(CO) = 0.5$ kPa and a temperature of 288 °C.

The transition from a low catalytic activity state to a high catalytic activity state has been identified by other authors on supported and unsupported Pt single crystals upon increasing the $p(O_2)/p(CO)$ ratio at various pressures. Hendriksen et al. has shown that Pt (110) surfaces undergo a structural phase transition, which correlates with an enhanced catalytic rate at sufficiently low carbon monoxide to oxygen ratio [Hend02]. Ackermann et al. was the first to study the restructuring of Pt (110) surfaces under reaction conditions at pressures up to 50 kPa and temperatures up to 350 °C [Acke05]. Other work has shown that Pt (111) surfaces also exhibit a significant increase in activity in going from a reducing to oxidising gas atmosphere [Chen07]. Rinnemo [Rinn97] showed that this steap increase in activity over Pt (111) depends on the carbon monoxide and oxygen partial pressures ($p(CO)$ and $p(O_2)$ respectively). As the $p(O_2)/p(CO)$ increases, the step transition to a higher activity state is shifted to higher temperatures. Somorjai et al. [Somo97] reported a similar step increase in TOF values from 20 s^{-1} to 1400 s^{-1} at 450 °C for carbon dioxide production over unsupported Pt (557) single crystals at a total pressure of 102 kPa for $p(O_2)/p(CO) = 2.5$. They also observed qualitative similarities for (111) and (100) Pt crystal faces. Similar results have been obtained for supported Pt single crystals. Farkas et al. [Fark13] studied the carbon monoxide oxidation over Pt (111) thin films supported on YSZ similar to the sample with 400 m ($4.9{\cdot}10^6 \frac{m}{m^2}$) l(TPB) used in this study under mildly oxidizing reaction conditions with excess oxygen and total pressures up to 1.3 kPa. They observed a transition to a higher catalytic activity state with TOF values rising from 650 s^{-1} to 950 s^{-1} at 388 °C at $p(O_2)/p(CO) = 1.6$. At higher tem-

perature (484 °C) the transition to a higher catalytic activity state was observed at lower $p(O_2)/p(CO) = 0.7$.

Clearly the nature of the transition from a lower to higher activity state is complex and depends upon both operating temperature and pressure. While TOF values are of similar orders of magnitude to the literature, our work also demonstrates that the kinetics of carbon dioxide formation over the YSZ-supported samples is dependent upon the l(TPB) with the rate transition being shifted to lower $p(O_2)/p(CO)$ for higher l(TPB). To our best of knowledge this relationship has not been seen before by anyone working with model systems.

It is possible that the Pt active sites close to the three phase boundaries are modified due to the presence of YSZ support. This can modify the adsorption/desorption energies of the reacting species and influence the overall catalytic activity of the Pt. It is also possible that discrete Pt particles (atoms or clusters of atoms) located on the YSZ in the close proximity of the three phase boundaries and not visible by SEM may offer additional active sites for reaction. The surface area of these Pt particles would be very small to influence the activity unless they were modified electronically by the support. It is also possible that this change in the kinetic behaviour is due to the chemical potential difference of oxygen between the YSZ or Al_2O_3 surface and the Pt surface. This oxygen chemical potential difference is a natural consequence of the difference in carbon monoxide oxidation activity of the YSZ or Al_2O_3 surface (low activity) and the Pt surface (high activity). The albeit low electronic conductivity of YSZ may facilitate such transfer of oxygen. We speculate that this low electronic conductivity per-

mits oxygen reduction on the YSZ surface. In turn these oxygen species may spillover onto the Pt surface under the chemical potential driving force mentioned above resulting in the formation of surface oxygen species which may influence the catalytic activity of the Pt.

CO kinetics with different constant oxygen partial pressures

Additionally, experiments at different $p(\mathrm{CO})$ were performed over four different Pt/YSZ samples with different $l(\mathrm{TPB})$ and two different Pt/Al_2O_3 sample with 1 m ($1.2{\cdot}10^4 \frac{m}{m^2}$) and approximately 400 m ($4.9{\cdot}10^6 \frac{m}{m^2}$) $l(\mathrm{TPB})$ (Fig. 4.6). The $p(O_2)$ was held constant, while $p(\mathrm{CO})$ was increased. It is well established that strong adsorption of carbon monoxide at this temperature will lead to a reaction rate that will eventually decrease with increasing $p(\mathrm{CO})$ [Berl88].

Figure 4.6 shows that the rate appears to decrease for $p(\mathrm{CO}) <$ 1 kPa as expected for all samples. However, for all but the YSZ supported sample with 400 m ($20{\cdot}10^4 \frac{m}{m^2}$) l (TPB), increasing rates with $p(\mathrm{CO})$ are eventually attained for the YSZ-supported samples (at high $p(\mathrm{CO})$). We speculate that this rate may be due to reverse oxygen spillover from the YSZ over onto the catalyst surface which would result in a rate increase as a result of the spillover oxygen consumed but may also result in a secondary rate increase because of the modified coverage in the affected interfacial region. It is noteworthy that the rate for the Pt/Al_2O_3 samples is below measurable limit.

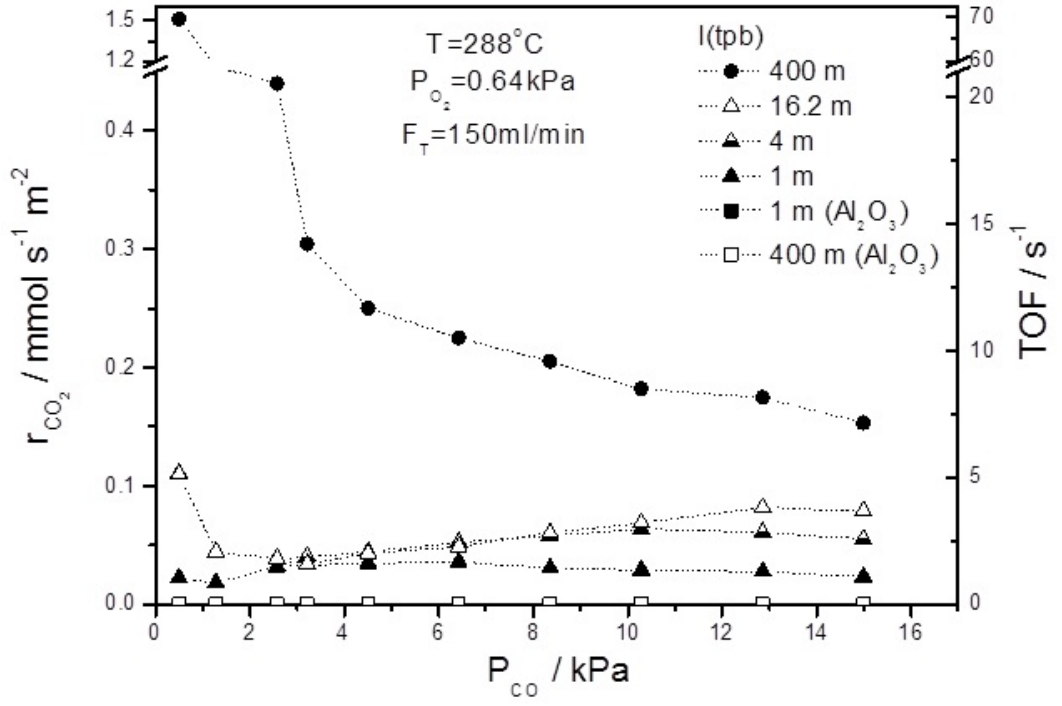

Figure 4.6: p(CO) dependence for CO oxidation at $p(O_2)$ = 0.64 kPa and a temperature of 288 °C.

4.1.3 Conclusion

In this study the role of the length and the nature of the TPB on the kinetics of patterned Pt (111) single crystal catalysts for CO oxidation was studied as a function of temperature and $p(O_2)$ and p(CO) at atmospheric pressure. We studied a series of supported platinum catalysts (supported on single crystal YSZ or Al_2O_3 support) which exhibit lengths of three phase boundary that vary over four orders of magnitude from $3.6{\cdot}10^{-2}$ m ($4.5{\cdot}10^2 \frac{m}{m^2}$) to 400 m ($4.9{\cdot}10^6 \frac{m}{m^2}$). The results suggest that the reaction rate of carbon dioxide formation undergoes a transition from a low rate regime to a high catalytic activity state at a particular $p(O_2)/p$(CO) ratio. The $p(O_2)/p$(CO) for the transition to the higher catalytic activity state depends upon the length of TPB with $p(O_2)/p$(CO) associ-

ated with the transition shifted to lower values for higher lengths of TPB. At the high catalytic activity state TOF values of 80 s^{-1} were obtained at 288 °C under atmospheric total pressure for the YSZ-supported samples with l(TPB) higher than 16.2 m ($2{\cdot}10^5 \frac{m}{m^2}$). It is hypothesized that this change in kinetic behaviour is due to the role of a surface oxygen species that undergoes reverse spillover at the three phase interface.

4.2 Investigation of the origin of electrochemical promotion in terms of surface oxidation under reaction conditions

4.2.1 Introduction

The following part of this chapter deals with the electrochemical behaviour of the platinum metal electrodes at ambient pressure conditions and focuses especially on the electrochemical promotion. The main goal is to identify the (pre)conditions which are necessary to obtain electrochemical promotion and help to explain the ambiguous results obtained in literature.

The catalytic oxidation of hydrocarbons to carbon dioxide and water over platinum group metals has attracted major attention in the last years due to its importance in exhaust after-treatment in automobiles [Plia97, Barb94, Harm00]. Ethylene oxidation over the catalyst/electrode system Pt/YSZ was one of the first reactions which was investigated in terms of the NEMCA effect and which shows the highest lambda values so far, meaning that it provides the most efficient enhancement in terms of polarization [Bebe89].

From the thermodynamic point of view, the anodic polarization of a metal electrode on an oxygen solid electrolyte corresponds to a local increase of the chemical potential of oxygen at the potential-controlling electrode interface and may easily lead to oxidation of a metal electrode [Hörl13, Pöpk11.3, Pöpk12, Pöpk13]. In this context it is important to note that heterogeneous catalytic systems often work at the edge of oxide stability and can exhibit oscillations in the catalytic conversion rate - indicating two different states of activity at the surface. Depending on the catalytic system the nature of these oscillations may have their origin in the coverage-dependent heat of adsorption [Sche77, Piki77, Slin78], reconstruction of the surface due to formation and decomposition of a metal oxide [Fark13, Hend10], and surface temperature oscillations [Dago76]. Also impurities which can activate or poison the surface can drive the system from an inactive state to an active one and vice versa [Yent88, Ibra12]. Potential driven segregation to the surface and back has also been demonstrated [Muto08.2, Hube12, Hube12.2, Muto12]. For ethylene oxidation over platinum and other metals like Ag and Rh as well as for the CO oxidation over different metals formation and decomposition of an oxide species is the most likely explanation for oscillations [Fark13, Bara05, Onke92, Jime12.2].

In this study we used the model type electrode system Pt/YSZ(111) for the electrochemically promoted catalytic oxidation of ethylene to investigate the NEMCA effect and to shed more light on the origin of the effect and on the nature of the proposed spillover species - taking platinum oxide formation into account. We investigated three different types of platinum electrodes (dense films, porous and

pasted films) to cover most of the electrode types used in previous work so far. To reduce the disturbing influence of impurities we prepared both porous and dense electrodes by pulsed laser deposition of nominally pure platinum. The first part of this chapter deals with the temperature dependence of the open circuit reaction rate of ethylene oxidation on freshly prepared electrodes and the same electrodes after deactivation for 24 hours as well as with the influence of temperature cycling with a constant heating/cooling rate. The second part focuses on the changes of the conversion rate during a temperature-controlled deactivation step and subsequent reactivation with and without polarization. The last part shows the influence of the sample treatment on the catalytic activity enhancement during electrochemical polarization.

4.2.2 Experimental Part

The catalytic reaction experiments were carried out in a continuous flow atmospheric pressure single-chamber quartz reactor with a volume of 50 cm^3. C_2H_4 (Linde, 99.9 %) and O_2 (PRAXAIR, 99.999 %) were used as reactive gases to investigate the total oxidation of ethylene:

$$C_2H_4 + 3O_2 \rightarrow 2CO_2 + 2H_2O \tag{4.2}$$

A fixed flux of 420 $\frac{cc}{min}$ was adjusted with a fixed gas composition of $p(O_2) = 8.0$ kPa and $p(C_2H_4) = 0.2$ kPa and He as carrier gas. The reaction product concentration (CO_2) was analyzed with an infrared analyzer (X-Stream, Emerson Process Management). For electrochemical measurements a galvanostat-potentiostat (Gamry

Reference 600) was used to apply a constant current of 10 μA for 1800 seconds. All electrochemical measurements were carried out at a temperature of 300 °C, as it has been reported that Pt/YSZ electrodes typically exhibit very high ρ and Λ values at this temperature [Vaye01].

4.2.3 Results

Sample characterization

Pt electrodes with geometrical surfaces of 64 mm^2 and three different morphologies (paste, porous and de-wetted) have been investigated. A detailed description of the sample preparation is given in chapter 2. For electrochemical measurements a catalytically inactive gold paste counter electrode (Du Pont 5771 Conductor paste) was placed in a symmetrical face to face arrangement on the opposite side of the YSZ pellet next to the reference electrode to ensure a symmetrical current and potential distribution. To stabilize the morphology and to sinter the gold paste the Pt paste electrodes and the porous Pt electrodes were annealed for 3 hours at 750 °C in air. For the de-wetted Pt electrodes the counter and reference electrodes were painted on the YSZ single crystals and sintered at 750 °C for 3 hours before the PLD process was started and no after-treatment was performed.

The thickness of the electrodes, determined by profilometric measurements using an Alpha-Step instrument (Alpha-Step IQ, KLA Tencor), was estimated as being 1 μm - 2 μm for the paste electrodes, 100 nm - 200 nm for the porous electrodes and 50 nm - 100 nm for the de-wetted electrodes. The different surface mor-

phologies were confirmed by scanning electron microscopy (SEM, Merlin (Zeiss)) and the composition was investigated with X-ray photoelectron spectroscopy (PHI 5000 VersaProbe (ULVAC-PHI, inc.)). The analysis shows that the samples prepared with PLD contain no impurities (within the detection limits) whereas the Pt paste electrodes contain small amounts of Si and Fe [Muto08, Muto09].

Temperature cycling

Fig. 4.7 shows the temperature dependence of the open circuit catalytic rate for ethylene oxidation in a fixed gas mixture ($p(O_2)$ = 8.0 kPa, $p(C_2H_4)$ = 0.2 kPa) at a fixed flow rate of 420 $\frac{\text{cc}}{\text{min}}$ STP (standard temperature and pressure) for a porous PLD electrode. The catalytic rate is given in terms of $\frac{\text{mol}}{\text{s}}$ of CO_2 formed. The geometric catalyst area was 0.64 cm^2, but as we do not know the surface area of the catalyst exactly, we refer to absolute numbers in order to avoid errors. In the forward scan the onset temperature for significant conversion is around 200 °C with about 30 $\frac{\text{nmol}}{\text{s}}$ of CO_2 formation. A further increase in temperature leads to a steap increase in the reaction rate reaching a plateau with a maximum value of 335 $\frac{\text{nmol}}{\text{s}}$ at around 400 °C. The temperature of 450 °C is held for 24 h and afterwards stepwise decreased to 100 °C (reverse scan). An appreciable deactivation in the rate is visible. A comparison of the conversion rate at 300 °C in the forward and reverse scan shows an activity loss of 18 % from 290 $\frac{\text{nmol}}{\text{s}}$ to 230 $\frac{\text{nmol}}{\text{s}}$. In the lower temperature range the conversation rate of the activated and deactivated state converge indicating that the deactivation effect diminishes by reducing the temperature.

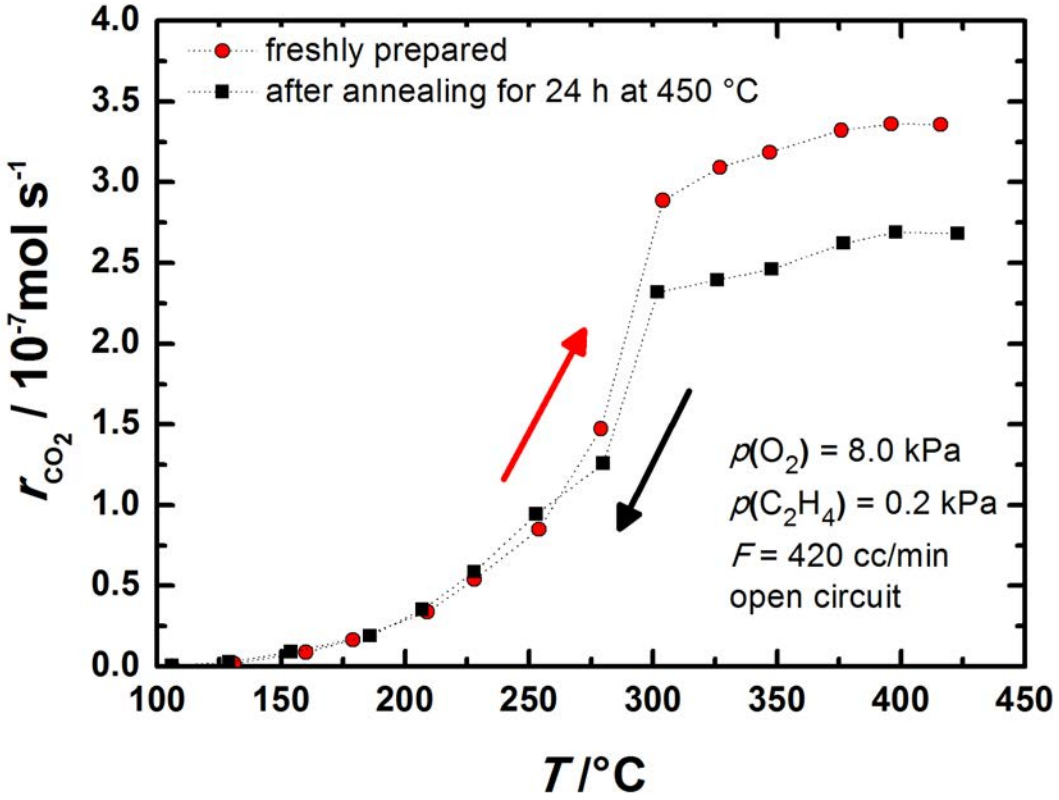

Figure 4.7: Temperature dependence of the open circuit rate of a porous Pt sample on YSZ (111) with a reaction composition of 0.2 kPa ethylene and 8.0 kPa oxygen and a volumetric flow rate of 420 $\frac{cc}{min}$ STP. A clear hysteretic behaviour between the forward scan (freshly prepared sample) and the reverse scan (obtained after 24 hours of annealing) is visible.

Another freshly prepared porous PLD sample has been cycled with a fixed gas mixture ($p(O_2) = 8.0$ kPa, $p(C_2H_4) = 0.2$ kPa) at a fixed flow rate of 420 $\frac{\text{cc}}{\text{min}}$ STP with a constant temperature scan rate of 0.4 $\frac{°C}{min}$ from 300 °C to 550 °C and back to 300 °C (Fig. 4.8). The initial conversion rate at 300 °C is about 200 $\frac{\text{nmol}}{\text{s}}$ and exhibits a maximum of 350 $\frac{\text{nmol}}{\text{s}}$ at 390 °C before decreasing steeply to 51 $\frac{\text{nmol}}{\text{s}}$ at 550 °C. In the reverse scan the rate stabilizes at around 60 $\frac{\text{nmol}}{\text{s}}$ for the whole temperature range. Comparing the two states at 300 °C (before and after) an activity loss of $\approx$ 83 % can be seen, indicating a very strong deactivation at high temperatures (550 °C).

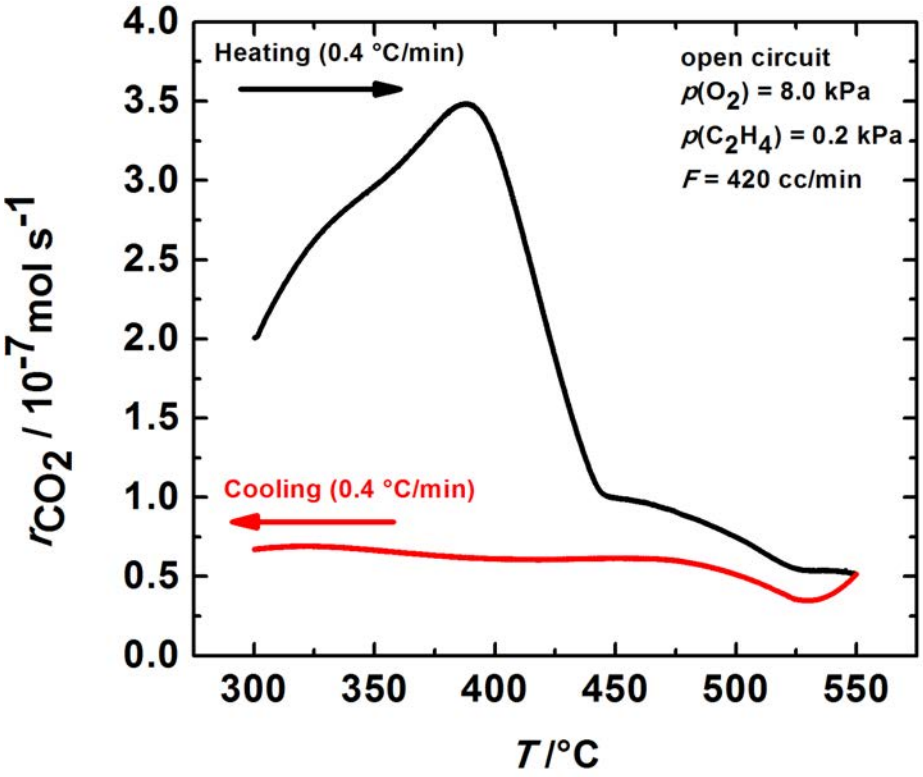

Figure 4.8: Open circuit reaction rate of a porous Pt sample on YSZ (111) during temperature cycling with a scan rate of 0.4 $\frac{^\circ C}{min}$ and a gas reaction composition of $p(C_2H_4) = 0.2$ kPa and $p(O_2) = 8.0$ kPa and a volumetric flow rate of 420 $\frac{\text{cc}}{\text{min}}$ STP. In the forward scan a rate maximum at around 390 °C is achieved followed by a strong deactivation. Upon cooling down the rate stabilizes at around 60 $\frac{\text{nmol}}{\text{s}}$.

At 300 °C a slow reactivation of the catalyst takes place, with the conversion rate increasing slowly to the initial open circuit steady state rate (conversion rate before cycling) after 60 h (Fig. 4.9).

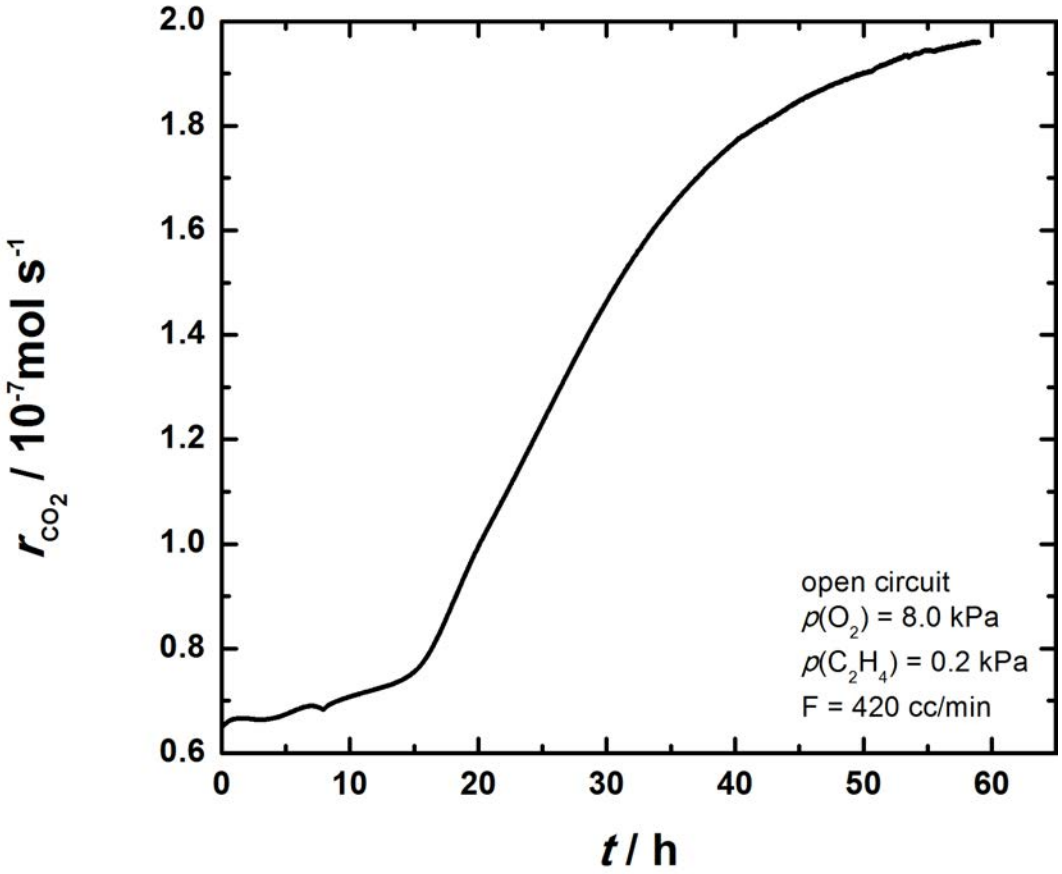

Figure 4.9: Reactivation of a porous sample from a deactivated state at 300 °C after temperature cycling (see Fig. 4.8). The reactivation of the catalyst takes around 60 hours until the steady state reaction rate is reached.

Deactivation and activation procedures

To understand the deactivation process at higher temperatures a porous sample was kept at 300 °C for 2.5 hours with a steady state rate of 270 $\frac{\text{nmol}}{\text{s}}$ and heated up to 450 °C (150 $\frac{^\circ\text{C}}{\text{min}}$) and held for 24 hours (Fig. 4.10). During the heating step an increase in the open circuit rate occurs with a maximum of 345 $\frac{\text{nmol}}{\text{s}}$ CO_2 formed. After reaching the higher temperature the rate starts immediately to decrease to 280 $\frac{\text{nmol}}{\text{s}}$ and a small reactivation to a new steady state rate at around 290 $\frac{\text{nmol}}{\text{s}}$. After that the reactor is cooled down rapidly to 300 °C (Fig. 4.11).

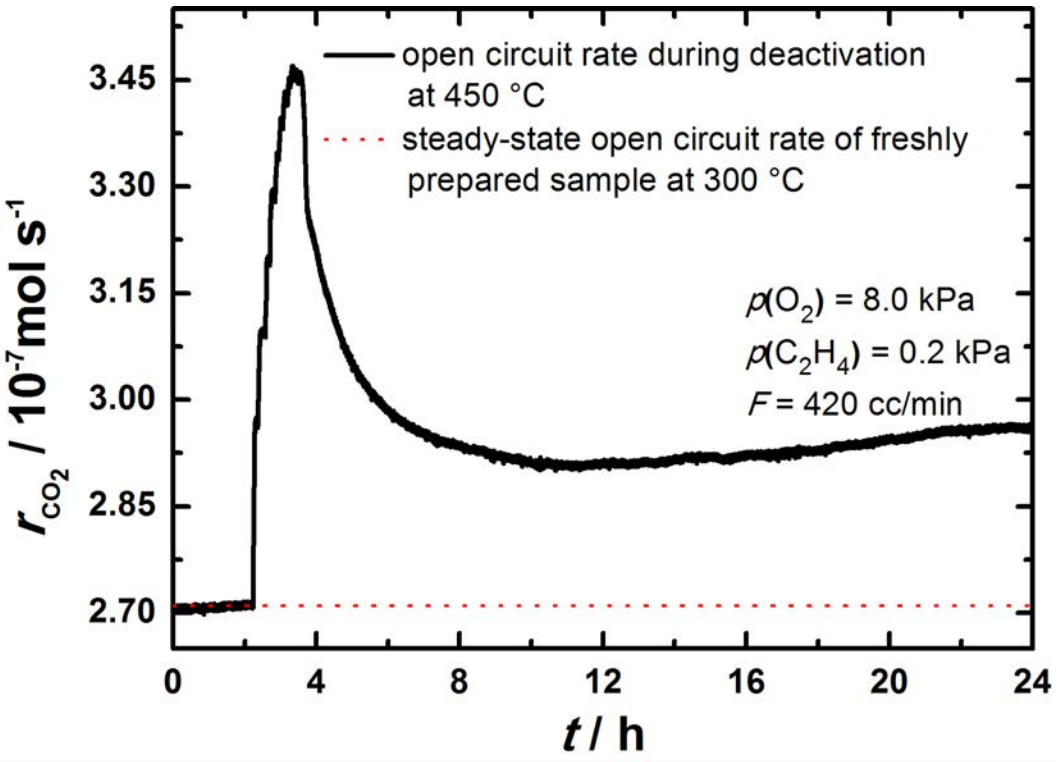

Figure 4.10: Open circuit rate of a porous Pt sample on YSZ (111) at two different temperatures with a reaction composition of $p(C_2H_4) = 0.2$ kPa and $p(O_2) = 8.0$ kPa and a volumetric flow rate of 420 $\frac{cc}{min}$ STP. At 300 °C a steady state rate of 270 $\frac{nmol}{s}$ is obtained. Heating up to 450 °C the sample exhibits a strong increase in the rate followed by a deactivation leading to a new open circuit rate of 290 $\frac{nmol}{s}$.

During the cooling step (Fig. 4.11) the rate drops almost immediately to 230 $\frac{nmol}{s}$ showing an activity loss of almost 15 % in comparison to the fresh sample. However, at this temperature and the given conditions the catalytic activity returns to open circuit steady state rate, following a very slow transient. Interestingly, at the beginning of the reactivation, oscillations occur, which vanish during return to the steady state rate.

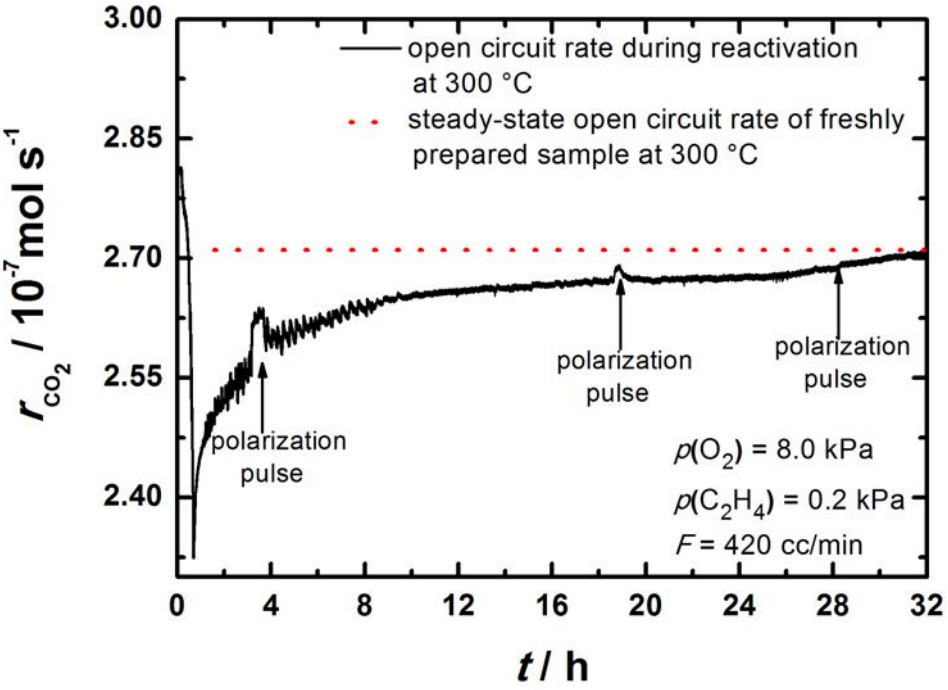

Figure 4.11: Open circuit rate of a porous Pt sample on YSZ(111) at 300 °C with a reaction composition of 0.2 kPa ethylene and 8.0 kPa oxygen and a volumetric flowrate of 420 $\frac{cc}{min}$ STP. By cooling down from 450 °C after deactivation for 24 h the rate drops to 230 $\frac{nmol}{s}$ followed by a very slow reactivation of the catalyst. Electrochemical pulses during reactivation show different rate enhancements depending on the progress of reactivation.

Electrochemically induced reactivation

In order to shed more light onto the reactivation behaviour of the cell a series of polarization pulses were applied (Fig. 4.11). Every polarization pulse lasts 30 minutes with a constant current of +10 μA between the catalyst and a gold counter electrode and a potential of approximately + 300 mV between the catalyst and a gold reference electrode. Three pulses were applied during the reactivation of the porous electrode at minute 190 (3,2 h), minute 1120 (18,7 h) and minute 1700 (28,3 h). The first two pulses lead to an appreciable increase in the rate. After switching off the polarization

the open circuit rate drops rapidly to a value higher than before polarization. Both pulses lead to different rate enhancements, showing a clear dependence on the state of reactivation of the sample. In both cases the initial steady state open circuit value is not reached. The rate enhancement for the first pulse at minute 190 is $\rho = 1.02$ and $\Lambda = 289$ showing a clear non-faradic behaviour. For the second pulse at minute 1120 the values of $\rho = 1.01$ and $\Lambda = 116$ show a less pronounced modification of the catalytic activity. It is worth mentioning that the third pulse applied close to the steady state value (minute 1700) causes no appreciable rate increase.

To verify this behaviour a second porous electrode has been investigated (Fig. 4.12). The sample shows an open circuit rate of 302 $\frac{\text{nmol}}{\text{s}}$ before the reactor was heated up to 450 °C for 24 hours to deactivate to a new rate of 270 $\frac{\text{nmol}}{\text{s}}$. After cooling down to 300 °C the rate drops to 220 $\frac{\text{nmol}}{\text{s}}$ followed by a slow reactivation (Fig. 4.12).

Three polarization pulses are carried out with a time delay of 30 minutes between two pulses (Fig. 4.13). As can be clearly seen the rate enhancement generated by the pulses is reduced as the reactivation progresses. The ρ and Λ values for the three pulses are given in table 4.2 showing a reduced enhancement by every further pulse.

No. of polarization pulse	Λ	ρ
1	521	1.04
2	405	1.03
3	347	1.03

Table 4.2: Λ and ρ values during electrochemically induced reactivation.

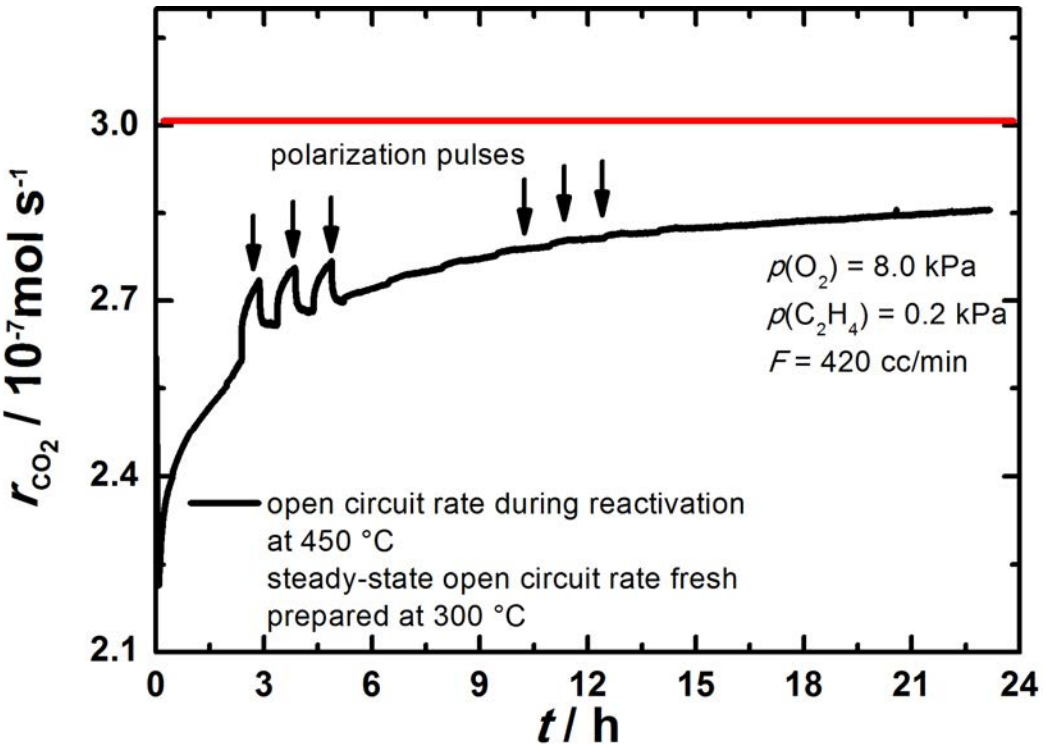

Figure 4.12: Open circuit rate of a freshly prepared sample at 300 °C and reactivation of the rate by time and polarization pulses after heat treatment.

Comparison of activated and deactivated state in terms of electrical polarization for different geometries

The quite different reactivity of activated and deactivated porous samples becomes obvious in Fig. 4.14. The activated state of the porous sample has an open circuit rate of 266 $\frac{\text{nmol}}{\text{s}}$ (black) and is obtained by a freshly prepared sample. The deactivated state of the sample has an 20 % reduced open circuit rate of 214 $\frac{\text{nmol}}{\text{s}}$ and is obtained after heating at 450 °C for 24 h and cooling down to 300 °C (red). Application of the same electrical pulses to both states shows that only the deactivated state can be promoted and thus, only its rate be enhanced ($\Lambda = 1084$, $\rho = 1.08$). It is worth mentioning

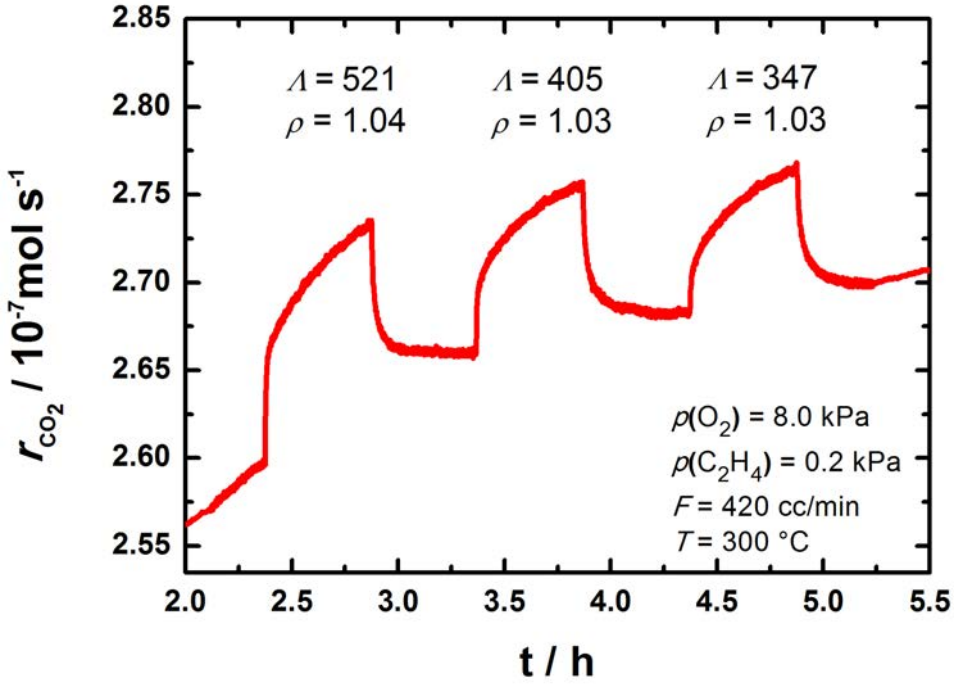

Figure 4.13: Open circuit rate of a porous sample at 300 °C after deactivation for 24 h at 450 °C with a reaction gas composition of $p(C_2H_4) = 0.2$ kPa and $p(O_2) = 8.0$ kPa and a volumetric flow rate of 420 $\frac{cc}{min}$ STP. During reactivation electrical pulses cause rate enhancements depending on the progress of reactivation.

that the increase of the rate by polarization for the inactive state leads to a rate which is still lower than the open circuit rate for the active state; even at higher polarization rates the open circuit rate of the activated state is not reached.

This behavior has also been demonstrated for de-wetted samples as well as for pasted samples.

The samples were characterized by SEM as well as XPS to rule out morphological and chemical changes during the measurements. Fig. 4.15 shows the results for the porous sample. There is no appreciable difference visible in the SEM images before and after the measurement indicating that the experimental procedure leads to no substantial morphological changes.

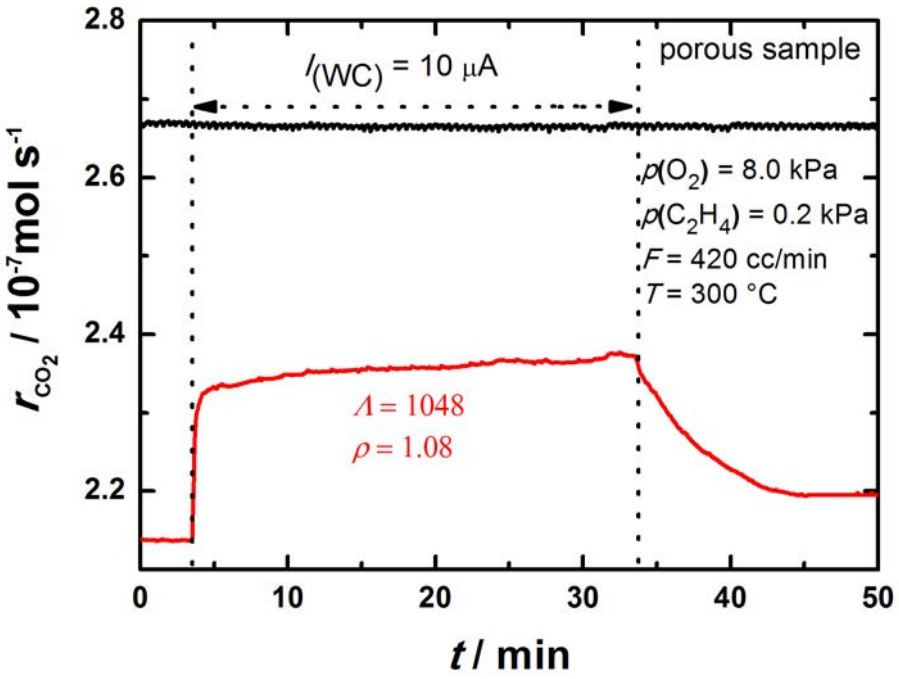

Figure 4.14: Comparison of the activated (black curve) and deactivated (red curve) state open circuit rates of a porous Pt sample on YSZ (111) at 300 °C with a reaction composition of 0.2 kPa ethylene and 8.0 kPa oxygen and a volumetric flowrate of 420 $\frac{cc}{min}$ STP. Application of 10 μA current for 30 minutes does only promote the deactivated state.

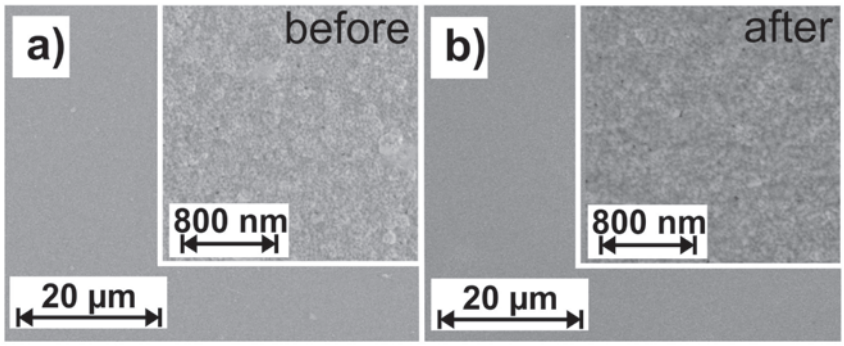

Figure 4.15: SEM pictures of a porous Pt sample on YSZ (111) before and after measurements. From the images no morphological changes are visible.

The XPS investigation of the same sample before and after deactivation (Fig. 4.16) also shows no difference in the Pt 4f signal. This indicates negligible oxide formation, although a surface platinum oxide which would be mainly located close to the TPB is difficult to detect by XPS.

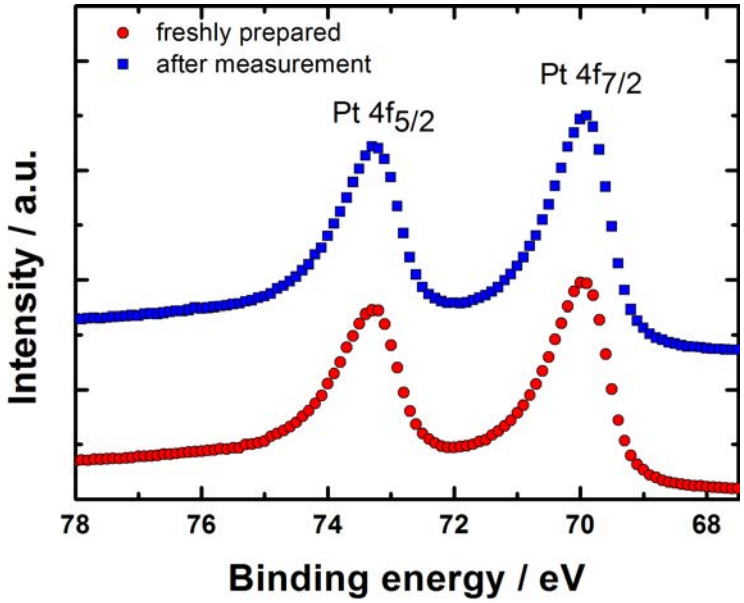

Figure 4.16: Comparison of the Pt 4f doublet XPS peaks of a porous Pt sample on YSZ (111) before and after measurements. From the spectra no difference is visible.

4.2.4 Discussion

As shown in Fig. 4.7 and 4.8 pronounced deactivation occurs by annealing the Pt/YSZ samples at high enough temperature in the reaction gas mixture. This annealing leads to a hysteresis of the reaction rate ending up with 2 different states of activity. There are different possible explanations for the appearance of two states with different activities on a catalyst surface. Due to the increase of temperature, impurities from the substrate and or the catalyst

can segregate to the active positions on the catalyst thereby lowering the conversion rate [Ridd02]. A poisoning of the surface by the reactive gas (ethylene) resulting in carbon deposition can take place [Togh10, Togh10.1] and a reconstruction of the surface due to changed thermodynamic parameters is possible.

Impurities in solid electrolyte systems like catalysts, batteries or solid oxide fuel cells (SOFC) have always played an important role in the explanation of performance changes. Especially the amount of sodium and calcium on the surface and/or at the TPB seems to have a tremendous influence on the behaviour of catalysts and SOFC electrodes [Ibra12]. Even though we cannot rule out the influence of impurities completely, a directed flux of an impurity only by changing the temperature to and away from the surface is not likely [Ibra12]. In addition, cation mobility is extremely small in zirconia [Kilo03] . Furthermore, we used single crystalline YSZ as well as nominally pure Pt for deposition of the electrode to minimize the amount of impurities. We were not able to detect impurities by EDX or XPS on the samples before and after the measurement.

Carbonization of the surface by ethylene decomposition can be ruled out, since there is no carbon enrichment in the XPS spectra visible. Furthermore, carbon deposition under highly oxidizing conditions (fuel lean conditions, 1 : 40 ethylene : oxygen) is highly improbable and on comparable systems like Pt wires and rods no coke formation could be found under fuel lean conditions [Wu85, Wu86, Wu88].

From the thermodynamic point of view a reconstruction of the surface linked to oxide formation or decomposition is likely. In Fig. 4.17 the phase diagram of platinum in equilibrium with platinum

oxide as calculated by Vayenas [Vaye81,Vaye82] and Berry [Berr78] is illustrated. As can be seen from the diagram, and as thermodynamically reasonable, the formation of platinum oxide becomes more favourable with decreasing temperature. The conditions chosen in this study are close to the equilibrium between platinum and its oxide. This might well explain oxide decomposition at higher temperatures and (slow) oxide formation at lower temperatures, although one should keep in mind that the exact position of the equilibrium will be different for different Pt facets and may be influenced by the presence of YSZ, i.e. it may depend on sample preparation and on the support. The reactivation as illustrated in Fig. 4.11 takes hours indicating a metastable state of the system.

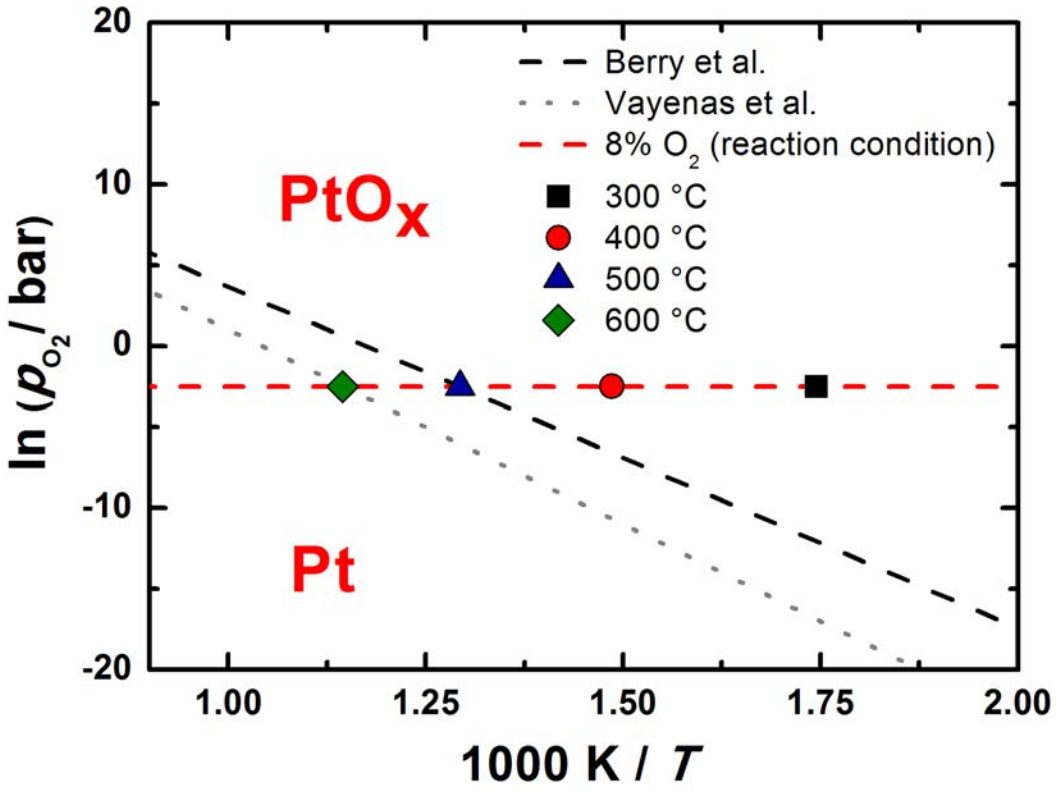

Figure 4.17: Phase equilibrium between platinum and platinum oxide according to Berry et al. [Berr78] and Vayenas et al. [Vaye82]. The reaction conditions (temperature and oxygen partial pressure) are marked in the diagram.

We were not able to detect a change in the Pt 4f doublet after the deactivation steps which could refer to oxide formation or decomposition. This might be due to the need to cool the samples down after the experiments and to expose to UHV for the ex situ XPS studies. But even if platinum oxide would survive this procedure; the obtained XPS spectra are averaged over a large electrode area and local oxide formation close to the TPB could most probably not be detected. Besides that, we found evidence for the formation of platinum oxide during anodic oxygen pumping in earlier studies [Pöpk11.3, Pöpk12] which might be taken as a hint for possible oxide formation also in the present case. Following anodic electrochemical polarization a rate increase is observed during reactivation of the electrodes which depends in size on the progress of reactivation. A possible explanation for this behaviour is that the anodic polarization triggers the transition from an inactive state to an active state. Due to the strong increase of the oxygen activity at the electrode upon polarization the system reaches a new thermodynamic state. The obtained rate enhancements during polarization are clearly non-faradaic, but decreasing during reactivation which means that a huge rate increase by polarization is only possible for a strongly deactivated sample. Finally, in the fully reactivated state only faradaic behavior is seen. It is important to note that the enhanced rates upon polarization observed during reactivation are always below the steady state rate of the activated state (Fig. 4.9, 4.10, 4.11). It appears that the activity of deactivated state can be improved by applying of a current, but that the catalytic activity can not become higher than in the activiated state. More explicitly, it appears that electrochemical polarisation can diminish the

effect of deactiviation, but that it cannot promote the activity of platinum in excess of its intrinsic properties in the activated state. Thus, in the present study we did not observe any electrochemical promotion of active samples. Samples had to be thermally treated in the reaction gas mixture in order to be deactivated and then to become EPOC-active. We feel that this observation will finally help to overcome the controversies on the NEMCA or EPOC effect. As we show with our experiments, the actual NEMCA effect depends strongly on the pretreatment of a Pt/YSZ sample, which explains that researchers sometimes were not able to reproduce the effect. Once a Pt/YSZ sample is in its catalytical active state, electrochemical polarisation will not improve the activity, and thus, the NEMCA effect is most probably not a tool to further promote the intrinsic high activity of active Pt surfaces. But once a Pt catalyst supported by YSZ has been aged and deactiviated, then electrochemical polarization may restore a part of the original activity. We presume that EPOC studies in literature which report strong NEMCA effects have dealt with deactivated electrodes, as these were usually kinetically characterized at higher temperatures prior to electrochemical polarization - leading to a metastabile deactivated state. We admit that this study is far from being complete in the sense that we have so far not been able to identify the microscopic mechanism for the deactivation/activation step - but the phenomenological results give unequivocal evidence for a mechanism different from a mere spillover effect. In line with previous studies of the Pt/YSZ system we believe that platinum oxides and their electrochemical and catalytic properties are responsible for the observed phenomena. Only in operando spectroscopic surface

studies of polarized electrodes in reaction gas mixtures with high spatial resolution close to well defined TPB will help to get a deeper understanding.

4.2.5 Conclusion

In this study the kinetic and electrochemical behavior of different platinum catalyst films on YSZ was investigated in a reaction mixture of 0.2 % ethylene and 8 % oxygen. By increasing the temperature the conversion rate exhibits a maximum at around 450 ° C followed by a decrease in the conversion rate (the formation rate of CO_2) rate at higher temperatures. We assign this decrease to a deactivated state most likely resulting from a change of stability of surface phases upon increased temperature. According to thermodynamics the active state (at lower temperatures) must be the platinum oxide modified catalyst surface and the deactivated state (at higher temperatures) must be the oxide-free platinum surface. Due to the fixed gas composition the temperature triggers the transition between both states. Additionally, anodic electrochemical polarization forces the transition from the deactivated state to an activated state most likely by formation of an oxide phase close to the TPB. The influence of impurities and their temperature and potential-dependent segregation cannot be ruled out completely, but we consider impurities not as key factor. Ex situ XPS did not show any oxide formation or decomposition, which could be due to the nature of the investigations (ex situ, high vacuum conditions, insufficient spatial resolution). Further investigations, especially in operando studies under reaction conditions are required in order

to identify the nature of the deactivating/activating species. We suggest that the NEMCA/EPOC effect is primarily related to surface changes related to oxide formation and that is is rather an re-activation process of a formerly deactivated catalyst than a true promotion effect.

Chapter 5

Results and Discussion - Part 3: Investigation of the PtO_x formation

The change of the catalytic activity [Stou81, Vaye88], the appearance of two different peaks in TDS [Neop95, Neop98, Tsip99] and XPS spectra [Luer00] and the change in work function [Vaye90, Tsip01] are explained by the formation of a charged oxygen species which originates from the electrolyte and spills over onto the surface of the catalyst. All these experimental results might also be explainable by the formation or decomposition of an active compound layer at the metal surface with a variable composition depending on the oxygen activity. For platinum electrodes on YSZ the formation or decomposition of PtO_x layers during electrochemical polarization at the Pt/YSZ interface as well as in the bulk have been analyzed by different indirect methods [Chao91, Kenj93, Brei97, Stan99, Jacc07, Foti09, Muto09, Poep11.2]. The formation or decomposition of an oxide on the metal surface might occur. In this case the oxygen activity should be fixed by the equilibrium

with the underlying Pt. Theoretical investigations [Seri06] as well as oxidation experiments [Berr78, Elli08, Fark13] on platinum surfaces show that different platinum oxides are formed depending on the temperature, oxygen partial pressure and crystallographic orientation. Under atmospheric pressure an α-PtO_2 structure with stacked O-Pt-O trilayers is stable up to 870 K. Above that temperature Pt_3O_4 ($c = PtO_{2-x}$; $x = 0{,}66$) becomes favorable up to 970 K which leads to a pure platinum surface above that temperature [Seri06]. Experiments at 500 mbar show stability of α-PtO_2 up to 840 K [Elli08]. Further investigations of Berry et al. [Berr78] and Vayenas et al. [Vaye81, Vaye82] lead to phase diagrams which show that the transition between the blank platinum surface and the oxidized surface lies in the region of typical EPOC conditions (10 mbar - 100 mbar oxygen partial pressure and 550 K - 850 K). The formation of platinum oxide phases at the contact area between the electrolyte and the metal or at the TPB between the electrolyte, the metal electrode and the gas phase may occur at different conditions. Unfortunately, these interphases may be hidden from the detection of many surface sensitive techniques which makes an in situ proof extremely difficult or even impossible. However, some investigations have been done in order to identify the nature of the metal surface at different oxygen partial pressures and also at different oxygen activities resulting also from polarization steps. Typical surface sensitive techniques to analyze surfaces with respect to structure and composition are XPS and surface-XRD (S-XRD).

5.1 X-ray photoelectron spectroscopy (XPS) under vacuum and high pressure conditions

5.1.1 Introduction

In XPS investigations of Pt electrodes on YSZ the focus has been set to the identification of potential spillover species, therefore looking only at the formation of new oxygen peaks in the XPS spectra or the shift and broadening of an existing peak (see chapter 1.4). Taking also possible metal oxide formation into account the peaks corresponding to the metal element are also important. Only a few investigations have focused on the identification of metal oxide species during polarization. Jaccoud et al. [Jacc07.2] investigated sputtered platinum films in terms of EPOC and analyzed the surface composition by XPS afterwards. They found differences in the Pt 4f (5/2) and the Pt 4f (7/2) doublet before and after EPOC measurements depending on the gas treatment during measurement. However, the XPS measurements were only conducted ex situ after the EPOC experiments and the exact same surface position for the XPS measurement cannot be found again. Additionally, the change in the peak signals before and after EPOC measurements are minor. In situ XPS investigations [Poepk11.1] of porous Pt/YSZ electrodes show a very small increase of the valley between the Pt 4f (5/2) and the Pt 4f (7/2) peaks during anodic polarization indicating a superposition of a Pt^0 doublet with an oxidized Pt^{4+} doublet. Nonetheless the change in the peaks is very little and the results are not unequivocal. In order to shed more light on the change of surface composition during a polarization

step XPS and high pressure XPS measurements were performed in collaboration with the research group of Prof. Dr. Steinrueck at the Friedrich-Alexander-University of Erlangen-Nürnberg.

5.1.2 Experimental Part

Experimental setup for XPS measurements under high pressure conditions

The investigations have been conducted in a differentially pumped "pressure gap" photoelectron spectrometer, which is able to operate in a pressure range of 10^{-10} mbar to 1 mbar. The background pressure was around $1 \cdot 10^{-9}$ mbar. The X-ray source (SPECS XR50) as well as the hemispherical analyzer (OMICRON EA 125) has been modified for elevated pressure. The detection angle of the electrons is 0° to the surface normal of the sample. Additionally, the analyzer is equipped with a quadrupole mass spectrometer. For the high pressure investigations the reaction chamber was fed by oxygen and the pressure was measured by a Baratron. A schematic view of the setup is given in Fig. 5.1. A detailed description of the setup is given in [Pant05].

Sample holder

To perform the measurements a new sample holder has been designed which had to fulfill the following requirements:

- The sample should be heated up to 500 °C.
- The sample should be contacted by 2 wires for electrical polarization.

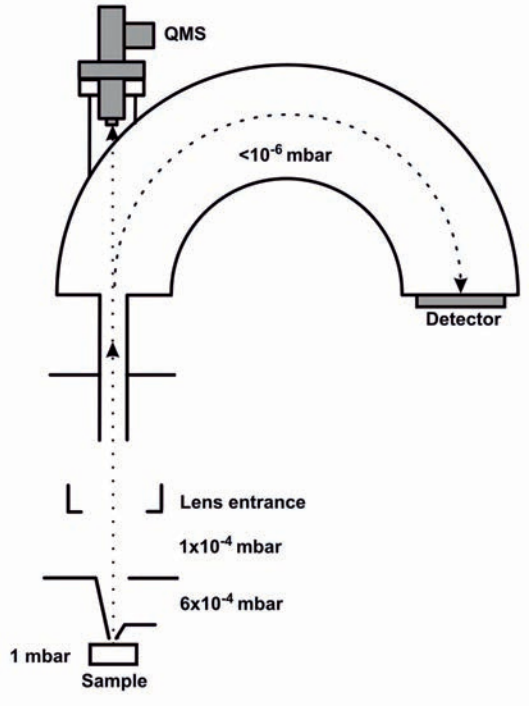

Figure 5.1: Schematic picture of the HP-XPS equipment [Hank09].

- The sample should be accessible to the gas atmosphere and the X-ray beam.

From the technical requirements the sample holder could not exceed certain dimensions, because of constructural restrictions (e.g. sample holder transfer system of the machine, incident angle of the X-ray beam). In order to fulfill all requirements a commercially available boraelectric heater (Tectra, Germany) with a specially designed layout with a heating area in the size of the YSZ substrate was utilized. The heater was mechanically and electrically connected with the sample holder input via 2 bended copper bars allowing to heat up the sample and fixing the sample holder in the input system (Fig. 5.2).

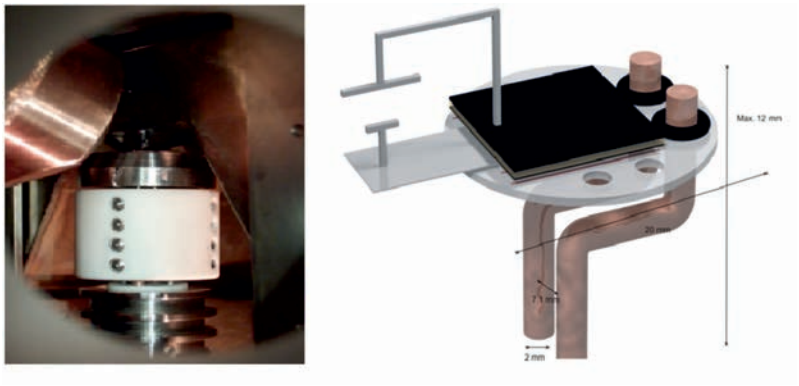

Figure 5.2: Sample holder positioned in the XPS machine (left) and schematic drawing of the high pressure XPS sample holder (right).

The sample consisted of a symmetric face to face 2 electrode arrangement on YSZ. The working electrode was facing the gas atmosphere while the counter electrode was facing the heater. The working electrode was fixed and electrically contacted by a metal base. The counter electrode was electrically contacted by a Pt mesh (Fig. 5.3).

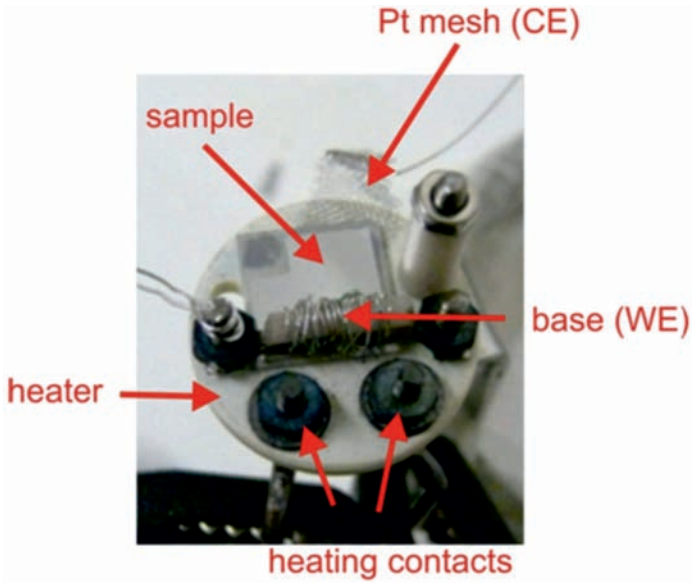

Figure 5.3: Top view of the sample holder with an attached sample.

An exact temperature measurement during operation was not possible as not enough electrical contacts were available for the polarization and the temperature measurement. Therefore, a type K thermocouple was placed close to the working electrode surface prior to the measurement and a temperature calibration curve was taken by applying different potentials to the heater and looking for the temperature response of the thermocouple.

5.1.3 Results

In order to investigate possible PtO_x formation during anodic polarization different types of platinum model electrodes were utilized: lithographic electrodes, dense electrodes and dewetted electrodes. The measurements have been conducted at ultra high vacuum conditions ($1{\cdot}10^{-9}$ mbar), 0.1 mbar oxygen partial pressure and 1 mbar oxygen partial pressure. The temperature was adjusted between 400 °C and 500 °C and the polarization voltage between − 2 V and + 3 V. The oxygen signals (527 eV - 536 eV) and the Pt signals (66 eV - 80 eV) were recorded. The intensity of all recorded spectra were normalized to the Pt 4f (7/2) peak in order to identify changes in the height ratio of the Pt 4f (7/2) peak and the Pt 4f (5/2) peak. The peak ratio is related to the amount of platinum.
The lithographic samples had a TPB of 16.2 m and were produced by a lithographic method (see chapter 2.2.3). The lithographic samples were measured under different oxygen partial pressures at 500 °C and under polarization conditions at 400 °C. For the polarization experiments different potentials were applied for 20 minutes and XPS spectra were taken during that time. In Fig. 5.4 the mea-

surements at UHV, 0.1 mbar and 1 mbar for the Pt 4f signal are shown. It can be seen that by increasing the oxygen partial pressure the signal to noise ratio is decreased revealing a higher background noise and a smaller valley between both Pt 4f peaks. The ratio between both peaks (7/2 and 5/2) remained constant and is therefore unaffected by the oxygen partial pressure.

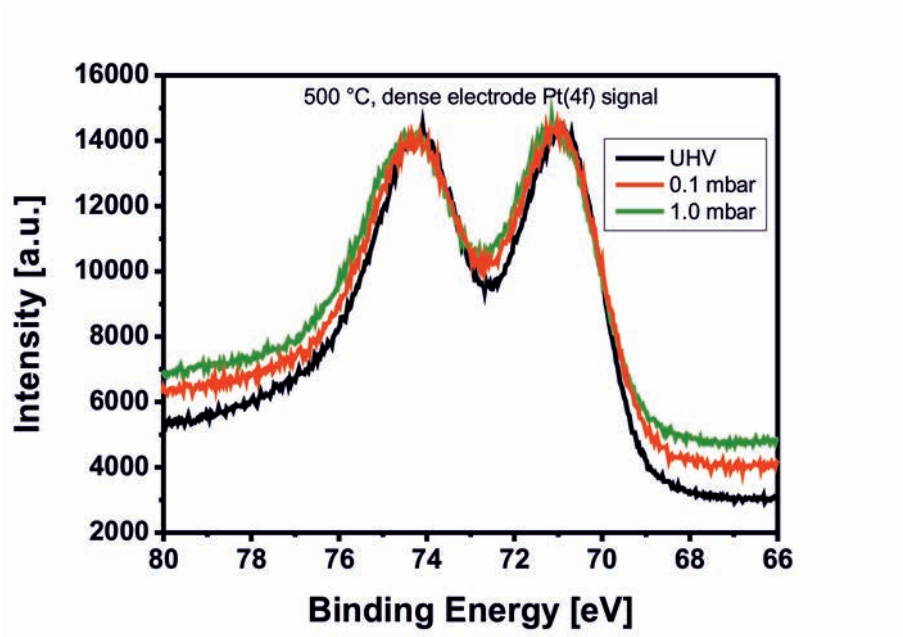

Figure 5.4: XPS measurements of the Pt 4f signal at 500 °C and different oxygen partial pressure.

In Fig. 5.5 the XPS spectra measured under UHV conditions at the end of different polarization steps (anodic: left, cathodic: right) are shown. One can see that the polarization has no influence on the shape or intensity of the Pt 4f doublet. The ratio between both peaks remains constant.

The oxygen signal at around 530 eV without and at the end of anodic (left) and cathodic (right) polarization is shown in Fig. 5.6. One can see that the signal intensity is reduced upon polarization by positive polarization as well as negative polarization.

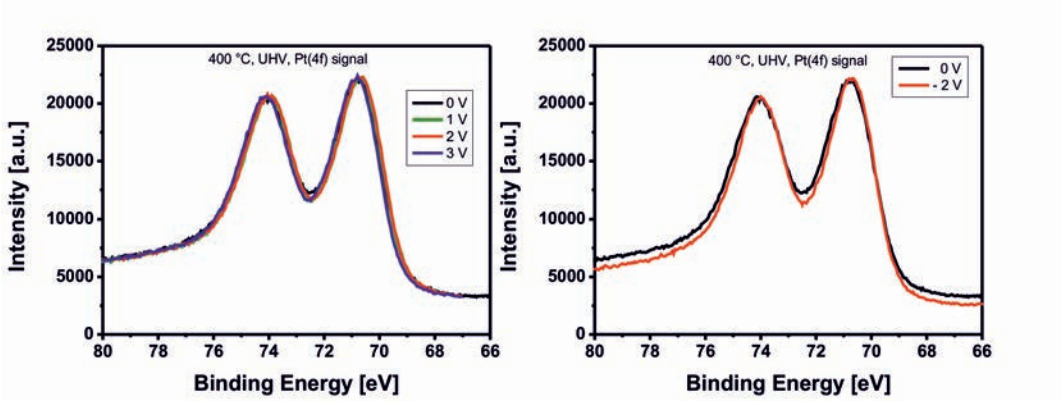

Figure 5.5: XPS measurements of the Pt 4f signal at 400 °C for different polarization steps: anodic polarization steps (left) and cathodic polarization steps (right).

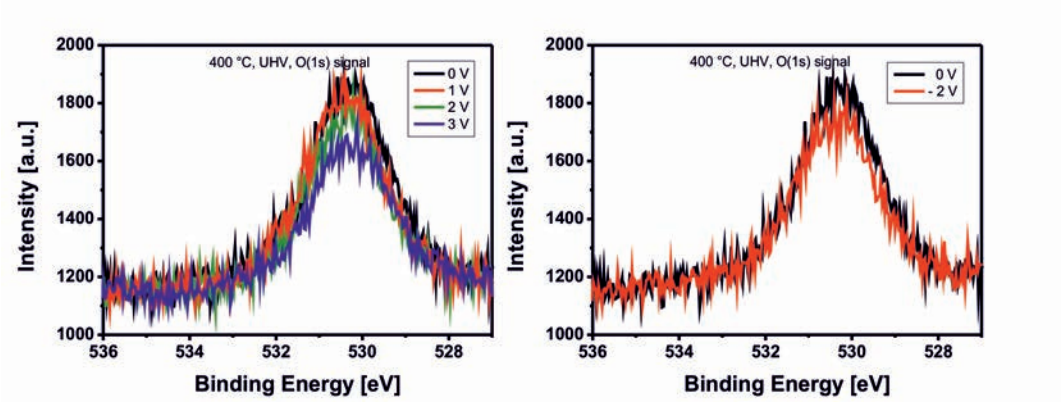

Figure 5.6: XPS measurements of the O 1s signal at 400 °C at UHV conditions for different polarization steps: anodic polarization steps (left) and cathodic polarization steps (right).

The same measurements have been conducted at an oxygen partial pressure of 1 mbar in order to enhance and increase a possible oxide formation. Similar to the measurements under UHV conditions no change in the peak ratio upon polarization is visible (Fig. 5.7).

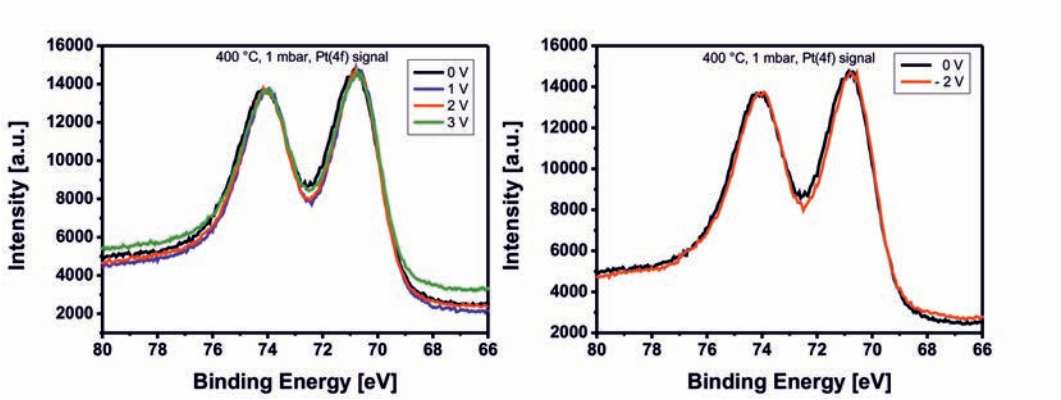

Figure 5.7: XPS measurements of the O 1s signal at 400 °C and 1 mbar oxygen partial pressure for different polarization steps: anodic polarization steps (left) and cathodic polarization steps (right).

The O 1s signal at 1 mbar shows a second peak centered at around 538 eV [Fig. 5.8]. This peak originates from gas phase oxygen which is also ionized by the X-ray beam. The chemisorbed oxygen peak at around 530 eV seems to be mainly unaffected by polarization except a little shift during negative polarization.

5.1.4 Discussion

PtO_x formation on the surface of the examined sample should be detectable by photoelectron spectroscopy once it forms with sufficient coverage. Pure metallic platinum is causing a doublet with maxima at around 70.5 eV and 74 eV in the XPS spectra. Due to the inherent character of platinum as noble metal the formation of an oxide requires special conditions, especially if the oxide should penetrate the surface [Fark13, Elli08]. Experiments with plasma

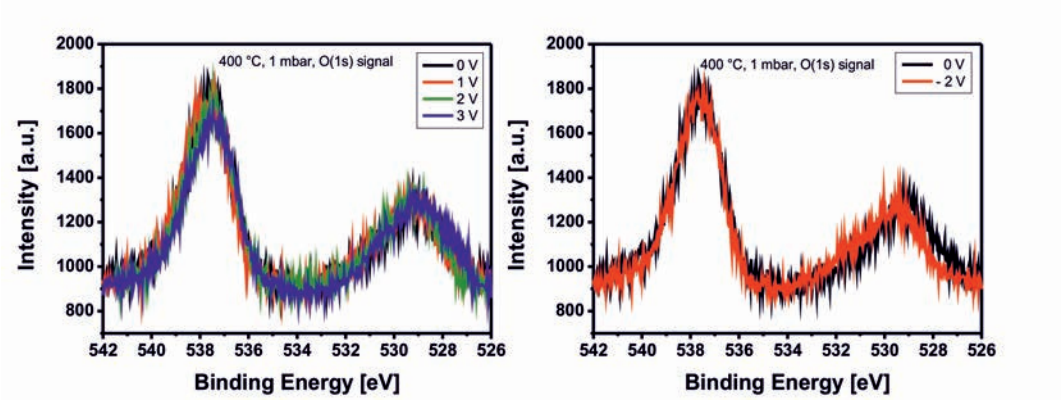

Figure 5.8: XPS measurements of the O 1s signal at 400 °C at 1 mbar oxygen partial pressure conditions for different polarization steps: anodic polarization steps (left) and cathodic polarization steps (right).

oxidation [Blac05] or reduction of previously formed PtO_x [Zhu12] show the difference between both states. At the beginning of the PtO_x formation a shoulder at the Pt 4f (5/2) peak is formed and the valley between both peak maxima is reduced. Ongoing oxidation leads to the formation of a new doublet shifted by 4 eV in comparison to the original platinum doublet. At the same time the original doublet vanishes (Fig. 5.9). This shift of the doublet is easily explainable by the oxidic character of the platinum leading to a higher bonding energy of the electrons.

In the XPS measurements performed in this study no change of the peak ratio of the Pt 4f (7/2) and Pt 4f (5/2) peak is found. The formation of a shoulder cannot be seen either. In literature the formation of a PtO_x related doublet out of the Pt 4f doublet has barely been described [Pöpk11.2, Zhu12]. The changes in ratio between the peaks as well as the shoulder formation during an anodic polarization or oxidation by increased oxygen partial pressure are not very pronounced. In the investigation of Pöpke et al. [Pöpk11.2] a synchrotron source was used and the spectra were taken out of a

microspot of 150 μm around the TPB, therefore imaging a reaction with oxygen and platinum at the place where an oxidation reaction is most likely. In the present study no noteworthy spatial resolution was possible and mainly unoxidized platinum was probably rather investigated than oxidized platinum close to the TPB. Additionally, due to the use of high pressures and the construction of the differential pumped system the signal intensity is reduced.
Further investigations under high pressure conditions are needed in order to confirm or refute the formation of a surface oxide during polarization. Especially a lack of spatial resolution could be crucial, therefore high pressure synchrotron facilities (BESSY Berlin, Advanced light source, Berkeley) which can also operate at pressures up to 10 torr are needed.

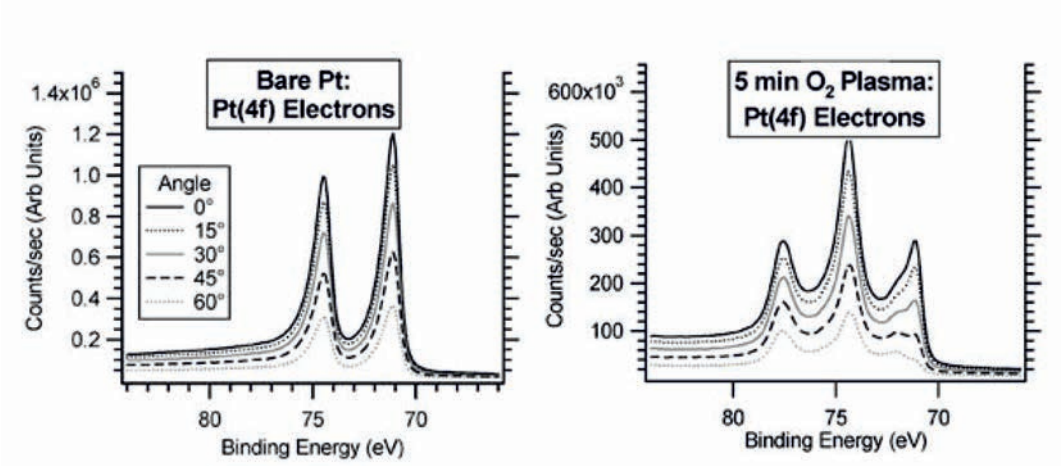

Figure 5.9: XPS comparison of the Pt 4f signals: a) a bare Pt surface and b) a partially oxidized surface [Blac05].

5.2 Surface X-ray diffraction (S-XRD) under reaction conditions

At first glance the surface of a crystal appears smooth and similar to the bulk material. However, electron microscopy and STM reveals that the surface structure is heterogeneous with its steps and defects. This local variation in surface structure leads to different electronic properties with reference to the bulk material. Besides that, the atomic structure and composition which determine the reactivity of a surface can be completely different from the bulk. This will often tend to force the surface to undergo mainly two different processes, surface reconstruction and surface relaxation. Surface reconstruction is a process where the periodicity of the lattice is changed by a rearrangement of the surface atoms. This happens mostly at less stable metal surfaces and leads to a minimization of the surface free energy. It is also dependent on the surrounding gas phase. Surface relaxation is a small rearrangement of the upper surface layer which just involves the compression of the layers perpendicular to the surface. This leads also to a minimization of the surface free energy.

One of the best techniques to obtain information about the atomic structure of crystalline surfaces is S-XRD. Due to the very low scattering intensity of the surface in comparison to the bulk (10^5 orders less) very intense X-ray beams are needed. Therefore, S-XRD measurements can only be conducted with synchrotron radiation. Although the analysis of XRD spectra of bulk materials is well established the analysis of surfaces shows some important differences. By analyzing a bulk structure the X-ray beam is reflected on the lat-

tice planes of the crystal satisfying the three Laue conditions (h,k,l) giving a point in the reciprocal space. In the case of a surface the third Laue condition is truncated due to the 2 dimensionality of the surface. Therefore, diffraction takes place on rods instead of points in the reciprocal space. Due to the fact that the surface as well as parts of the bulk are measured a superimposed pattern of rods (from the surface) and points (from the bulk) are obtained leading to the so-called crystal truncation rods (CTR). These rods can be measured with a 6-circle diffractometer.

A big advantage of this technique is that it averages over a large ensemble of atoms therefore ruling out defects. Furthermore, investigations under high pressure are possible in contrast to electron microspectroscopic methods. Both criteria allow the investigation of surfaces during catalytic reactions.

The CO oxidation on platinum has been studied intensively [Voelk00, Lang22, Camp80, Su97, Somo97, Hend02, Hend04, Acke05, Chen07, Gao09, Gao09.2, Clur09, Clur09.2]. Pioneer experiments of Ertl et al. [Camp80] under UHV conditions revealed that the reaction is following a Langmuir-Hinshelwood mechanism. Further important investigations at higher pressures have been conducted by Somorjai et al. [Su97, Somo97], Frenken et al. [Hend02, Hend04, Acke05] and Goodman et al. [Chen07, Gao09, Gao09.2, Clur09] in order to overcome the pressure and material gap and to get more insight into the processes taking place under "real" catalyst conditions (ambient pressures and polycrystalline samples). Somorjai et al. found that the mechanism of the CO oxidation depends strongly on the ratio of CO and O_2. Under oxidative conditions ($p(\mathrm{CO})/p(\mathrm{O_2}) < 2$) the surface reaction can be divided

into two regimes of different activity. The low activity regime is found at low temperatures (< 600 K) where the surface is predominantly covered with CO molecules and the activation energy for the reaction is determined by desorption of CO molecules from the surface (42 kcal/mol). At higher temperatures (> 600 K) enough surface sites for the adsorption of molecular oxygen are available and the rate limiting step is the reaction of adsorbed CO with adsorbed atomic oxygen (11 kcal/mol) on the surface. The reaction occurs at the perimeter of oxygen and CO islands on the surface [Ertl97, Wint00]. Investigations of Frenken et al. on Pt (110) and Pt (111) surfaces in a flow reactor equipped with STM and QMS devices show a change from a low reactivity regime to a high reactivity regime upon changing the ratio of CO to oxygen to more oxidizing ratios. The transition from a low reactivity regime to a high reactivity regime is explained by the formation of a more active thin platinum oxide layer. As can be seen from STM images the surface is roughened by time, which is attributed to a change of the Langmuir-Hinshelwood mechanism to a Mars-Van-Krevelen mechanism. Comparable experiments from Goodman et al. did not show the very high reactivity regime which Frenken et al. [Rijn10] had found. Instead Goodman et al. [Chen07] found 3 different regimes of activity corresponding to the CO desorption limitation at low temperature, a transient regime, and a higher activity regime which corresponds to a gas phase mass transfer limitation of CO. PM-ERAS measurements did not show platinum oxide formation at any of these regimes. Goodman et al. have argued that the metal phase should be more active than the oxide phase. Ongoing discussion between Frenken et al. and Goodman et al. about the

state of the catalyst and whether an oxide formation is present or not show that still much research has to be done.

The identification of a platinum oxide during catalysis should be clearly visible in S-XRD investigations. The formation of a platinum oxide including its structural properties has been investigated by S-XRD measurements by Stierle et al. in detail [Elli08]. They observed the formation of an oxide at 520 K and 500 mbar oxygen partial pressure. The obtained surface oxide is a slightly distorted and perpendicular to the surface compressed (bulk) α-PtO_2 which consists of 2 hexagonal platinum layers surrounded by oxygen.

The formation of an oxide as shown by Stierle et al. supports the experimental results of Frenkel et al., but has yet to be proven by S-XRD measurements under reaction conditions (CO oxidation).

For this reason the kinetics of the CO oxidation over Pt (111) thin films was investigated in situ by infrared spectroscopy and S-XRD in collaboration with Dr. A. Farkas, K. Zalewska-Wierzbicka, J Goritzka, D. Langsdorf and Prof. Dr. H. Over from the institute of Physical Chemistry, Giessen, Germany and O. Balmes from the beamline ID03, European Synchrotron Radiation Facility (ESRF), Grenoble, France.

Both setups (RAIRS and S-XRD) were equipped with capacitive gauge and a quadrupole mass spectrometer to monitor the total pressure of the gas mixture and the composition of the reacting gases. With infrared spectroscopy (RAIRS), the product CO_2 molecules in the gas phase and the surface CO species were monitored. With in situ S-XRD the ordered atomic structure of the catalyst surface during the CO oxidation was monitored, while with online total pressure measurements and mass spectrometry

measurements the reaction kinetics could be followed. Both in situ experiments show a steep increase in the activity when a certain O_2/ CO ratio is exceeded. These oxidizing conditions are strongly dependent on temperature. S-XRD shows that the active platinum phase is a mixture of oxidic Pt (111) surface and chemisorbed O covered Pt (111) surface. By RAIRS under these conditions it could be shown that the surface reaction is so fast that every CO molecule impinging on the surface is transferred to CO_2, therefore no CO surface molecule could be detected. The limiting factor for the reaction is the gas-phase diffusion which is shown by an activation energy for the reaction of 0 $\frac{kJ}{mol}$. Under mildly oxidizing conditions the metallic CO-covered Pt (111) surface is predominant with a high coverage of CO and O_2 which react at the perimeter of O islands. This is also reflected by an activation energy of (45 $\pm$ 3) $\frac{kJ}{mol}$. Detailed information can be found in A. Farkas, K. Zalewska-Wierzbicka, C. Bachmann, J. Goritzka, D. Langsdorf, O. Balmes, J. Janek, H. Over, „*High Pressure Carbon Monoxide Oxidation over Platinum (111)*", The Journal of Physical Chemistry C, 117, (2013), 9932-9942.

Chapter 6

Summary

The phenomenon of NEMCA has been investigated for over 30 years, but the results are often puzzling and the nature of the proposed spillover species - i.e. the detailed mechanism itself - has not been clarified without doubt. Despite the impression of a well-proven phenomenon the NEMCA effect has only been investigated experimentally by a small number of research groups, and only a few of them have reported a reasonable NEMCA effect. Most of the investigated catalysts were made out of metal pastes with an unknown composition and additives.

Model electrodes like they were used throughout the investigations in this thesis are chemically (free of additives) and structurally (orientation and crystallinity of the film) well defined and therefore exhibit a high reproducibility and are more suitable for fundamental NEMCA investigations.

The present investigations reveal that a sizeable NEMCA effect - under typical NEMCA conditions with pure and well defined platinum electrodes - can only be found under certain conditions. A pretreatment of the catalyst is necessary to elicit electrochemical promotion phenomena from the catalyst. This pretreatment in-

cludes temperature cycling which most probably leads to the formation of metastable surface states or the segregation of impurities. Due to fact that typical NEMCA operating conditions are close to the transition between platinum and platinum oxide a metastable oxide state might be formed, and an electrochemical trigger could then switch between both states. Clear spectroscopic evidence for the formation or decomposition of platinum oxide during polarization has not been found in this study so far which is due to the difficulty of in operando surface investigations with a sufficient spacial resolution to detect species close to the TPB.

This experimental result could easily explain why the NEMCA effect has not been found by all research groups before. Some of the samples simply have not received the necessary pretreatment to see the NEMCA effect. Further investigations are required to find out how and in which way the pretreatment and therefore the history of the catalyst influence the NEMCA effect in detail. Overall the results show that the NEMCA effect cannot be explained easily by a special spillover species, rather the pretreatment of the investigated catalyst has to be understood. Further in operando investigations are necessary to reveal the nature of the rate changing species at the edge of phase stability.

Finally, there is experimental evidence that the NEMCA effect can only improve the activity of a Pt catalyst once this catalyst has been deactivated (pretreated) before. Thus, further efforts in studying NEMCA will only make sense, if this catalyst state and the TOF in all different catalyst states can be documented properly. Otherwise, NEMCA studies can easily be missinterpreted.

Chapter 7

Bibliography

[Acke05] M. D. Ackermann, T. M. Pederson, B. L. M. Hendriksen, O. Robach, S. C. Bobaru, I. Popa, C. Quiros, H. Kim, B. Hammer, S. Ferrer, J. W. M. Frenken, *Structure and Reactivity of Surface Oxides on Pt(110) during Catalytic CO Oxidation*, Phys. Re. Lett., 95, (2005), 255505

[Alli11] A. D. Allian, K. Takanabe, K. L Fujdala, X. Hao, T. J. Truex, J. Cai, C. Buda, M. Neurock, E. Iglesia, *Chemisorption of CO and Mechanism of CO Oxidation on Supported Platinum Nanoclusters*, Journal of the American Chemical Society, 133, (2011), 4498-4517

[Alex97] F. A. Alexandrou, V. G. Papadakis, X. E. Verykios, C. G. Vayenas, *The promotional effect of Na on the NO reduction by CO on supportd Pt, Pd and Rh caalysts*, Proc. 4th Intnl. Congress on Catalysis and Automotive Pollution Control, 2, (1997), 1-16

[Anas93] N. A. Anastasijevic, H. Baltruschat, J. Heitbaum, *On the hydrogen evolution during electrochemical oxidation of aldehydes at Ib metal*, Electrochim. Acta, 38(8), (1993), 1067-1072

[Anas09] N. A. Anastasijevcic, *NEMCA - From discovery to technology* Catal. Today, 146, (2009), 308-311

[Andr13] E. S. Andreiadis, P.-A. Jacques, P. D. Tran, A. Leyris, M. Chavarot-Kerlidou, B. Jousselme, M. Matheron, J. Pecaut, S. Palacin, M. Fontecave, V. Artero, *Molecular engineering of a cobalt-based electrocatalytic nanomaterial for H_2 evolution under fully aqueous conditions*, Natur Chemistry, 5, (2013), 48-53

[Arch06] D. Archonta, A. Frantzis, D. Tsiplakides, C. G. Vayeans, *STM observation of the origin of electrochemical promotion on metal catalyst-electrodes interfaced with YSZ and β-Al_2O_3*, Solid State Ionics, 177, (2006), 2221-2225

[Balo04] S. Balomenou, D. Tsiplakides, A. Katsaounis, S. Thiemann-Handler, B. Cramer, G. Foti, C. Comninellis, C. G. Vayenas, *Novel monolithic electrochemically promoted catalytic reactor for environmentally important reactions*, Appl. Catal. B Environ., 52, (2004), 181-196

[Balo06] S. Balomenou, D. Tsiplakides, A. Katsaounis, S. Brosda, G. Foti, C. Comninellis, S. Thiemann-Handler, B. Cramer, C. G. Vayenas, *Monolithic electrochemically promoted reactors: A step for the practical utilization of electrochemical promotion*, Solid State Ionics, 177, (2006), 2201-2204

[Bara05] E. A. Baranova, A. Thursfield, S. Brosda, G. Foti, C. Comninellis, C. G. Vayenas, *Electrochemical promotion of ethylene oxidation over Rh catalyst thin films sputtered on YSZ and TiO_2/YSZ supports*, J. Electrochem. Soc., 152 (2), (2005), E40-E49

[Barb94] J. Barbier, D. Duprez, *Steam effects in three-way catalysis*, Appl. Catal., B., 4, (1994), 105-140

[Bart00] J. V. Barth, *Transport of adsorbates at metal surfaces: from thermal migration to hot precursors*, Surface Science Rep., 40, (2000), 75-149

[Bebe89] S. Bebelis, C. G. Vayenas, *Non-faradaic electrochemical modification of catalytic activity: The case of ethylene oxidation on Pt*, J. of Catalysis, 118, (1989), 125-146

[Beck07] G. Beck, H. Fischer, E. Mutoro, V. Srot, K. Petrikowski, E. Tchernychova, M. Wuttig, M. Ruhle, B. Luerssen, J. Janek, *Epitaxial Pt(111) thin film electrodes on YSZ(111) and YSZ(100) - Preparation and characterisation*, Solid State Ionics, 178, (2007), 327-337

[Beck11] G. Beck, H. Poepke, B. Luerssen, J. Janek, *Microstructure of platinum films on YSZ prepared by pulsed laser deposition*, Journal of Crystal Growth, 322, (2011), 95-102

[Beck14] G. Beck, C. Bachmann,*Oxygen removal at grain boundaries in platinum films on YSZ*, Solid State Ionics, 262, (2014), 508-511

[Bely00] V. D. Belyaev, T. I. Politova, V. A. Sobyanin, *Effect of non-Faradaic electrochemical modificationn of catalytic activity* Solid State Ionics, 136-137, (2000), 721-725

[Berl88] P. J. Berlowitz, C. H. F. Peden, D. W. Goodman, *Kinetics of carbon monoxide oxidation on single-crystal palladium, platinum, and iridium*, J. Phys. Chem., 92, (1988), 5213-5221

[Berr78] R. J. Berry, *Study of multilayer surface oxidation of platinum by electrical resistance technique*, Surface Science, 76, (1978), 415-442

[Bill07] A. Billard, P. Vernoux, *Electrochemical catalysts for hydrocarbon combustion*, Top. Catal., 44, (2007), 369-377

[Blac05] J.J. Blackstock, D.R. Stewart, Z. Li, *Plasma-produced ultrathin platinum-oxide films for nanoelectronics: physical characterization*, Appl. Phys. A, 80, (2005), 1343-1353

[Bonz75] H. P. Bonzel, J. J. Burton, *CO Oxidation on a Pt(110) Surface: Solution of a Reaction Model*, Surf. Sci., 52 (1), (1975), 223-229

[Brei97] M. W. Breitner, K. Leb, G. Fafilek, *Voltammetric studies of electrochemical processes at the interface Pt|YSZ between 300 and 600 °C*, J. Electroanal. Chem., 434, (1997), 129-137

[Cabr49] N. Cabrera, N. F. Mott, *Theory of the oxidation of metals*, Rep. Prog. Phys., 12, (1949), 163-184

[Camp80] C. T. Campbell, G. Ertl, H. Kuipers, J. Segner, *A molecular beam study of the catalytic oxidation of CO on a Pt (111) surface*, J. Chem. Phys., 73, (1980), 5862-5873

[Cava93] C. A. Cavalca, G. Larsen, C. G. Vayenas, G. Haller, *Electrochemical modification of methanol oxidation selectivity and activity on a platinum single-pellet catalytic reactor*, J. Phys. Chem., 97, (1993), 6115-6119

[Cava98] C. A. Cavalca, G. L. Haller, *Solid electrolytes as active catalyst support: Electrochemical modification of benzene hydrogenation activity on Pt/β(Na)Al$_2$O$_3$*, J. Catal., 177, (1998), 389395

[Chao91] T. Chao, K. J. Walsh, P. S. Fedkiw, *Cyclic voltammetric study of the electrochemical formation of platinum oxide in a Pt/yttria-stabilized zirconia cell*, Solid State Ionics, 47, (1991), 277-285

[Chen07] M. S. Chen, Y. Cai, Z. Yan, K. K. Gath, S. Axnanda, D. W. Goodman, *Highly active surfaces for CO oxidation on Rh, Pd and Pt*, Surf. Science, 601, (2007), 5326-5331

[Chen10] A. C. Chen, P.Holt-Linde, *Platinum-Based Nanostructured Materials: Synthesis, Properties, and Applications*, Chem. Rev., 110 (6), (2010), 3767-3804

[Chen13] M. Chen, Y. Zheng, H. Wan, *Kinetics and Active Surfaces for CO Oxidation on Pt-Group Metals Under Oxygen Rich Conditions*, Topics in Catalysis, 56, (2013), 1299-1313

[Clur09] S. M. McClure, D. W. Goodman, *New insights into catalytic CO oxidation on Pt-group metals at elevated pressures*, Chem. Phys. Lett., 469, (2009), 1-13

[Clur09.2] S. M. McClure, M. Lundwall, Z. Zhou, F. Yang, D. W. Goodman, *Characterization of Pt/SiO_2 Model Catalysts at UHV and Near Atmospheric Pressures*, Catal. Lett., 133, (2009), 298-306

[Dago76] R. Dagonnier, J. Nuyts, *Oscillating CO oxidation on a Pt surface*, J. Chem. Phys., 65, (1976), 2061-2066

[Daus90] A. Dauscher, L. Hilaire, F. Le Normand, W. Müller, G. Maire, A. Vasquez, *Characterization by XPS and XAS of supported Pt/TiO_2-CeO_2 catalysts*, Surface and Interface Analysis, 16, (1990), 341-346

[deLu07] A. de Lucas-Consuegra, F. Dorado, J. L. Valverde, R. Karoum, P. Vernoux, *Low-temperature propene combustion over Pt-K-βAl_2O_3 electrochemical catalyst: Characterization, catalytic activity measurements and investigation of the NEMCA effect*, J. of Catalysis, 251(2), (2007), 474-484

[Dora07] F. Dorado, A. De Lucas-Consuegra, C. Jimenez, J. L. Valverde, *Influence of the reaction temperature on the electrochemical promoted catalytic behaviour of platinum impregnated catalysts for the reduction of nitrogen oxides under lean burn conditions*, Appl. Catal. A Gen., 321, (2007), 86-92

[Douv02] S. L. Douvartzides, P. E. Tsiakaras, *Electrochemically Promoted Catalysis: The Case of Ethanol Oxidation over Pt*, J. Catal., 211, (2002), 521-529

[Eich02] A. Eichler, *CO Oxidation on Transition Metal Surfaces: Reaction rates from First Principles*, Surface Science, 498 (3), (2002), 314-320

[Elli08] C. Ellinger, A. Stierle, I. K. Robinson, A. Nefedov, H. Dosch, *Atmospheric pressure oxidation of Pt(111)*, J. of Physics: Cond. Matter, 20, (2008), 184013

[Emer98] D. A. Emery, P. H. Middleton, I. S. Metcalfe, *The effect of electrochemical current pumping on the work fuction of solid electrolyte supported catalysts*, Surf. Sci., 405, (1998), 308-315

[Ertl97] J. Wintterlin, S. Völkening, T.V.W. Janssens, T. Zambelli, G. Ertl, *Atomic and Macroscopic Reaction Rates of a Surface-Catalyzed Reaction*, Science, 278, (1997), 1931-1933

[Etse70] T. H. Etsell, S. N. Flengas, *Electrical properties of solid oxide eletrolytes*, Chem. Rev., 70, (1970), 339-376

[Falg10] C. Falgairette, *Stored Electrogenerated Promoters Inducing Sustainable Enhanced Pt Catalyst activity*, Dissertation, Ecole Polytechnique Federale de Lausanne, (2010)

[Falg10.2] C. Falgairette, C. Xia, YD Li, W. Harbich, G. Foti, C. Comninellis, *Investigation of the Pt/YSZ interface at low oxygen partial pressure by solid electrochemical mass spectroscopy under high vacuum conditions*, J. Appl. Electrochem., 40, (2010), 1901-1907

[Fark13] A. Farkas, K. Zalewska-Wierzbicka, C. Bachmann, J. Gortzka, D. Langsdorf, O. Balmes, J. Janek, *High Pressure Carbon Monoxide Oxidation over Platinum (111)*, Journal of Physical Chem. B, 117, (2013), 9932-9942

[Flei05] J. Fleig, J. Jamnik, *Work function changes of polarized electrodes on solid electrolytes*, J. Electrochem. Soc. 152(4), (2005) E138-E145

[Foti09] G. Foti, A. Jaccoud, C. Falgairette, C. Comninellis, *Charge storage at the Pt/YSZ interface*, J. Electroceram., 23, (2009), 175-179

[Freu01] H.-J. Freund, H. Kuhlenbeck, J. Libuda, G. Rupprechter, M. Bäumer, H. Hamann, *Bridging the pressure and materials gaps between catalysis and surface science: clean and modified oxide surfaces*, Topics in Catalysis, 15, (2001), 201-209

[Gao09] F. Gao, Y. Wang, Y. Cai, D. W. Goodman, *CO Oxidaion on Pt-Group Metals from Ultrahigh Vacuum to Near Atmospheric Pressures. 2. Palladium and Platinum*, J. Phys. Chem., 113, (2009), 174-181

[Gao09.2] F. Gao, S. M. McClure, Y. Cai, K. K. Gath, Y. Wang, M. S. Chen, Q. L. Guo, D. W. Goodman, *CO oxidation trends on Pt-goup metals from ultrahigh vacuum to near atmospheric pressures: A combined in situ PM-IRAS and reaction kinetic study*, Surf. Science, 603, (2009), 65-70

[Gao12] F. Gao, D. W. Goodman, *Model Catalysts: Simulating the Complexities of Heterogeneous Catalysts*, Annual Reviews of Physical Chemistry, 63, (2012), 265-286

[Gara11] I. Garagounis, V. Kyriakou, C. Anagnostou, V. Bourganis, I. Papachrsitou, M. Stoukides, *Solid Electrolytes: Applications in Heterogeneous Catalysis and Chemical Cogeneration*, IEC Reasearch, 50, (2011), 431-472

[Gauc11] Thomas Ryll, Henning Galinski, Lukas Schlagenhauf, Pierre Elser, Jennifer L. M. Rupp, Anja Bieberle-Hutter, Ludwig J. Gauckler, *Microscopic and Nanoscopic Three-Phase-Boundaries of Platinum Thin-Film Electrodes on YSZ Electrolyte*, Adv. Func. Mat., 21, (2011), 565-572

[Hank09] M. Hank, *Untersuchung von Goldkatalysatoren mittels Hochdruck-Röntgenphotoelektronenspektroskopie*, Diploma Thesis, Naturwissenschaftliche Fakultät der Friedrich-Alexander-Universität Erlangen-Nürnberg, (2009)

[Harm00] J. M. A. Harmsen, J. H. B. J. Hoebink, J. C. Schouten, *Transient kinetic modeling of the ethylene and carbon monoxide oxidation over a commercial automotive exhaust gas catalyst*, Ind. Eng. Chem. Res., 39 (3), (2000), 599-609

[Hein12] N. Heinemann, J. Grunau, T. Leissner, O. Andreyev, S. Kuhn, U. Jung, D. Zargarani, R. Herges, O. Magnussen, M. Bauer, *Reversible switching in self-assembled monolayers of azobenzene thiolates on Au (111) probed by threshold photoemission*, Chem. Phys., 402, (2012), 22-28

[Hend02] B. L. M. Hendriksen, J. W. M. Frenken, *CO oxidation on Pt(110): Scanning Tunneling Microscopy Inside High-Pressure Flow Reactor*, Phys. Rev. Lett., 89, (2002), 046101

[Hend04] B. L. M. Hendriksen, S. C. Bobaru, J. w. M. Frenken, *Oscillatory CO oxidation on Pd(100) studied with in situ scanning tunneling microscopy*, Surf. Science, 552, (2004), 229-242

[Hend05] B. L. M. Hendriksen, S. C. Bobaru, J. w. M. Frenken, *Looking at heterogeneous catalysis at atmospheric pressure using tunnel vision*, Topics in Catalysis, 36, (2005), 43-54

[Hend10] B. L. M. Hendriksen, M. D. Ackermann, R. van Rijn, D. Stoltz, I. Popa, O. Balmes, A. Resta, D. Wermeille, R. Felici, S. Ferrer, J. W. M. Frenken, *The role of steps in surface catalysis and reaction oscillations*, Nat. Chem., 2, (2010), 730-734

[Henr98] C. R. Henry, *Surface studies of supported model catalysts*, Surface Science Reports, 31, (1998), 235-325

[Hörl13] M. P. Hörlein, A. K. Opitz, J. Fleig, *On the variability of oxygen exchange kinetics of platinum model electrodes on yttria stabilized zirconia*, Solid State Ionics, 247, (2013), 56-65

[Hube12] A. K. Huber, M. Falk, M. Rohnke, B. Luerssen, M. Amati, L. Gregoratti, D. Hesse, J. Janek, *In situ study of activation and de-activation of LSM fuel cell cathodes - Electrochemistry and surface analysis of thin-film electrodes*, J. Catal. 294, (2012), 79-88

[Hube12.2] A. K. Huber, M. Falk, M. Rohnke, B. Luerßen, L. Gregoratti, D. Matteo, J. Janek, *In situ study of electrochemical activation and surface segregation of the SOFC electrode material* $La_{0.8}Sr_{0.25}Cr_{0.5}Mn_{0.5}O_{3\pm\delta}$, Phys. Chem. Chem. Phys. 14, (2012), 751-758

[Ibra12] N. Ibrahim, M. R. Jalil, D. Poulidi, I. S. Metcalfe, *The role of low coverage sodium surface species on electrochemical promotion in a Pt/YSZ system*, Solid State Ionics, 225, (2012), 386-389

[Imbi10] R. Imbihl, *Electrochemical promotion of catalytic reactions*, Progress in Surface Science, 85, (2010), 241-278

[Imbi11] R. Imbihl, A. Toghan, *Comment on the Note by Vayenas and Vernoux on - The Electrochemical Promotion of Ethylene Oxidation at a Pt/YSZ Catalyst* -, Chem. Phys. Phys. Chem., 12 (9), (2011), 1764-1766

[Jacc07] A. Jaccoud, C. Falgairette, G. Foti, C. Comninellis, *Charge storage in the* $O_{2(g)}$*, Pt/YSZ system*, Electrochim. Acta, 52, (2007), 7927-7935

[Jacc07.2] A. Jaccoud, *Electrochemical Promotion of Pt Catalysts for Gas Phase Reactions*, Dissertation, Ecole Polytechnique Federale de Lausanne, (2007)

[Jane99] J. Janek, C. Korte, *Electrochemical blackening of yttria-stabilized zirconia - morphological instability of the moving reaction front*, Solid State Ionics, 116, (1999), 181-195

[Jane00] J. Janek, M. Rohnke, B. Luerssen, R. Imbihl, *Promotion of catalytic reactions by electrochemical polarization*, PhysChem-ChemPhys, 2(9), (2000), 1935-1941

[Jime97] R. Jiménez, T. Kloid, M. Kleitz, *Reaction Zone Expansion and Mechanism of the O_2, Ag-Yttria-Stabilized Zirconia Electrode Reaction*, J. Electrochem. Soc., 144, (1997), 582-585

[Jime12] C. Jimenez-Borja, S. Brosda, M. Makrj, F. Sapountzi, F. Dorado, J. L. Valverde, C. G. Vayenas, *Mathane oxidation on Pd/YSZ by electrochemical promotion*, Solid State Ionics, 225, (2012), 376-381

[Jime12.2] C. Jimenez-Borja, A. de Lucas-Consuegra, F. Sapountzi, F. Dorado, A. Katsaounis, J. L. Valverde, *Oscillatory behavior of Rh/YSZ under electropromoted conditions*, Chem. Phys. Lett., S19-S20, (2012), 89-92

[Jung10] . Jung, O. Filinova, S. Kuhn, D. Zargarani, C. Bornholdt, R. Herges and O. Magnussen, *Photoswitching Behavior of Azobenzene-Containing Alkanethiol Self-Assembled Monolayers on Au Surfaces*, Langmuir, 26, (2010), 1391313923

[Kamb12] A. Kambolis, L. Lizarraga, M. N. Tsampas, L. Burel, M. Rieu, J. P. Viricelle, P. Vernoux, *Electrochemical promotion of catalysis with highly dispersed Pt nanoparticles*, Electrochem. Comm., 19, (2012), 5-8

[Karo08] R. Karoum, A. De Lucas-Consuegra, F. Dorado, J. L. Valverde, A. Billard, P. Vernoux, *Towards a new definition of EPOC parameters for anionic electrocheemical catalysts: case of propene combustion* J. Appl. Electrochem., 38, (2008), 1083-1088

[Kats04] A. Katsaounis, Z. Nikopoulou, X. E. Verykios, C. G. Vayens, *Comparative isotope-aided investigation of electrochemical promotion and metal-support interactions 1.* $^{18}O_2$ *TPD of electropromoted Pt films deposited on YSZ and of dispersed Pt/YSZ catalysts*, J. Catalysis, 222, (2004), 192-206

[Kats04.2] A. Katsaounis, Z. Nikopoulou, X. E. Verykios, C. G. Vayens, *Comparative isotope-aided investigation of electrochemical promotion and metal-support interactions 2. CO oxidation by* $^{18}O_2$ *on electropromoted Pt films deposited on YSZ and of dispersed Pt/YSZ catalysts*, J. Catalysis, 226, (2004), 197-209

[Kats10] A. Katsaounis, *Recent developments and trends in the electrochemical promotion of catalysis (EPOC)* J. of Applied Electrochem., 40(5), (2010), 885-902

[Kenj93] T. Kenjo, Y. Yamakoshi, K. Wada, *An Estimation of the Electrode-Electrolyte Contact Area by Linear Sweep Voltammetry in Pt/ZrO_2 Oxygen Electrodes*, J. Electrochem. Soc., 140, (1993), 2151-2157

[Kenj94] T. Kenjo, H. Takiyama, *Oxygen Permeation in Ag/YSZ Air Cathodes*, Electrochimica Acta, 39, (1994), 2685-2692

[Kiuk57] K. Kiukkola, C. Wagner, *Measurements of Galvanic Cells Involving Solid Electrolytes*, J. Electrochem. Soc., 104, (1957), 379-387

[Kilo03] M. Kilo, M. A. Taylor, C. Argirusis, G. Borchardt, B. Lesage, S. Weber, S. Scherrer, H. Scherrer, M. Schroeder, M. Martin, *Cation self-diffusion of Ca-44, Y-88, and Zr-96 in single-crystalline calcia- and yttria-doped zirconia*, J. Appl. Phys., 12, (2003), 7547-7552

[Kont91] I. Kontoulis, B. C. H. Steele, *Determination of oxygen diffusion in solid Ag by an electrochemical technique*, Solid State Ionics, 47, (1991), 317-324

[Kout06] C. Koutsodontis, A. Katsaounis, J. C. Figueroa, C. Cavalca, C. Pereira, C. G. Vayenas, *The effect of catalyst film thickness on the electrochemical promotion of ethylene oxidation on Pt*, Topics in Catalysis, 39, (2006), 97-100

[Labo07] D. Labou, S. G. Neophytides, *Promotional effects on a PtRu/C catalyst-electrode interfaced with aqueous electrolytes: electrochemical metal support interaction (EMSI) and electrochemical promotion of catalysis (EPOC)*, Top. Catal., 44, (2007), 451-460

[Lada93] S. Ladas, S. Kennou, S. Bebelis, and C.G. Vayenas, *Origin of Non-Faradaic Electrochemical Modification of Catalytic Activity*, J. Phys. Chem. 97, (1993), 8845-8847

[Lang22] I. Langmuir, *Heterogeneous reaction: Chemical Reactions on surfaces*, Trans. Faraday Soc., 17, (1922), 607-620

[Larr11] A. Larrea, D. Sola, M. A. Laguna-Bercero, *Self-supporting thin yttria-stabilised zirconia electrolytes for solid oxide fuel cells prepared by laser machining*, J. of the Electrochemical Soc., 158 (10), (2011), B1193-1197

[Lawl74] K.R. Lawless, *The oxidation of metals*, Rep. Prog. Phys., 37, (1974), 231-316

[Leiv08] E. P. M. Leiva, C. Vazquez, M. I. Rojas, M. M. Mariscal, *Computer simulation of the effective double layer occuring on a catalyst surface under electro-chemical promotion conditions*, J. Applied Electrochem., 38, (2008), 1065-1073

[Lewi68] R. Lewis, R. Gomer, *Adsorption of oxygen on platinum*, Surface Science, 12, (1968), 157-176

[Libu05] J. Libuda, S. Schauermann, M. Laurin, T. Schalow, *Model studies in heterogeneous catalysis. From structure to kinetics*, Monatshefte der Chemie, 136 (1), (2005), 59-75

[Lin08] W.Lin, A. A. Herzing, C. J. Kiely, I. E. Wachs, *Probing Metal-Support Interactions under Oxidizing and Reducing Conditions: In Situ Raman and Infrared Spectroscopic and Scanning Transmission Electron Microscopic-X-ray Energy-Dispersive Spectroscopic Investigation of Supported Platinum Catalysts*, J.Phys. Chem. C., 112, (2008), 5942-5951

[Lint08] A. Lintanf, E. Djurado, P. Vernoux, *Pt/YSZ electrochemical catalysts prepared by electrostatic spray deposition for selective catalytic reduction of NO by C_3H_6*, Solid State Ionics, 178, (2008), 1998-2008

[Luca08] A. De Lucas-Consuegra, F. Dorado, J. L. Valverde, R. Karoum, P. Vernoux, *Electrochemical activation of Pt catalyst by potassium for low temperature CO deep oxidation*, Catal. Commun., 9, (2008), 17-20

[Luer00] B. Luerßen, S. Günther, H. Marbach, M. Kiskinoval, J. Jank, R. Imbihl, *Photoelectron spectromicroscopy of electrochemically induced oxygen spillover at the Pt/YSZ interface*, Chem. Phys. Lett., 316, (2000), 331-335

[Luer06] B. Luerssen, E. Mutoro, H. Fischer, S. Günther, R. Imbihl, J. Janek, *In Situ Imaging of Electrochemically Induced Oxygen Spillover on Pt/YSZ Catalysts*, Angewandte Chemie International Edition, 20, (2006), 1473-1476

[Makr96] M. Makri, C. G. Vayenas, S. Bebelis, K. H. Besocke, C. Cavalca, *Atomic resolution STM imaging of electrochemically controlled reversible promoter dosing of catalysts*, Surface Science, 369, (1996), 351-359

[Mar92] O. A. Mar'ina, V. A. Sobyanin, *The effect of electrochemical oxygen pumping on the rate of CO oxidation on Au electrode-catalyst*, Catal. Lett., 13, (1992), 61-69

[Marw98] M. Marwood, C. G. Vayenas, *Electrochemical Promotion of Dispersed Platinum Catalyst*, J. of Catalysis, 178, (1998), 429-440

[Mate13] F. Matei, C. Jimenez-Borja, J. Canales-Vazquez, S. Brosda, F. Dorado, J. L. Valverde, D. Ciuparu, *Enhanced electropromotion of methane combustion on palladium catalysts deposited on highly porous supports*, Appl. Catalysis B. Environmental, 132, (2013), 80-89

[Metc01] I. S. Metcalfe, *Electrochemical Promotion of Catalysis I: Thermodynamic Considerations*, J. of. Catalysis, 199, (2001), 247-258

[Metc02] I. S. Metcalfe, *Electrochemical promotion of catalysis: the use of transition state theory for the prediction of reaction rate modification*, Solid State Ionics, 152-153, (2002), 669-674

[Mich03] A. Michaelides, M.-L. Bocquet, P. Sautet, A. Alavi, D. A. King, *Structures and thermodynamic phase transition for oxgen and silver oxide phases on Ag(111)*, Chem. Phys. Letters, 367, (2003), 344-350

[Möbi66] H. Möbius, B. Rohland, *Sauerstoffionenleitende Festelektrolyte und ihre Anwendungsmöglichkeiten; Über den Einfluss des Elektrodenmaterials auf das Ergebnis von Messungen zur elektrischen Leitfähigkeit fester Elektrolyte*, Z. Chem., 158-159, 1966

[Muto05] E. Mutoro, *Photoelektronenmikroskopie und Polariationsuntersuchungen an katalytisch aktiven Elektroden auf Festelektrolyten*, Diplomarbeit, Justus-Liebig Universität Gießen, 2005

[Muto08] E. Mutoro, B. Luerssen, S. Guenther, J. Janek, *Structural, morphological and kinetic properties of model type thin film platinum electrodes on YSZ*, Solid State Ionics, 179, (2008), 21-26

[Muto08.2] . Mutoro, S. Günther, B. Luerßen, I. Valov, J. Janek, *Electrode activation and degradation: Morphology changes of platinum electrodes on YSZ during electrochemical polarisation*, Solid State Ionics, 179, (2008), 1835-1848

[Muto09] E. Mutoro, B. Luerßen, S. Günther, J. Janek, *The electrode model system Pt(O_2)|YSZ: Influence of impurities and electrode morphology on cyclic voltammograms*, Solid State Ionics, 180, (2009), 1019-1033

[Muto10] E. Mutoro, C. Koutsodontis, B. Luerssen, S. Brosda, C. G. Vayenas, J. Janek, *Electrochemical promotion of Pt(111)/YSZ(111) and Pt-FeO_x/YSZ(111) thin catalyst films: Electrocatalytic, catalytic and morphological studies*, Appl. Catalysis B Environmental, 100(1-2), (2010), 328-337

[Muto12] E. Mutoro, E. J. Crumlin, H. Pöpke, B. Luerssen, M. Amati, M. K. Abyaneh, M. D. Biegalski, H. M. Christen, L. Gregoratti, J. Janek, Y. Shao-Horn, *Reversible Compositional Control of Oxide Surfaces by Electrochemical Potentials*, J. Phys. Chem. Lett., 3, (2012), 40-44

[Nako10] A. Nakos, S. Souentie, A. Katsaounis, *Electrochemical promotion of methane oxidation on Rh/YSZ*, Appl. Catalysis B Environmental, 101, (2010), 31-37

[Neop94] S. G. Neophytides, D. Tsiplakides, P. Stonehart, M. M. Jaksic, C. G. Vayenas, *Electrochemical enhancement of a catalytic reaction in aqueous solution*, Nature, 370, (1994), 45

[Neop95] S. G. Neophytides, C. G. Vayenas, *TPD and Cyclic Voltammetric Investigation of the Origin of Electrochemical Promotion in Catalysis*, J. Phys. Chem., 99, (1995), 17063-17067

[Neop96] S. G. Neophytides, D. Tsiplakides, P. Stonehart, M. M. Jaksic, C. G. Vayenas, *Non-Faradaic Electrochemical Modification of the Catalytic Activity of Pt for H_2 Oxidation in Aqueous Alkaline Media*, J. Phys. Chem., 100, 1996, 14803-14814

[Neop98] S. G. Neophytides, D. Tsiplakides, C. G. Vayenas, *TPD of Oxygen from Pt Films Interfaced with Y_2O_3-Doped ZrO_2*, J. Catalysis, 178, (1998), 414-428

[Neub04] T. Neubrand, S. Günther, A. Fenske, R. Imbihl, *Work function changes and eletrochemical pumping of platinum electrodes on yttrium stabilized zirconia*, Physical Chemistry Chemical Physics, 6, (2004), 3569-3575

[Neum10] J. Neumeier, *Morphologische und elektrochemische Untersuchungen an Pt/YSZ-Modellelektroden*, Diplomarbeit, Justus-Liebig Universität Gießen, 2010

[Neum13] J. Neumeier, *Elektrochemische Untersuchungen an mikrostrukturierten Modellelektroden auf sauerstoffionenleitenden Festelektrolyten*, Masterarbeit, Justus-Liebig Universität Gießen, 2013

[Onke92] H. U. Onken, E. E. Wolf, *Self-sustained and forced oscillations during ethylene and carbon monoxide oxidation on Pt-SiO_2*, Chem. Eng. Sci., 47 (7) (1992), 1659-1667

[Opit10] A. K. Opitz, J. Fleig, *Investigation of O_2 reduction on Pt/YSZ by means of thin film miroelectrodes: The geometry dependence of the electrode impedance*, Solid State Ionics, 181, (2010), 684-693

[Opit10.1] A. K. Opitz, A.Schintlmeister, H. Hutter, J. Fleig, *Visualization of oxygen reduction sites at Pt electrodes on YSZ by means of ^{18}O tracer incorporation: the width of the electrochemically active zone*, Phys. Chem. Chem. Phys., 12, (2010), 12734-12745

[Opit12] A. K. Opitz, M. P. Hoerlein, T. Huber, J.Fleig, *Current-Voltage Characteristics of Platinum Model Electrodes on Yttria-Stabilized Zirconia*, J. Electrochem. Soc., 159, (2012), B502-B513

[Pant05] J. Pantförder, *Photoelektronenspektroskopie im „Pressure Gap" - Aufbau einer neuen Apparatur für Messungen im Druckbereich von 10^{-10} bis 1 mbar*, Dissertation, Naturwissenschaftliche Fakultät der Friedrich-Alexander-Universität Erlangen-Nürnberg, (2005)

[Patt71] J. W.Patterson, *Conduction Domains for Solid Electrolytes*, J.Electrochem. Soc, 118, (1971), 1033-1039

[Petr00] I. M. Petrushina, V. A. Bandur, F. Cappeln, N. J. Bjerrum, *Electrochemical Promotion of Sulfur Dioxide Catalytic Oxidation*, J. Electrochem. Soc., 147, (2000), 3010-3013

[Piki77] C. A. Pikios, D. Luss, *Isothermal concentration oscillations on catalytic surfaces*, Chem. Eng. Sci., 32 (1977), 191-194

[Plia96] C. Pliangos, I. V. Yentekakis, S. ladas, C. G. Vayenas, *Non-Faradaic Electrochemical Modification of Catalytic Activity: 9. Ethylene Oxidation on Pt Deposited on TiO_2*, J. of Catalysis, 159, (1996), 189-203

[Plia97] C. Pliangos, I. V. Yentakis, V. G. Papadakis, C. G. Vayenas, X. E. Verykios, *Support-induced promotional effects on the activity of automotive exhaust catalysis: 1. The case of oxidation of light hydrocarbons (C_2H_4)*, Appl. Catal., B., 14, (1997), 161-173

[Ploe97] L. Ploense, M. Salazar, B. Gurau, E. S. Smotkin, *Proton spillover promoted isomerization of n-butylenes on Pd-black Cathodes Nafion 117*, J. American. Chem. Soc., 119, (1997), 11550-11551

[Poli90] T. I. Politova, V. A. Sobyanin, V. D. Belyaev, *Ethylene hydrogenation in electrochemical cell with solid proton-conducting electrolyte*, React. Kinet. Catal. Lett., 41, (1990), 321-326

[Popp99] J. Poppe, S. Völkening, A. Schaak, E. Schütz, J. Janek, R. Imbihl, *Electrochemical promotion of catalytic CO oxidation on Pt/YSZ catalysts under low pressure conditions*, Phys. Chem. Chem. Phys., 1, (1999), 5241-5249

[Poul07] D. Poulidi, A. Thursfield, I. S. Metcalfe, *Electrochemical promotion of catalysis controlled by chmical potential difference across a mixed ionic-electronic conducting ceramic membrane - an example of wireless NEMCA*, Top. In Catal., 44(3), (2007), 435

[Pöpk11] H. Pöpke, E. Mutoro, B. Luerßen, J. Janek, *The potential of in situ-scanning electron microscopy - Morphology changes of electrically polarized thin film Pt(O_2)/YSZ model electrodes*, Solid State Ionics, 189, (2011), 56-62

[Pöpk11.2] H. Pöpke, E. Mutoro, C. Raiß, B. Luerßen, M. Amati, M. K. Abyaneh, L. Gregorattie, J. Janek, *The role of platinum oxide in the electrode system Pt(O_2)/yttria-stabilized zirconia*, Electrochimica Acta, 56, (2011), 10668-10675

[Pöpk11.3] H. Pöpke, E. Mutoro, B. Luerßen, M. Amati, L. Gregoratti, J. Janek, *Platinum Oxide Formation in the Electrode System Pt(O_2)/YSZ Investigated by In situ Scanning Photoelectron Emission Microscopy*, Electrochim. Acta, 56, (2011), 10668-10675

[Pöpk12] H. Pöpke, E. Mutoro, B. Luerssen, J. Janek, *Oxidation of Platinum in the Epitaxial Model system Pt (111) / YSZ (111): Quantitative Analysis of an Electrochemically Driven PtO_x Formation*, J. Phys. Chem. C, 116, (2012), 1912-1920

[Pöpk13] H. Poepke, E. Mutoro, B. Luerssen, J. Janek, *Oxygen reduction and oxidation at epitaxial model-type Pt(O-2)/YSZ electrodes - On the role of PtOx formation on activation, passivation, and charge transfer*, Catal. Today, 202, (2013), 12-19

[Ridd02] M. D. Ridder, R. G. van Welzenis, H. H. Brongersma, S. Wulff, W.-F. Chu, W. Weppner *Discovery of the rate limiting step in solid oxide fuel cells by LEIS*, Nucl.Instr. and Meth. in Phys. Res. B., 190, (2002), 732-735

[Rijn10] R. Van Rijn, O. Balmes, R. Felici, J. Gustafson, D. Wermeille, R. Westerström, E. Lundgren, J. W. M. Frenken, *Comment on CO Oxidation of Pt-Goup Metals from Ultrahigh Vacuum to Near Atmospheric Pressure. 2. Palladium and Platinum* J. Phys. Chem. C, 114, (2010), 6875-6879

[Rinn97] M. Rinnemo, D. Kulginov, S. Johansson, K.L. Wong, V.P. Zhdanov, B. Kasemo, *Catalytic ignition in the CO-O_2 reaction on platinum: experiment and simulations*, Surface Science, 376, (1997), 297-309

[Roch08] V. Roche, R. Karoum, A. Billard, A. Revel, P. Vernoux, *Electrochemical promotion of deep oxidation of methane on Pd/YSZ*, J. Appl. Electrochem., 38, (2008), 1111-1119

[Roch10] V. Roche, R. Revel, P. Vernoux, *Electrochemical promotion of YSZ moolith honeycob for deep oxidation of methane*, Catal. Comm., 11(13), (2010), 1076-1080

[Sala06] M. Salazar, E. S. Smotkin, *Electrochemically promoted olefin isomerization reactions at polymer electrolyte fuel cell membrane electrode assemblies*, J. Applied Electrochem., 36, (2006), 1237-1240

[Sapo07] F. Sapountzi, M. N. Tsampas, C. G. Vayenas, *Electrocatalysis and electrochemical promotion of CO oxidation in PEM fuel cells: the role of oxygen crossover*, Top. Catal., 44, (2007), 461-468

[Sapo07.2] F. Sapountzi, M. N. Tsampas, C. G. Vayenas, *Methanol reformate treatment in a PEM fuel cell-reactor*, Catal. Today, 127, (2007), 295-303

[Sche77] M. Scheintuch, R. A. Schmitz, *Oscillations in Catalytic Reactions*, Catal. Rev. Sci. Eng., 15, (1977), 107-172

[Seri06] N. Seriani, W. Pompe, L. C. Ciacchi, *Catalytic Oxidation Activity of Pt_3O_4 Surfaces and Thin Films*, J. Phys. Chem. B., 110, (2006), 14860-14869

[Shig78] R. A. Shigeishi, D. A. King, *The Oxidation of Carbon Monoxide on Platinum (111): Reflection-Absorption Infrared Spectroscopy*, Surf. Science, 75 (2), (1978), L397-L400

[Slin78] M. G. Slin´ko, M. M. Slin´ko, *Self-Oscillattion of Heterogeneous Catalytic Reaction Rates*, Catal. Rev. Sci. Eng., 17, (1978),119-153

[Soby92] V. A. Sobyanin, V. I. Sobolev, V. D. Belyaev, A. K. Demin, O. A. Mar'ina, *Oxygen isotope exchange over a Pt electrode in a cell with solid oxide electrolyte*, React. Kinet. Catal. Lett., 47(2), (1992), 327

[Soby93] V. A. Sobyanin, V. I. Sobolev, V. D. Belyaev, O. A. Marina, A. K. Demin, A. S. Lipilin, *On the origin of the non-faradaic electrochemical modification of catalytic activity (NEMCA) phenomena. Oxygen isotope exchange on Pt electrode in cell with solid oxide electrolyte*, Catalysis Letters, 18, (1993), 153-164

[Somo97] G. A. Somorjai, *New model catalysts (platinum nanoparticles) and new tehniques (SFG and STM) for studies of reaction intermediates and surface restructuring at high pressures during catalytic reactions*, Applied Surface Science, 121-122, (1997), 1-19

[Soue08] S. Souentie, A. Hammad, S. Brosda, G. Fori, C. G. Vayenas, *Electrochemical promotion of NO reduction by C_2H_4 in 10 % O_2 using a monolithic electropromoted reactor with Rh/YSZ/Pt elements*, J. Appl. Electrochem., 38, (2008), 1159-1170

[Stan99] . Stancovski, S. Sridhar, U. B. Pal, *Thermodynamic Stability and Interfacial Impedance of Solid-Electrolyte Cells with Noble Metal Electrodes*, J. Electrceram., 3, (1999), 279-299

[Stou81] M. Stoukides, C. G. Vayenas, *The effect of electrochemical oxygen pumping on the rate and selectivity of ethylene oxidation on polycrystalline silver*, J. of Catalysis, 70, (1981), 137-146

[Stou84] M. Stoukides, C. G. Vayenas, *Electrocatalytic Rate Enhancement of Propylene Epoxidation on Porous Silver Electrodes Usind a Zirconia Oxygen Pump*, J. Electrochem. Soc., 131(4), (1984), 839-845

[Stou88] M. Stoukides, *Application of solid electrolytes in heterogeneous catalysis*, Ind. Eng. Chem. Res., 27, (1988), 1745-1750

[Su97] X. Su, P. S. Cremer, Y. R. Shen, G. A. Somorjai, *High-Pressure CO Oxidation on Pt(111) Monitored with Infrared-Visible Sum Frequency Generation (SFG)*, J. Am. Chem. Soc., 119, (1997), 3994-4000

[Thur03] A. Thursfield, S. Brosda, C. Pliangos, T. Schober, C. G. Vayenas, *Electrochemical pomotion of an oxidation reaction using a proton conductor*, Electrochim. Acta, 48, (2003), 3779-3788

[Thel12] D. Theleritis, S. Souentie, A. Siokou, A. Katsaounis, C. G. Vayenas, *Hydrogenation of CO_2 over Ru/YSZ Electropromoted Catalysts*, ACS Catalysis, 2(5), (2012), 770-780

[Togh10] A. Toghan, L. M. Rösken, R. Imbihl, *Origin of non-Faradayicity in electrochemical promotion of catalytic ethylene oxidation*, Phys. Chem. Chem. Phys., 12, (2010), 9811-9815

[Togh10.2] A. Toghan, L. M. Rösken, R. Imbihl, *The Electrochemical Promotion of Ethylene Oxidation at a Pt/YSZ Catalyst*, Chem. Phys. Chem., 11, (2010), 1452-1459

[Tsam09] M. N. Tsampas, F. M. Sapountzi, C. G. Vayenas, *Electrochemical promotion of CO oxidation on Pt/YSZ: The effect of catalyst potential on the induction of highly active stationary and oscilatory states*, Catalysis Today, 146, (2009), 351-358

[Tsam13] M. N. Tsampas, F. M. Sapountzi, A. Boreave, P. Vernoux, *Isotopical labeling mechanistic studies of electrochemical promotion of propane combustion on Pt/YSZ*, Electrochem. Comm., 26, (2013), 13-16

[Tsia02] P. E. Tsiakaras, S. L. Douvatzides, A. K. Demin, V. A. Sobyanin, *The oxidation of ethanol over Pt catalyst-electrodes deposited on ZrO_2 (8 mol %)*, Solid State Ionics, 152-153, (2002), 721-726

[Tsip99] D. Tsiplakides, C. G. Vayenas, *Temperature-Programmed Desorption of Oxygen from Ag Films Interfaced with Y_2O_3-Doped ZrO_2*, J. Catalysis, 185, (1999), 237-251

[Tsip01] D. Tsiplakides, C. G. Vayenas, *Electrode Work Function and Absolute Potential Scale in Solid-State Electrochemistry*, 148, (2001), E189-E202

[Tsip05] D. Tsiplakides, A. Katsaounis, D. Archonta, C. Koutsodontis, C. G. Vayenas, *Electrochemical promotion of catalysis: mechanistic investigations and monolithic electropromoted reactors*, Catal. Today, 100, (2005), 133-144

[Tsip09] D. Tsiplakides, S. Balomeneou, *Milestones and perspectives in electrochemically promoted catalysis*, Catalysis Today, 146, (2009), 312-318

[VanH94] J. Van Herle, A. J. McEvoy, *Oxygen diffusion through silver cathodes for solid oxide fuel cells*, J. Phys. Chem. Solids, 55 (4), (1994), 339-347

[Vark95] E. Varkaraki, J. Nicole, E. Plattner, C. Comninellis, C. G. Vayenas, *Electrochemical promotion of IrO_2 catalyst for the gas phase combustion of ethylene*, J. Appl. Electrochem., 25, (1995), 978-981

[Vatt08] Luca Vattuone, L. Savio, M. Rocca, *Bridging the structure gap: Chemistry of nanostructured surfaces at well-defined defects*, Surface Science Reports, 63, (2008), 101-168

[Vaye81] C. G. Vayenas, C. Georgakis, J. Michaels, J. Tormo, *The role of PtOx in the Isothermal Rate Oscillations of Ethylene Oxidation on Platinum*, J. Catal., 67, (1981), 348-361

[Vaye82] C. G. Vayenas, J. Michaels, *On the stability limit of surface platinum oxide and its role in oscilation phenomena of platinum catalyzed oxidations*, Surf. Science, 120, (1982), L405-408

[Vaye88] C. G. Vayenas, S. Bebelis, S. Neophytides, *Non-Faradaic electrochemical modification of catalytic activity*, J. Phys. Chem., 92, (1988), 5083 -5085

[Vaye90] C. G. vayenas, S. Bebelis, S. Ladas, *Dependence of catalytic rates on catalyst work function*, Nature, 343, (1990), 625 - 627

[Vaye01] C. G. Vayenas, S. Bebelis, C. Pliangos, S. Brosda, D. Tsiplakides, *Electrochemical Activation of Catalysis - Promotion, Electrochemical Promotion, and Metal-Support Interaction*, Kluwer Academin/ Plenum Publisher, New York, (2001)

[Vaye03] C. G. Vayenas, S. Brosda, C. Pliangos, *The double-layer approach to promotion, electrocatalysis, electrochemical promotion and metalsupport interactions*, J. Catal., 216, (2003), 487-504

[Vaye06] C. G. Vayenas, D. Archonta, D. Tsiplakides, *Scanning tunneling microscopy observation of the origin of electrochemical promotion and metal-supported interactions*, J. Electroanal. Chem., 554-555, (2006), 301-306

[Vaye11] C. G. Vayenas, P. Vernoux, *Note on - The Electrochemical Promotion of Ethylene Oxidation at a Pt/YSZ Catalyst*, Chem. Phys. Phys. Chem., 12 (9), (2011), 1761-1763

[Vern11] P. Vernoux, C. G. Vayenas, *Note on - Electrochemical promotion of catalytic reactions*, Prog. in Surf. Science, 86, (2011), 83-93

[Völk00] S. Völkening, J. Wintterlin, *CO oxidation on Pt(111)-Scanning tunneling microscopy experiments and Monte Carlo simulation*, J. Chem. Phys., 114, (2001), 6382-6395

[Wang79] D.Y.Wang, A.S. Nowick, *Cathodic and anodic polarization phenomena at platinum electrodes with doped CeO_2 as electrolyte. I. Steady-state overpotential*, J. Electrochem. Soc., 126, (1979), 1155-1165

[Wang79.2] D.Y.Wang, A.S. Nowick, *Cathodic and anodic polarization phenomena at platinum electrodes with doped CeO_2 as electrolyte. II. Transient overpotential and A-C*, J. Electrochem. Soc., 126, (1979), 1166-1172

[Wang81] D.Y.Wang, A.S. Nowick, *Diffusion-controlled polarization of Pt, Ag, and Au electrodes with doped ceria electrolyte*, J. Electrochem. Soc., 128(1), (1981), 55-163

[West13] C. J. Weststrate, A. M. Saib, J. W. Niemantsverdriet, *Promoter segregation in Pt and Ru promoted cobalt model catalysts during oxidation reduction treatments*, Catalysis Today, 215, (2013), 2-7

[Wint96] J. Wintterlin, R. Schuster, G. Ertl, *Existence of a Hot Atom Mechanism for the Dissociation of O_2 on Pt(111)*, Phys. Rev. Lett., 77, (1996), 123-126

[Wint20] S. Völkening, J. Wintterlin, *CO oxidation on Pt (111)scanning tunneling microscopy experiments and Monte Carlo simulations*, J. Chem. Phys., 114, (2000), 6382-6395

[Wu85] N. L. Wu, J. Phillips, *Catalytic Etching of Platinum during Ethylene Oxidation*, J. Phys. Chem., 89, (1985), 591-600

[Wu86] N. L. Wu, J. Phillips, *Reaction-enhanced sintering of platinum thin films during ethylene oxidation*, J. Appl. Phys., 59, (1986), 769-779

[Wu88] N. L. Wu, J. Phillips, *Carbon deposition on Platinum during Ethylene Oxidation*, J. Catal., 113, (1988), 383-397

[Yent88] I. V. Yentekakis, C. G. Vayenas, *The effect of electrochemical oxygen pumping on the steady-state and oscillation behavior of CO oxidation on polycrystalline Pt*, J. Catal., 11, (1988), 170-188

[Yent92] I.V. Yentekakis, S. Bebels, *Study of the NEMCA effect in a single-pellet catalytic reactor*, J. of Catalysis, 137, (1992), 278-283

[Yent98] I. V. Yentekakis, R. M. Lambert, M. S. Tikhov, M. Konsolakis, V. Kiousis, *Promotion by Sodium Emission Control Catalysis: A Kinetic and Spectroscopic Study of the Pd-Catalyzed Reduction of NO by Propene*, J. Catal., 176, (1998), 82-92

[Yiok00] C. G. Yiokari, G. E.Pitselis, D. G. Polydoros, A. D. Katsaounis, C. G. Vayenas, *High-Pressure Electrochemical Promotion of Ammonia Synthesis over an Industrial Iron Catalyst*, J. Phys. Chem. A, 104, (2000), 10600-10602

[Zhan00] C. J. Zhang, H. Hu, *Why Must Oxygen Atoms be Activated from Hollow Sites to Bridge Sites in Catalytic CO Oxidation*, J. Am. Chem. Soc., 122, (2000) 2134-2135

[Zhu12] Z. Zhu, F. Tao, F. Zheng, R. Chang, Y. Li, L. Heinke, Z. Liu, M. Salmeron, G. A. Somojai, *Formation of Nanometer-Sized Surface Platinum Oxide Clusters on a Stepped Pt(557) Single Crystal Surface Induced by Oxygen: A High-Pressure STM and Ambient Pressure XPS Study*, Nano Lett., 12, (2012), 1491-1497